SPA-LEED study of the morphology and nucleation of a novel growth mode and the "devil's staircase" on Pb/Si(111)

by

Wang-Chi Vincent Yeh

A dissertation submitted to the graduate faculty

in partial fulfillment of the requirements for the degree of

DOCTOR OF PHILOSOPHY

Major: Condensed Matter Physics

Program of Study Committee:
Michael C. Tringides, Major Professor
Kai-Ming Ho
James W. Evans
David Lynch
Jianwei Qiu

Iowa State University

Ames, Iowa

2003

Graduate College
Iowa State University

This is to certify that the doctoral dissertation of

Wang-Chi Vincent Yeh

has met the dissertation requirements of Iowa State University

Major Professor

For the Major Program

Graduate College
Iowa State University

This is to certify that the doctoral dissertation of

Wang-Chi Vincent Yeh

has met the dissertation requirements of Iowa State University

M. C. Trivedi

Major Professor

For the Major Program

TABLE OF CONTENTS

IS-T 1995

CHAPTER 1. General introduction

Discovery of a novel growth mode: where all these began

Recently, a novel growth mode was discovered on Pb thin film grown on Si(111)-7×7 reconstructed surface [1]: nano-scale islands of uniform 7-layer height with steep edges and flat tops can form below room temperature (180 K $\sim$ 240 K). Further study showed that different stable heights were observed over a wider temperature range, with a bi-layer difference between stable heights. For example, for a total of 4 ML (monolayer, 1 ML = 1 adsorbate atom per substrate unit cell) Pb deposited on Si(111)-7×7 surface, 5-layer high islands were grown from 150 K to 175 K, while 7-layer islands were formed from 175 K to 250 K. If Pb coverage was increased to 6ML, 9-layer islands were observed between 200 K and 230 K. These observed stable heights (5, 7 and 9) are separated by two instead of one layer difference. This growth mode was unexpected because it does not belong to any of the three growth modes that have always been discussed: layer-by-layer (Frank-van der Merwe) mode; three dimensional (Volmer-Weber) mode; and mixed or layer by layer followed by three dimensional (Stranski-Krastanov) mode. Figure 1.1 shows schematically the three commonly referred growth modes and the newly discovered one. In the layer-by-layer mode, each single layer completes before the next layer starts to grow. In the three dimensional mode, new layer can start to grow on top of one layer before lower layer is completed. The result is that islands of multi-layer height with single-stepped edges will grow. In the mixed mode, the thin film starts to grow in layer-by-layer mode for the first one or more layers, then followed by three dimensional

mode. The three usual growth modes can be understood by considering the difference in total surface tensions (surface free energy), $\Delta\gamma = \gamma_a - \gamma_s$, where γ_a is the surface tension of the surface with one layer of adsorbate, while γ_s is that of the clean substrate. If the difference $\Delta\gamma \leq 0$, meaning the clean substrate has higher or the same surface tension as the single-layer adsorbate covered surface, growth mode will be layer by layer in order not to increase the surface tension. On the other hand, if the clean substrate has lower surface tension, i.e., $\Delta\gamma > 0$, the substrate surface tends to remain uncovered and three dimensional growth mode is expected. The mixed mode, however, requires that $\Delta\gamma < 0$ for the first or more layers so they grow in layer by layer manner, then a change of sign in $\Delta\gamma$ should happen after some critical coverage to switch to three dimensional mode. This newly discovered novel growth mode could not be explained by this thermodynamic consideration. Instead, it could be explained by quantum size effects (QSE). QSE states that, to confine electrons inside a well, the dimensions of the well have to meet the requirement of energy quantization: the electron wavefunctions have to form standing waves within the confining well. Therefore, assuming infinite well, the following relation must be satisfied for the islands in the direction normal to the surface,

$$nd = s\lambda_F/2, \tag{1.1}$$

where λ_F is the Fermi wavelength and d the single step height of the grown crystal, with n, s both integers. Figure 1.2 shows a schematic of quantum size effects. If an island has a height that satisfies Eq. (1.1), it will be stable; otherwise it will not. Table 1-1 lists a calculation of Eq. (1.1) from $n = 3$ to $n = 11$. It is seen that only for $n = 5$, 7, 9 and 11 can the value of s be closest to an integer (7.2, 10.1, 13.0, 15.9, respectively). This explains the observed stable heights and the bi-layer increment results. After the discovery of this novel growth mode, related questions were raised immediately, such as: "How stable are those islands?" "How to increase the stability of the islands?" "Will

the results change if grown on a different type of Si(111) surface such as Pb/Si(111)-$\sqrt{3} \times \sqrt{3}$-β?" "What is the critical size of nucleation for such kind of islands?" To answer these questions, we performed experiments on such a system with the SPA-LEED technique. We have found that the 7-layer islands are stable at coverage between 3.5 and 8 monolayers (ML) and temperatures between 180 K and 240K K [2]. Islands covered with oxygen are found to stay at the same height (but coarsen laterally) up to almost room temperature [3]. Islands of different height (5-layer) and larger size are grown on a different surface Pb/Si(111)-$\sqrt{3} \times \sqrt{3}$-β at the same growth conditions (coverage, temperature, deposition flux) [Chapter 2], which is possibly caused by charge transfer at the metal-semiconductor interface. Chapter 3 tries to determine the critical size of nucleation for the 7-layer islands grown on the Si(111)-7×7 substrate. Although a definite conclusion could not be drawn without some theoretical calculations, the measured results are consistent with published works [4, 5].

In addition to the questions related to the novel growth mode, another interesting question was investigated and some of the results presented in this thesis. The question is: What phase or phases does it form on Pb/Si(111) when the coverage is between 6/5 ML and 4/3 ML? This question was raised because 1) more than one phase were reported in publications [6, 7, 8] and 2) there existed inconsistent descriptions about the higher coverage phases during this coverage range [9, 10]. It was found that actually a novel "devil's staircase" could be formed within this coverage range [11][Chapter 4]. Further study [12] using SPA-LEED found that even more of such "devil's staircase" phases could be formed at low temperatures ($T \sim$120 K), where atoms are not expected to be mobile! High symmetry site occupation change, a small effect of a shift of $\frac{\sqrt{3}}{3} \times 3.84 = 2.2$ Å in real space, was observed clearly in reciprocal space [Chapter 4].

Thesis organization

In the rest of this introductory chapter, the basics of diffraction by a perfect, flat surface will be given, followed by introducing the effects that a non-flat surface has in the reciprocal space and the method of observing such effects using SPA-LEED. Thereafter, the different growth results obtained on different surface will be presented in Chapter 2. Experimental results to determine the critical size of nucleation for the 7-layer Pb islands on Si(111)-77 are given in Chapter 3. The observation of "devil's staircase" phases at low temperature and the high symmetry site occupation change are then discussed in Chapter 4.

Literature review

Understanding LEED: waves scattered by a perfect and flat 2-dimensional lattice

A single lattice consists of a domain of a repeated structure called the unit cell. On a three-dimensional lattice, one can define lattice vectors, $\boldsymbol{a}_1, \boldsymbol{a}_2$ and $\boldsymbol{a}_3$, which correspond to the distances and directions of the repeating of the unit cell. Once such vectors are defined, the position of any unit cell (the lattice point) on the whole lattice can be specified by

$$\boldsymbol{R}_{uc} = n_1\boldsymbol{a}_1 + n_2\boldsymbol{a}_2 + n_3\boldsymbol{a}_3, \tag{1.2}$$

where (n_1, n_2, n_3) are all integers. Each single atom inside one unit cell can then be specified relative to the origin of the unit cell. For example, for the kth atom in a unit cell, its position vector can be given by $\boldsymbol{R}_k = \boldsymbol{R}_{uc} + \boldsymbol{r}_k$, where $\boldsymbol{r}_k$ is the position vector of the kth atom relative to the unit cell. On a two-dimensional lattice, $\boldsymbol{a}_3 = 0$. Figure 1.3 shows a two-dimensional lattice with a choice of lattice vectors $\boldsymbol{a}_1$ and $\boldsymbol{a}_2$ that can specify all the lattice points for such a lattice. When monochromatic waves are

scattered by a perfect and flat two-dimensional lattice, the total scattered wave is given by

$$\Psi = A_0 \exp(i\boldsymbol{S}_s \cdot \boldsymbol{r} - \omega t) \sum_{k,allatoms} f_k \exp(-i\Delta\boldsymbol{s} \cdot \boldsymbol{R}_k),$$

where A_0 is the amplitude of the wave, $\boldsymbol{S}_s$ the momentum vector of the scattered wave, f_k the scattering factor of the kth atom, and $\Delta\boldsymbol{s} = \boldsymbol{S}_s - \boldsymbol{S}_i$ the momentum transfer, which is the difference of momentum between the scattered and incident waves. Since the important quantity in diffraction is the intensity of the scattered wave, we are safe to drop the amplitude (since it's a constant) and the plane wave term (since it will not affect intensity calculation) without losing generality. Thus, the total scattered wave can be written as

$$\begin{aligned}
\Psi &= \sum_{k,allatoms} f_k \exp(-i\Delta\boldsymbol{s} \cdot \boldsymbol{R}_k) \\
&= \sum_{n_1,n_2} \sum_{k,unitcell} f_k \exp(-i\Delta\boldsymbol{s} \cdot (n_1\boldsymbol{a}_1 + n_2\boldsymbol{a}_2 + \boldsymbol{r}_k)) \\
&= \sum_{k=1}^{n} f_k \exp(-i\Delta\boldsymbol{s} \cdot \boldsymbol{r}_k) \left[\sum_{n_1=1}^{N_1} \exp(-i\Delta\boldsymbol{s} \cdot n_1\boldsymbol{a}_1) \sum_{n_2=1}^{N_2} \exp(-i\Delta\boldsymbol{s} \cdot n_2\boldsymbol{a}_2) \right] \\
&= F(\Delta\boldsymbol{s})G(\Delta\boldsymbol{s}), \qquad (1.3)
\end{aligned}$$

where $F(\Delta\boldsymbol{s})$, the first summation, is the structure factor while $G(\Delta\boldsymbol{s})$, the product of the last two summations, is the long range cell contribution. The long range cell contribution is equivalent to the diffraction pattern from many unit cells with only one atom inside, while the structure factor is the contribution from all atoms inside one unit cell. The summation of structure factor $F(\Delta\boldsymbol{s})$ runs over all atoms in one unit cell consisting of n atoms, while that of the cell contribution $G(\Delta\boldsymbol{s})$ go over all unit cells along the directions of both $\boldsymbol{a}_1$ and $\boldsymbol{a}_2$, with N_1 and N_2 the number of unit cells along each of them. The summations in $G(\Delta\boldsymbol{s})$ can be carried out explicitly, which are

$$\sum_{n_j=1}^{N_j} \exp(-i\Delta\boldsymbol{s} \cdot n_j\boldsymbol{a}_j) = \frac{\exp(-iN_j\Delta\boldsymbol{s} \cdot \boldsymbol{a}_j)}{\exp(-i\Delta\boldsymbol{s} \cdot \boldsymbol{a}_j)} \frac{\sin(\frac{1}{2}N_j\Delta\boldsymbol{s} \cdot \boldsymbol{a}_j)}{\sin(\frac{1}{2}\Delta\boldsymbol{s} \cdot \boldsymbol{a}_j)}, \qquad (1.4)$$

where $j = 1, 2$. The intensity of the scattered wave is then given by

$$\begin{aligned} I &= |\Psi|^2 = |F(\Delta \boldsymbol{s})|^2 |G(\Delta \boldsymbol{s})|^2 \\ &= \left| \sum_{k=1}^{N} f_k \exp(-i \Delta \boldsymbol{s} \cdot \boldsymbol{r}_k) \right|^2 \left| \frac{\sin(\frac{1}{2} N_1 \Delta \boldsymbol{s} \cdot \boldsymbol{a}_1)}{\sin(\frac{1}{2} \Delta \boldsymbol{s} \cdot \boldsymbol{a}_1)} \right|^2 \left| \frac{\sin(\frac{1}{2} N_2 \Delta \boldsymbol{s} \cdot \boldsymbol{a}_2)}{\sin(\frac{1}{2} \Delta \boldsymbol{s} \cdot \boldsymbol{a}_2)} \right|^2 . \end{aligned} \tag{1.5}$$

If $N \gg 1$, the behavior of $|\frac{\sin(Nx)}{\sin(x)}|^2$ is like a series of delta functions peaked at all points where x equals an integral multiple of π, with a maximum intensity of N^2 and Full-Width-at-Half-Maxima (FWHM) $1/N$ (figure 1.4). That is, given large enough domains such that $N_1 \gg 1$ and $N_2 \gg 1$, the long range cell contribution $|G(\Delta \boldsymbol{s})|^2$ is a collection of delta functions, with a maximum intensity of $N_1^2 N_2^2$, peaked at wherever

$$\Delta \boldsymbol{s} \cdot \boldsymbol{a}_1 = h 2\pi \qquad \Delta \boldsymbol{s} \cdot \boldsymbol{a}_2 = k 2\pi \qquad (h, k \text{ integers}), \tag{1.6}$$

and the width of each peak equals $1/N_1 \times 1/N_2$. Different peaks correspond to different values of h and k, therefore each peak is identified by the indices in the form (hk). The separations between peaks are proportional to 2π times the inverse of unit cell dimensions, i.e. $2\pi/\boldsymbol{a}_1$ and $2\pi/\boldsymbol{a}_2$. Equations in (1.6) are the well known Laue conditions and can be solved for $\Delta \boldsymbol{s}$ in terms of the two vectors,

$$\boldsymbol{a}_1^* = 2\pi \frac{\boldsymbol{a}_2 \times \boldsymbol{n}}{\boldsymbol{a}_1 \cdot (\boldsymbol{a}_2 \times \boldsymbol{n})} \qquad \boldsymbol{a}_2^* = 2\pi \frac{\boldsymbol{n} \times \boldsymbol{a}_1}{\boldsymbol{a}_1 \cdot (\boldsymbol{a}_2 \times \boldsymbol{n})} \tag{1.7}$$

These are called the reciprocal vectors and they satisfy the following relations,

$$\boldsymbol{a}_i^* \cdot \boldsymbol{a}_j = 2\pi \delta_{ij} \qquad i, j = 1, 2. \tag{1.8}$$

Using such reciprocal vectors, the Laue conditions are satisfied if

$$\Delta \boldsymbol{s} = h \boldsymbol{a}_1^* + k \boldsymbol{a}_2^*, \qquad \text{with } (h, k) \text{ integers.} \tag{1.9}$$

In other words, the long range cell contribution $|G(\Delta \boldsymbol{s})|^2$ gives a spike wherever Eq. (1.9) is satisfied. In some cases, one can see all the delta functions in the diffraction pattern and the reciprocal vectors $\boldsymbol{a}_1^*$ and $\boldsymbol{a}_2^*$ can be easily determined. The real space unit cell

dimensions and orientations ($\boldsymbol{a}_1$ and $\boldsymbol{a}_2$) can thus be determined by using Eq. (1.7). The diffraction pattern of the 7×7 reconstruction of Si(111) surface and that of the Pb/Si(111)-$\sqrt{7} \times \sqrt{3}$ are good examples. In other cases, however, not all the delta functions will reveal themselves in the diffraction pattern because the intensity of spots are affected by the inter-atomic separation inside a unit cell through the structure factor squared $|F(\Delta \boldsymbol{s})|^2$. The reason why inter-atomic spacing can affect the spot intensity can be understood by carrying out explicitly the calculation of $|F(\Delta \boldsymbol{s})|^2$,

$$\begin{aligned} |F(\Delta \boldsymbol{s})|^2 &= \sum_{k=1}^{n} e^{-i\Delta \boldsymbol{s}\cdot \boldsymbol{r}_k} \sum_{j=1}^{n} e^{i\Delta \boldsymbol{s}\cdot \boldsymbol{r}_j} \\ &= \sum_{k=1}^{n} e^{-i\Delta \boldsymbol{s}\cdot \boldsymbol{r}_k} e^{i\Delta \boldsymbol{s}\cdot \boldsymbol{r}_k} \sum_{k=1}^{n} \sum_{j=1, j\neq k}^{n} e^{-i\Delta \boldsymbol{s}\cdot \boldsymbol{r}_k} e^{i\Delta \boldsymbol{s}\cdot \boldsymbol{r}_j} \\ &= n + \sum_{k=1}^{n-1} \sum_{j=k+1}^{n} \left(e^{-i\Delta \boldsymbol{s}\cdot(\boldsymbol{r}_k - \boldsymbol{r}_j)} + e^{i\Delta \boldsymbol{s}\cdot(\boldsymbol{r}_k - \boldsymbol{r}_j)} \right) \\ &= n + 2\sum_{k=1}^{n-1} \sum_{j=k+1}^{n} \cos(\Delta \boldsymbol{s}\cdot(\boldsymbol{r}_k - \boldsymbol{r}_j)). \end{aligned} \tag{1.10}$$

Equation (1.10) suggests that it is the relative positions, that is the inter-atomic separations, that determines the spot intensity. Figure 1.5 compares the diffraction pattern of a square lattice and that of a square lattice with one atom almost half way of the unit cell dimension along $\boldsymbol{a}_1$. It is seen in 1-5(d) that every other spot in the direction of $\boldsymbol{a}_1$ are weakened significantly due to the existence of the extra atom. In such cases, the determination of $\boldsymbol{a}_1^*$ and $\boldsymbol{a}_2^*$ is not easy and a simplified model and some kinematical calculations will help understand the diffraction pattern. The diffraction pattern of those ordered phases of Pb/Si(111) with coverage between 6/5 ML and 4/3 ML are such examples (Chapter 4).

Diffraction by a non-flat surface: use of Spot Profile Analysis LEED (SPA-LEED)

When the surface is not flat and has some kind of defect (point defect, steps, terraces, etc.), as in the newly discovered growth mode, the effects on diffraction pattern will be revealed in the changes of the profile of certain spots. Such changes include broadening without changing shape, splitting into multiple spots, or change of shape at different incident beam energies (from a sharp and strong spot to a weaker spot with shoulder or ring around, for example). The effects of different types of non-flat surfaces have on the spot profile had been studied thoroughly by Lent and Cohen [13], Pukite, Lent and Cohen [14] and Zhao, Luo and Henzler [15]. Assuming a two layer system, which is appropriate for Pb/Si(111) since Pb islands have steep edges and flat tops and only the top of islands and the area between islands are exposed to incident electrons (see lower right of figure 1.1), Ref [13, 14, 15] all had shown that, by the Fourier transform of the pair correlation function, the profile of the specular spot is given by

$$I(\Delta s) = [1 - I_1(\theta, \Delta s)]2\pi\delta(\Delta s_{//}) + I_1(\theta, \Delta s_n)C(\Delta s_{//}), \tag{1.11}$$

where θ is the coverage of the top layer, Δs_n is the normal component, $\Delta s_{//}$ the parallel component of the momentum transfer Δs, while $C(\Delta s_{//})$ is the Fourier transform of the pair correlation functions of the atoms on the top layer. In general Eq. (1.11) is a sharp delta function term, resulting from the long range order of the surface scatterers, plus a broad shoulder component that contains all the information on the lateral distribution of the top layer atoms, such as island size and separation. The relative intensities of the sharp and broad components depend on the incident energy through $I_1(\theta, \Delta s_n)$, whose explicit form is

$$I_1(\theta, \Delta s_n) = 2\pi(1 - \theta)[1 - \cos(\Delta s_n h)], \tag{1.12}$$

where h is the height of the top layer measured from the bottom. For a fixed coverage θ, at energies that satisfy the condition $\cos(\Delta s_n h) = 1, I_1(\theta, \Delta s_n)$ vanishes and only the

delta function term survives, so the spot profile will be sharp and strong. These are called the *in-phase* conditions. At other energies that give rise to $\cos(\Delta s_n h) = -1, I_1(\theta, \Delta s_n)$ has its maximum value $4\theta(1-\theta)$, the delta function term will be suppressed and spot profile becomes broad and weak. These are the *out-of-phase* conditions. Note that the function $4\theta(1-\theta)$ has a maximum value of 1 at $\theta = \frac{1}{2}$, therefore the delta function term will not give a negative contribution to the intensity in Eq. (1.11).

Lateral information

The explicit form of $C(\Delta s_{//})$ depends on the terrace length distributions of the two layers. If both layers have regular terrace length, that is, the separation S between islands is constant (see top left of figure 1.6), $C(\Delta s_{//})$ will be periodic and peaked at wherever $\Delta s_{//} S = 2\pi q$ [15], where q is an integer. As a result, new weak spots will appear close to the specular spot, with the position of the first new spot given by $K_1 = \Delta s_{//,1} = 2\pi/S$. The existence of these new spots is easy to understand because having regularly separated islands on top of a surface is identical to having another lattice with bigger unit cell on the substrate lattice, the resultant diffraction pattern is simply the superposition of that of the two lattices. If, however, the island separation has a finite width distribution centered at S, one would expect to see the same result but with broader new spots. Therefore, by measuring the position of the satellite spot around (00) spot at an out-of-phase condition, one can determine the average island separation S by

$$\frac{K_1}{K_{10}} = \frac{a_0}{S}, \tag{1.13}$$

where K_1 is the position of the satellite spot, a_0 the substrate lattice constant, $K_{10} = 2\pi/a_0$ is the distance between (00) and (10) spot. The bottom of figure 1.6 shows how to measure such a quantity.

The average size L of the islands can be measured from the FWHM (Full Width at

Half Maximal) of the superstructure spots, if there is any present, by [16]

$$\frac{\sigma_0}{K_{10}} = \frac{a_0}{L}, \tag{1.14}$$

where σ_0 is the FWHM of the superstructure spot. The top right of figure 1.6 shows how to do such measurement. If no superstructure spots are available, one can still obtain the average size, once the average separation S is known, from the FWHM of the broad component around (00) spot by

$$\frac{\sigma_1}{K_{10}} = a_0 \left(\frac{1}{S} + \frac{1}{L} \right), \tag{1.15}$$

where σ_1 is the FWHM of the broad shoulder of (00) spot. See lower right of figure 1.6 for example. This result was derived in Ref [13, 14] using geometric distribution with different average terrace lengths on the top (L_1) and the bottom (L_2) layers. That is, the probabilities of finding a terrace with length L on layer i is given by $P_i(x) = (1/L_i)\exp(-x/L_i)$, $i = 1, 2$. Using such distributions Eq. (1.11) becomes

$$I(\Delta s) = [1 - I_1(\theta, \Delta s_n)]2\pi\delta(\Delta s_{//}) + I_1(\theta, \Delta s_n)(\frac{1}{L_1} + \frac{1}{L_2})/[\Delta s_{//}^2 + (\frac{1}{L_1} + \frac{1}{L_2})^2]. \tag{1.16}$$

The broad shoulder component is a Lorentzian function with a half width equals the inverse sum of average terrace size of the two layers.

Vertical information

The height of islands nd, where d is the single step height while n is an integer, can be determined by measuring the $g(s)$ curve. A $g(s)$ curve is the relative intensity of the central spike to the whole (00) spot at different incident beam energies, defined by

$$g(s) = [1 - I_1(\theta, \Delta s_n)]2\pi\delta(\Delta s_{//})/I(\Delta s), \tag{1.17}$$

where s is the magnitude of the incident beam momentum. Such a curve can determine the island height nd because as the incident beam energy varies, the corresponding

wavelength λ changes, and so does the phase difference between the waves scattered off the island top and that off the bottom layer between islands. If this phase difference $\Delta\phi = 2\pi(2nd/\lambda)$ is an even-integral multiple of π, that is, the in-phase condition $\cos(\Delta s_n nd) = 1$, the profile of (00) spot will be the same as if the surface were flat, i.e., it will be a sharp and strong spot (see top of figure 1.7). On the other hand, if this phase difference is an odd-integral multiple of π, the out-of-phase condition $\cos(\Delta s_n nd) = -1$, the scattered waves from the top of island and that from the bottom layer between islands will cancel each other and give no contribution to the intensity of the (00) spot. In either case, the broad component around (00) spot caused by the existence of islands will still be present. Therefore the profile of (00) spot at out-of-phase conditions will look as shown in the bottom of figure 1.7. If the surface has only steps with single atomic height d, and the energy range in a $g(s)$ curve covers two in-phase conditions for a single step, it shall look like a cosine curve with only one oscillation, as shown in figure 1.8(a). If the surface has steps of multiple atomic heights, then within the same energy range, the $g(s)$ curve shall reveal multiple oscillations. The number of oscillations in a $g(s)$ is the height of the steps counted in single step height, which is n for islands of height nd. Figure 1.8(b) shows that islands of 7-layer height give 7 oscillations in the corresponding $g(s)$ curve. Experimentally, the (00) spot profiles taken at different energies are fitted with a Gaussian function for the central spike and two Lorentzian-3/2 functions for the broad component. The integrated intensities of the central spike and the broad component are denoted by A_0 and A_1, respectively, with A_0 corresponds to the first term while A_1 to the second in Eq. (1.16). The $g(s)$ curve defined by Eq. (1.17) is then written as

$$g(s) = \frac{A_0}{A_0 + A_1}.$$

The bottom of figure 1.7 shows such a definition.

Summary

This chapter introduces a novel growth mode discovered on Pb/Si(111) system: islands with 7-layer high, steep edges and flat tops can grow by deposition below room temperature. Quantum size effects (QSE) can explain such a growth mode. For comparison, the three commonly referred growth modes were briefly discussed. A summary of the basics of diffraction and a simple discussion on the spot profile were given. Methods of experimentally measuring average island size, separation, and island height were provided. The advantage of using SPA-LEED in determining those properties is that no complicated calculations are needed. Usually direct observations of the spot profiles can give qualitative conclusions about the defects present on the surface. For example, if the average separation of islands becomes larger by annealing to a higher temperature, the position of the satellite spot will be shifted closer to the specular spot (larger distance in real space, smaller distance in the reciprocal). In the following chapters we will provide experimental results and discussions on the following questions:

- Will the results change if grown on a different type of Si(111) surface such as Pb/Si(111)-$\sqrt{3} \times \sqrt{3}$-β? (Chapter 2).
- What is the critical size of nucleation for such kind of islands? (Chapter 3).
- What phase or phases does it form on Pb/Si(111) when the coverage is between 6/5 ML and 4/3 ML? (Chapters 4).

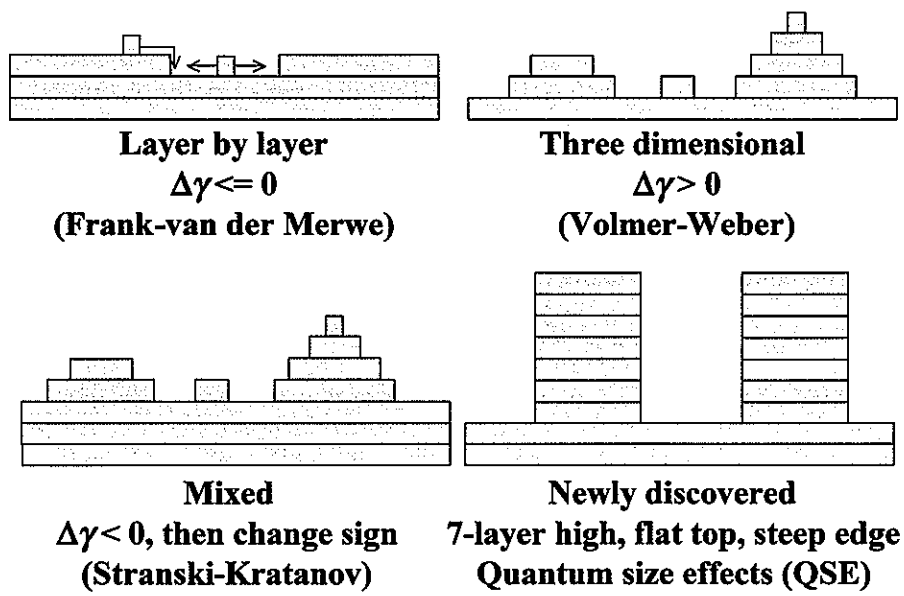

Figure 1.1 Different modes of thin film growth, including the three commonly referred modes: FM, VW, and SK modes, and the newly discovered islands with 7-layer height, flat tops and steep edges.

Table 1.1 A list of possible stable heights for Pb(111) crystal determined by Eq. (1.1). The single step height is $d = 0.286$ nm, while the Fermi wavelength of confined electrons is $\lambda_F = 0.395$ nm. The islands can be stable only when both n and s are integers. It is seen that $n = 5, 7, 9, 11$, corresponding to $s = 7.2, 10.1, 13.0, 15.9$, are the stable heights.

n	3	4	5	6	7	8	9	10	11
$s = 2nd/\lambda_F$	4.3	5.8	**7.2**	8.7	**10.1**	11.6	**13.0**	14.5	**15.9**

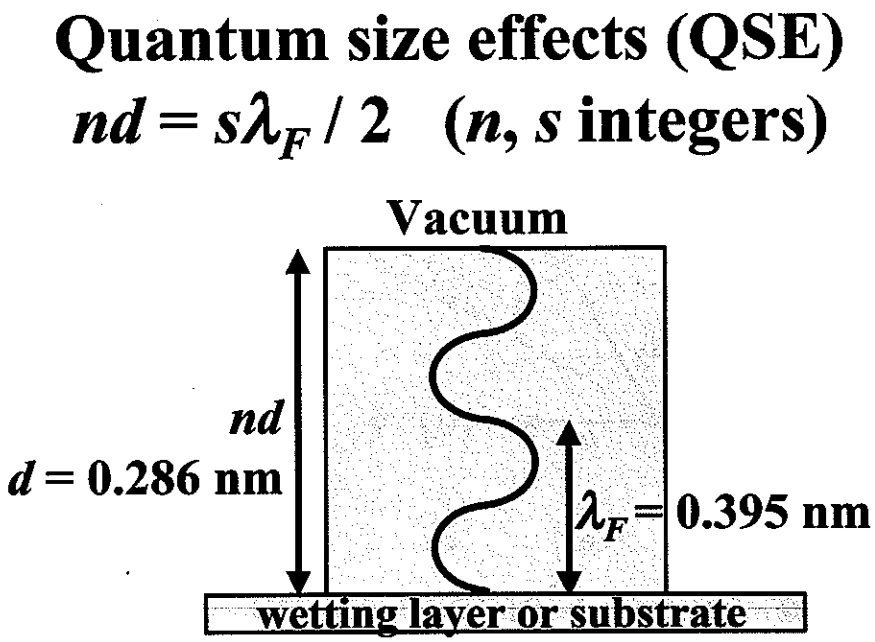

Figure 1.2 Schematic of quantum size effects (QSE): the dimensions of confining well have to satisfy the requirement of energy quantization that the electron wavefunctions have to form standing waves. These effects cause the island height to be stable only when the requirement is met.

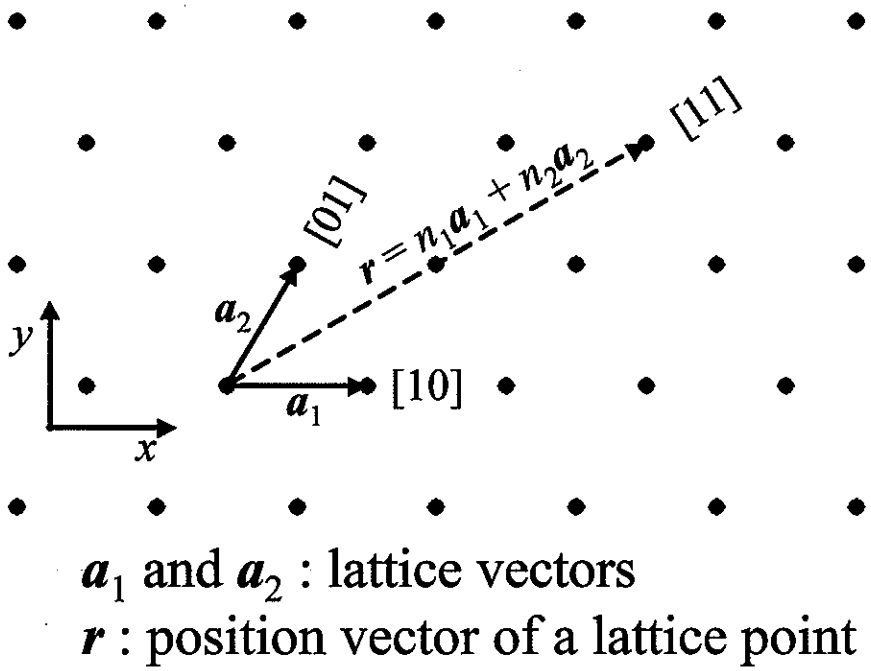

Figure 1.3 A two-dimensional lattice and a choice of lattice vectors $\boldsymbol{a}_1$ and $\boldsymbol{a}_2$ that can specify all the lattice points for such a lattice. Direction of a vector is specified by its components enclosed by a pair of square brackets. For example, [10] means the direction along $\boldsymbol{a}_1$, [11] means that along $\boldsymbol{a}_1 + \boldsymbol{a}_2$.

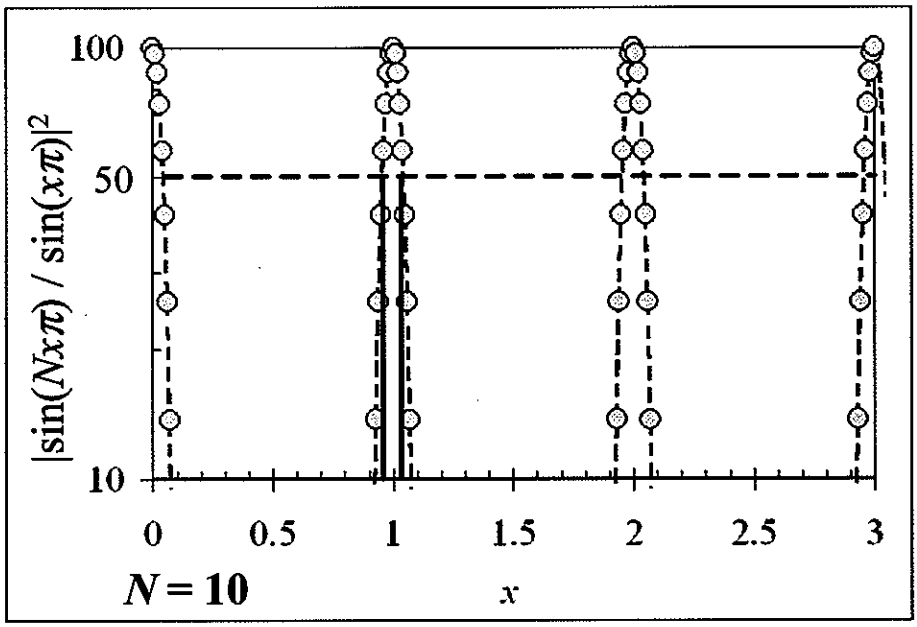

Figure 1.4 Plot of $|\frac{\sin(Nx)}{\sin(x)}|^2$ from $x = 0$ to $x = 3$ using $N = 10$. In this case, this function has a maximum intensity of $100 = 10^2$ whenever x is an integer, with the FWHM of each peak equals $0.1 = 1/10$. In general, this function is periodic with a period of π and maximum intensity of N^2, with FWHM of each peak equals $1/N$.

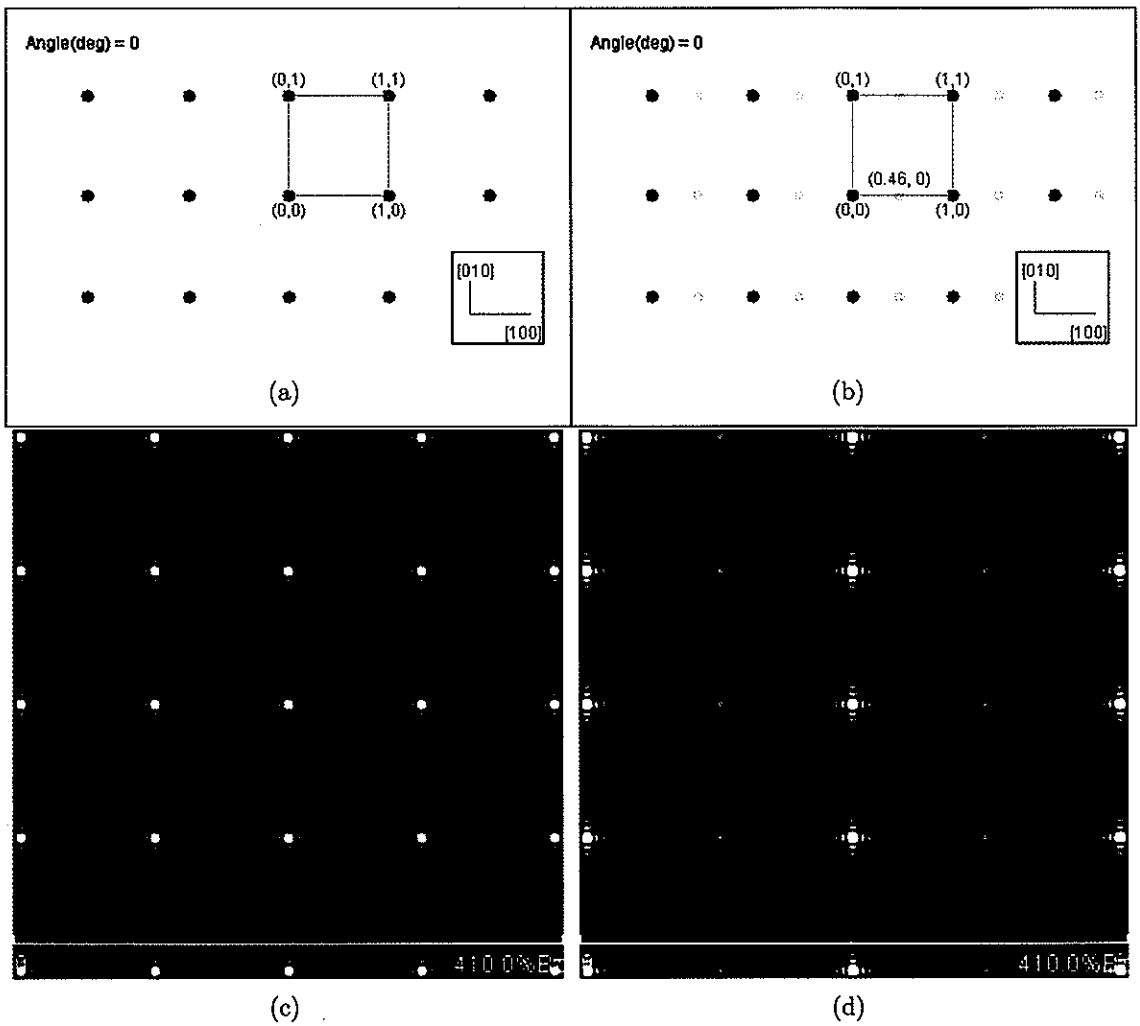

Figure 1.5 Calculated diffraction pattern showing how the inter-atomic spacing within a unit cell can affect the intensity of some diffraction spots. (a) A regular square lattice with $\boldsymbol{a}_1 = (1, 0)$ and $\boldsymbol{a}_2 = (0, 1)$. (b) Square lattice with an additional atom inside the unit cell at (0.46, 0), almost half way along $\boldsymbol{a}_1$. (c) Diffraction pattern of (a). (d) Diffraction pattern of (b). Note that in (d) every other spot along [100] is weakened considerably due to the existence of the extra atom in (b).

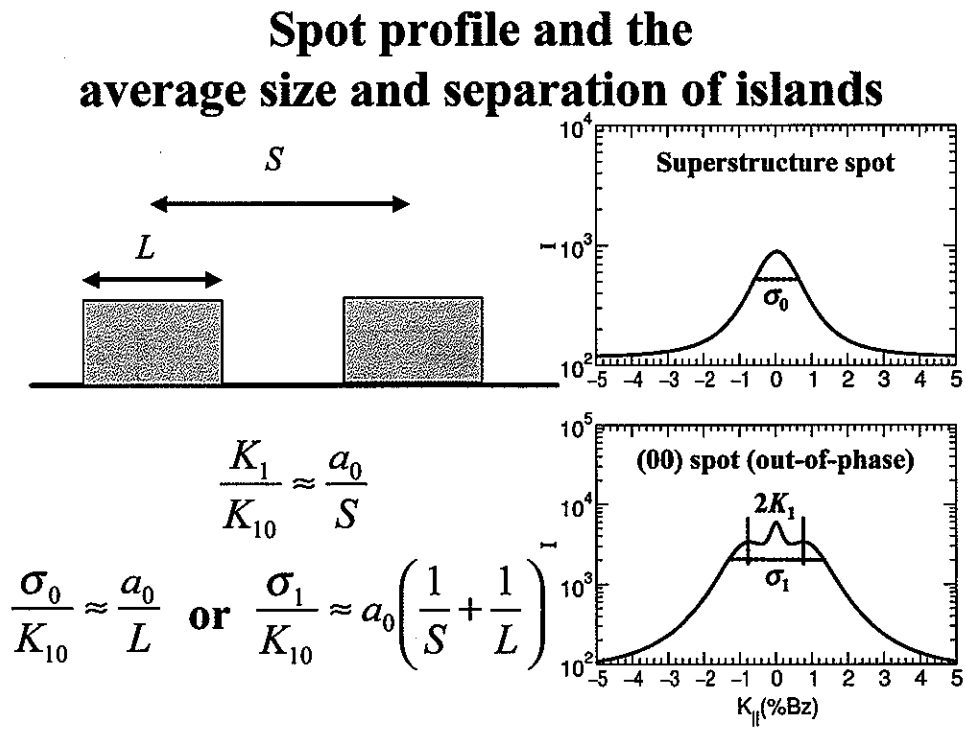

Figure 1.6 Measurement of average separation S and size L of terraces from spot profiles. Average separation S can be measured from the position of local maxima of the shoulder/ring around (00) spot. Average size L can be determined from the FWHM of the superstructure spot, if present, or the FWHM of the shoulder/ring around (00) once the separation S is known.

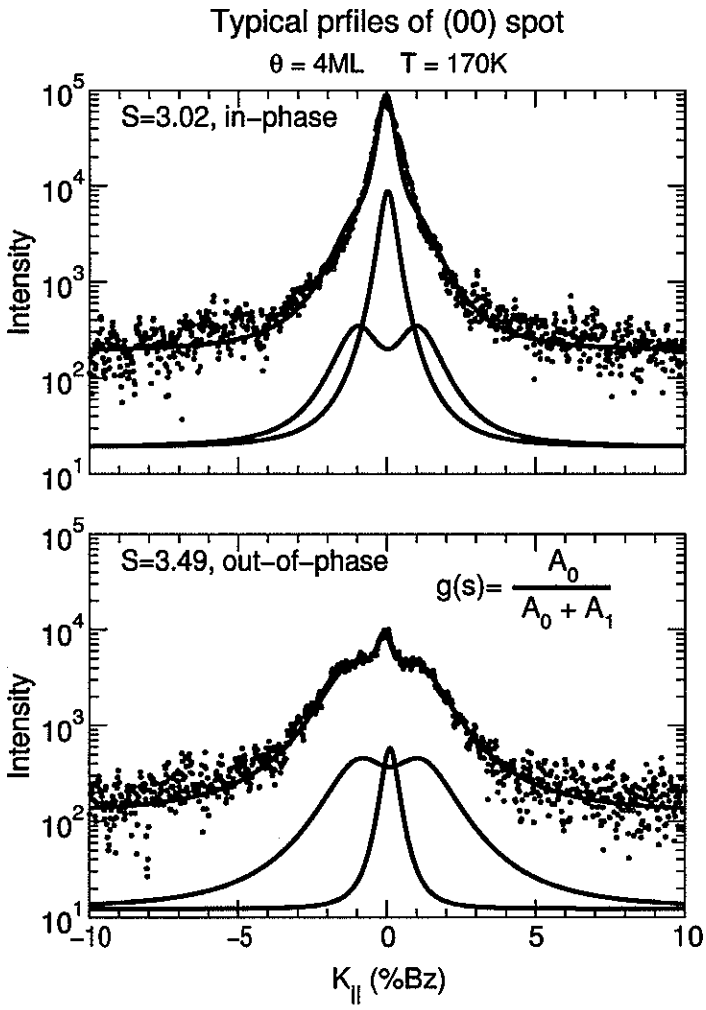

Figure 1.7 Typical profile of (00) spot at in-phase (top) condition and out-of-phase (bottom) condition, taken on a surface after a total of 4 ML Pb deposition at a temperature $T = 170$ K. Profiles were fitted with Gaussian function for the central spike and Lorentzian-3/2 function for the broad component. Fitted components were shown separately below the profile. The bottom half also shows that a $g(s)$ is obtained by taking the ratio of the integrated intensity of the central spike to the total intensity of the spot.

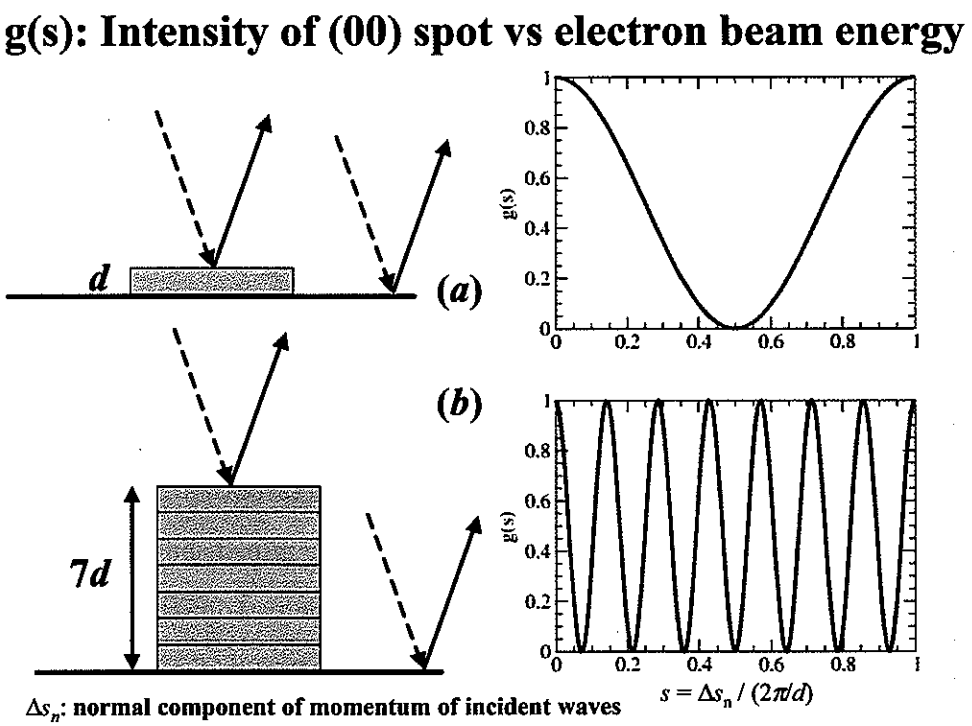

Figure 1.8 Measurement of step height by means of $g(s)$ curve. Within an energy range covering two in-phase conditions for single atomic height, the number of oscillations in a $g(s)$ curve shall correspond to the step height counted in atomic height. (a) Single step islands, one oscillation in $g(s)$. (b) 7-step islands, 7 oscillations in $g(s)$.

CHAPTER 2. The role of the metal/semiconductor interface in quantum size effects: Pb/Si(111)

A paper published in Physical Review Letter 85, 5158 (2000)

V. Yeh[1], L.Berbil-Bautista[2], C. Z. Wang[3], K. M. Ho[4] and M. C. Tringides[5]

Abstract

Self-organized islands of uniform heights can form at low temperatures on metal/semiconductor systems as a result of quantum size effects (QSE), i.e., the occupation of discrete electron energy levels in the film. We have examined the role of the metal/semiconductor interfaces by comparing the growth mode on two different substrates (Si(111)-(7×7) vs Si(111)-Pb($\sqrt{3} \times \sqrt{3}$)) measured with Spot Profile Analysis (SPA-LEED). For the same growth conditions (of coverage and temperature) 7-step islands are the most stable islands on the (7×7) phase while 5-step (but larger islands) are the most stable islands on the ($\sqrt{3} \times \sqrt{3}$). A theoretical calculation suggests that the height selection on the two interfaces can be attributed to differences in their electronic structure and the amount of charge transfer at the interface.

[1]Graduate student and primary researcher and author.
[2]Collaborating senior undergraduate student.
[3]Collaborating theoretical scientist.
[4]Collaborating theoretical researcher and committee member.
[5]Major professor and corresponding author.

Introduction

The search for methods to produce highly organized atomic scale structure during epitaxy is an intensively active research area since it holds the promise for novel technological applications. It is important to develop highly regular structures and there preferred sizes to be selected in a controlled way. Recently it was found unexpectedly that uniform height islands, with steep edges and flat tops, could be grown on several systems [17, 18, 19, 20, 1]. This was surprising since single steps are commonly observed during growth, separating the exposed island levels. In some systems the structures form, after annealing to room temperature, an amount which is initially deposited at lower temperatures [17, 18, 19, 20]; in Pb/Si(111)-(7×7) regular height islands form in situ during low temperature deposition T = 120-240K [1]. In this system depending on the growth conditions selected (i.e. coverage, temperature, kinetic pathway, etc) islands of uniform heights 5-, 7-, 9- steps can reproducibly form.

Although the kinetics controlling this unusual growth mode are not fully understood (i.e. how the deposited atoms have such high mobility to build the islands) the driving force of the self-organization is believed to be related to quantum size effects (QSE) i.e. the quantization of the energy of the electrons confined in the film at discrete levels. The minimization of the energy of the confined electrons favours a preferred thickness [21, 22, 23, 24, 25]. This is usually expressed in terms of the boundary conditions that the wavefunction should satisfy $nd = s\lambda_F/2$, where λ_F is the Fermi wavelength and d is the single step height of the grown crystal with n, s integer numbers. For the Pb(111) $\lambda_F = 0.366$ nm, $d = 0.286$ nm and since approximately $d = 3/4\lambda_F$ this leads to preferred island heights differing by $2d$.

Originally evidence of the presence of QSE during epitaxial growth was based on the observation of bilayer diffraction intensity oscillations Cu(111) [26], oscillations in the film conductivity during the growth of Pb/Si(111) [27], changes in the step height

as a function of film thickness in the growth of Pb/Ge(100) [28], imaging a buried interface of a Pb wedge grown epitaxially on stepped Si(111) [29] and the unusual island morphology (i.e. flat shape and uniform heights) described earlier [17, 18, 19, 20, 1]. A preliminary theoretical treatment [30] of the dependence of the electron energy on the film thickness takes into account two contributions: the increase of the confined electrons energy at small film thickness and the energy gain due to charge transfer at the metal-semiconductor interface as a result of differences in the Fermi level positions across the interface. The film energy vs thickness curve can have, in principle, several energy minima. The depth of the energy minima and the height at the saddle point depend on the relative contribution of the two components to the film energy.

For Pb/Si(111) several energy minima are expected because of the relation between and d mentioned above. More insight into the role of QSE can be obtained if the growth is studied on different metal/semiconductor interfaces. Different Pb-Si interfaces [(Si(111)-(7×7) vs Si(111)-Pb($\sqrt{3}\times\sqrt{3}$)] are well characterized from other experiments [31, 32] so both the atoms position and the electronic structure at these two interfaces are known independently.

Experiments and results

Our experiments are carried out with Spot Profile Analysis (SPA-LEED) [16]. The technique uses the distribution of diffracted intensity $I(k_{//}, k_z)$, the parallel and normal components of the momentum transfer to deduce the vertical and lateral distribution of atoms in the film. A measurement of the spot profile at fixed can be decomposed into two components, a narrow component that measures the long-range arrangement of atoms on lattice sites and a broad component which measures the average island size and separation. The step height is deduced from oscillations of the distribution of the intensity between the two diffraction components as a function of k_z.

Since different types of the $\sqrt{3} \times \sqrt{3}$ phase can be realized on the surface depending on the Pb coverage and the annealing process [31], it is important to describe the method of preparation of the $\sqrt{3} \times \sqrt{3}$ phase. Initially an amount 4ML Pb was deposited at 130K and the surface was heated to higher temperature. We first observe the reversible formation of the high coverage, so-called $\sqrt{3} \times \sqrt{3}$-α phase (with ideal coverage θ = 4/3ML) at T = 470K followed by partial desorption of Pb until the strongly bound $\sqrt{3} \times \sqrt{3}$-β phase remains (with ideal coverage θ = 1/3ML). Most of the growth experiments were carried out with Pb deposited on the $\sqrt{3} \times \sqrt{3}$-β but limited experiments were also carried out on the $\sqrt{3} \times \sqrt{3}$-α phase.

Since the main goal of this study is the comparison of the growth on the two different interfaces, we present results for the same growth parameters of θ = 4ML and T = 195K. Fig.1 shows σ_0 vs $k_z/(2\pi/d)$ where d = 2.86 Å is the single step height of Pb(111) and σ_0 the constant in the denominator of the Lorentzian-3/2 fits). The bottom figure is for the (7×7) and the top figure for the $\sqrt{3} \times \sqrt{3}$ interface. (σ_0 is smaller by a constant factor, approximately 1.5, than the Full-Width-Half-Maximum (FWHM)).

For growth on the (7×7) interface we see strong 7-step oscillations indicating that predominantly 7-step islands form as found earlier [1] and as confirmed with low temperature STM [33]; for the growth on the $\sqrt{3} \times \sqrt{3}$ phase we see a 5-step oscillation, which indicates that mainly 5-step islands form. The islands have steep edges as can be seen directly in the STM images or can be deduced with diffraction, by comparing the profiles at the different out-of-phase conditions of the multi-step periodicity. This result is intrinsic to the difference in the two interface structures, and not a result of the selected growth conditions. As found earlier for T = 195K on the (7×7) and for any Pb coverage (larger than 2ML needed to form the wetting layer) we always observe 7 step islands. 5-step islands are observed during growth on the (7×7) at lower temperature T¡165K and for smaller Pb amounts (θ < 5ML); but after annealing to the higher temperature T = 195K the 5-step islands transform to 7-step islands. This indicates that 7-step

islands are the most stable islands on the (7×7). On the other hand for the growth on the $\sqrt{3} \times \sqrt{3}$ phase and for coverage $\theta < 5.5$ML we first see 5-step oscillations, after an amount, of approximately 1ML, converts the $\sqrt{3} \times \sqrt{3}$-β to $\sqrt{3} \times \sqrt{3}$-α. The 5-step islands are stable and despite prolonged annealing at temperature as high as 240K they maintain their height although the height distribution broadens and the island edges are less steep as the islands coarsen.

Fig. 2 compares typical profiles of the (00) spot at in-phase and out-of-phase conditions for growth on the two different substrates. As can be seen from the comparison of the out-of-phase conditions (i.e. maxima in fig. 1), the profiles are sharper on the $\sqrt{3} \times \sqrt{3}$ than on the (7×7) .This directly indicates that larger islands are grown on the $\sqrt{3} \times \sqrt{3}$ than on the (7×7). The profiles at the out-of-phase conditions for growth on the $\sqrt{3} \times \sqrt{3}$ phase are sharper than the profiles on the (7×7) indicating that larger islands are grown on the $\sqrt{3} \times \sqrt{3}$ than on the (7×7). This difference in the island sizes is also supported from the comparison of the FWHMs of the Pb(10) spots on the two phases. The FWHM of the Pb(10) on the $\sqrt{3} \times \sqrt{3}$ is narrower by a factor of 2 from the FWHM of the Pb(10) spot on the (7×7). By using the FWHM of the Pb(10) which measures the average island size L, the position of the satellite spots of the (00) (when visible) which measures the island separation S and the width of the (00) spot which measures the geometric average of L and S, we deduce that $L = 180$ Å, $S = 700$ Å for the growth on the $\sqrt{3} \times \sqrt{3}$ and $L = 90$ Å, $S = 310$ Å for the growth on the (7×7) phase. This difference in the size indicates that either the kinetic barriers are lower or the energy minima are deeper for the growth on the $\sqrt{3} \times \sqrt{3}$ than the corresponding barriers for the growth on the (7×7).

Fig. 3 shows results of the growth on the $\sqrt{3} \times \sqrt{3}$ phase if larger Pb amounts $\theta > 5.5$ML are deposited at T = 195K. We observe islands with heights larger than 5 steps, by bilayer increments i.e. 7-, 9-, 11-steps depending on the coverage. For example for $\theta = 7.5$ML we observe 7-step islands with comparable island lateral sizes as observed

at lower coverage. If the film is annealed to higher temperature T = 210K, weak 9-step oscillations are observed with a decreased oscillation amplitude and a larger average σ_0 value. The amplitude of the oscillations measures the sharpness of the island height distribution (i.e. what fraction of the islands has the most probable height and/or the island steepness) and the average value of σ_0 measures the average island size. From the results in fig. 3 we deduce that as the islands grow the height distribution broadens and the islands become less steep. During the annealing process the Si(10) spot increases while the Pb(10) spot decreases in intensity indicating the transfer of Pb atoms already in the islands to higher levels However for smaller coverage $\theta < 5.5$ML we see 5-step islands that maintain their height despite annealing to higher temperatures, which shows that for lower coverage the 5-step islands are the most stable islands on the $\sqrt{3} \times \sqrt{3}$.

We only observe 7-step islands after Pb deposition (for the range in coverage after the formation of the wetting layer and before the film closes). The annealing results on the (7×7) are similar to the annealing results on the $\sqrt{3} \times \sqrt{3}$: if 7-step islands form at T = 195K, for smaller Pb amounts ($\theta < 5$ML), they remain 7-step high; otherwise for larger deposited amounts they grow, after annealing, to islands with the next bilayer increment i.e.9-step islands. Since no higher than 7-step islands are observed on the (7×7) directly after deposition, this indicates that a larger kinetic barrier exists, for Pb atoms to move to higher levels, on the (7×7) than on the $\sqrt{3} \times \sqrt{3}$ phase, which is consistent with the earlier observation that the island sizes are smaller for growth on the (7×7) than on the $\sqrt{3} \times \sqrt{3}$. In addition since the growth of the islands to heights larger than the stable ones, after annealing, requires a minimum coverage on the surface (approximately 5ML) and, since as seen in fig.3 this is carried out by atoms already in the islands, it suggests that the lateral size for the islands cannot be reduced below a minimum size.

It is worth mentioning a puzzling and unexpected feature for the growth on top of the $\sqrt{3} \times \sqrt{3}$ phase so the comparison of the differences of the growth on top of the two

interfaces is complete. If large amounts of Pb are deposited on top of the $\sqrt{3} \times \sqrt{3}$ phase at the same temperature T = 195K we observe (without annealing) larger height islands (we can easily resolve islands up to 11 step height otherwise the oscillations become too close in energy). However, the film does not close and the islands are still separated since the $\sqrt{3} \times \sqrt{3}$ phase is still visible.

We discuss now a possible explanation for the main result of this work; i.e. that the selected height depends on the type of interface present on the surface. Although this is physically expected it has not been observed experimentally before. Both interfaces have been extensively studied with angle-resolved photoemission experiments to probe the electronic structure and with in-situ conductivity measurements to determine the number and origin of the charge carriers on the interface [31, 32]. From the photoemmission spectra on the different interfaces one can deduce changes in the position of the Fermi level by measuring its energy shift from well-known bulk emission features used as a reference. It is found that the Fermi level is lower on the $\sqrt{3} \times \sqrt{3}$ than on the (7×7) both at low coverage θ = 1ML (0.08eV vs 0.18 above the valence band respectively [31]) and at multilayer Pb amounts deposited on the $\sqrt{3} \times \sqrt{3}$ vs (7×7) (0.19eV vs 0.42eV above the valence band respectively [32]). Under the assumption [30] that the charge transfer energy depends on the difference in the Fermi level positions between the metal and the substrate, the energy gain on the $\sqrt{3} \times \sqrt{3}$ phase will be larger than the energy gain on the (7×7) phase. A more accurate analysis of the energy gain due to charge transfer should take into account the number of carriers transferred between the two films and the substrate. In-situ conductivity measurements on the $\sqrt{3} \times \sqrt{3}$ phase (at 1.3ML) have shown that the number of charge carriers on the $\sqrt{3} \times \sqrt{3}$ is larger than what is expected from simply the space charge layer because of additional carrier contribution from a metallic surface state close to the Fermi level [31].

The total film energy vs thickness curve on the $\sqrt{3} \times \sqrt{3}$ interface should lie lower from the total energy of the film vs thickness curve on the (7×7), moved downward

by the larger charge transfer term. This will tend to lower all the kinetic barriers on the $\sqrt{3} \times \sqrt{3}$ and can explain why the island sizes on the $\sqrt{3} \times \sqrt{3}$ are larger (both the lateral size of the islands and the island height during deposition for high θ). In addition, since the gain due to charge transfer decreases with thickness, a larger contribution is expected at the 5-step than at the 7-step height, so the energy minimum will be affected more at 5- than 7-step height.

Based on the analysis of ref [30], the energy of the system can be expressed as $E = E_0 - E_c$ where E_0 is the energy of the Pb film (after subtracting the bulk energy) and E_c is an energy gain due to the charge transfer. E_0 is estimated by a model of free electron gas confined by an infinite hard wall at the Pb/Si(111) interface and a barrier step at the Pb/vacuum interface. The barrier step is equal to the sum of the Fermi energy (9.45 eV) of bulk Pb measured from the bottom of the conduction band and the work function (4.25 eV) of Pb. $E_c = C(\Delta E_F)^2$ where ΔE_F is the initial difference between the Fermi energies of the film and the substrate. Using the experimentally determined values of the Fermi level for the two different interfaces (4.75eV for the (7×7) and 4.98 eV for the $\sqrt{3} \times \sqrt{3}$ below the vacuum level) [32] and the calculated Fermi level position for the potential well of thickness L described above, the dependence of $E(L)$ on L is determined for the two interfaces. The results are shown in fig. 4. C is a phenomenological parameter, which is related to carrier changes and the strength of the chemical bonding, across the interface. We have chosen the value $C = 0.033\text{eV/Å}^2$ in the calculation, which is consistent with the measured work function change $\Delta\phi = 0.25$eV after Pb adsorption on Si(111)-(7×7) [32]. With this choice of C the energy minimum for the $\sqrt{3}\times\sqrt{3}$ phase is at $L = 5$ and for the (7×7) is at the next energy minimum (the next calculated minimum is at $L = 8$ instead of $L = 7$). The energy shift downward (17meV $\sim$ 170K) of the $\sqrt{3} \times \sqrt{3}$ curve below the (7×7) curve is comparable to the expected kinetic barrier decrease at the temperature range (T$\sim$190K) of the experiments, that produces islands on the $\sqrt{3} \times \sqrt{3}$ phase twice as big as the ones on the (7×7). Although

the model can capture the essential physics of the role of QSE in film growth, it is clearly an oversimplified approach. More realistic calculations based on ab initio methods are needed to fully understand the island structures with the lowest energy and the kinetic barriers in the system.

In summary we have studied how the self-organized growth mode of uniform height islands observed on Pb/Si(111) at low temperatures depends on the different type of interface structure of the substrate. 7-step island are the most stable islands for growth on top of the (7×7) while 5-step islands are the most stable islands for growth on top of the $\sqrt{3} \times \sqrt{3}$ phase. This difference apparently is related to the larger charge transfer on the $\sqrt{3} \times \sqrt{3}$ than on the (7×7) interface, in good agreement with the results of a theoretical model, based on the difference in the Fermi levels across the interface. The practical significance of these experiments is that they demonstrate that it is possible to select in another way ,(i.e. by varying the starting phase of the substrate), the preferred island height and to control the type of nanostructures formed in epitaxy.

Acknowledgment

Ames Laboratory is operated by the U.S. Department of Energy by Iowa State University under Contract NO. W-7405-Eng-82. This work was supported by the Director for Energy Research Office of Basic Energy Sciences.

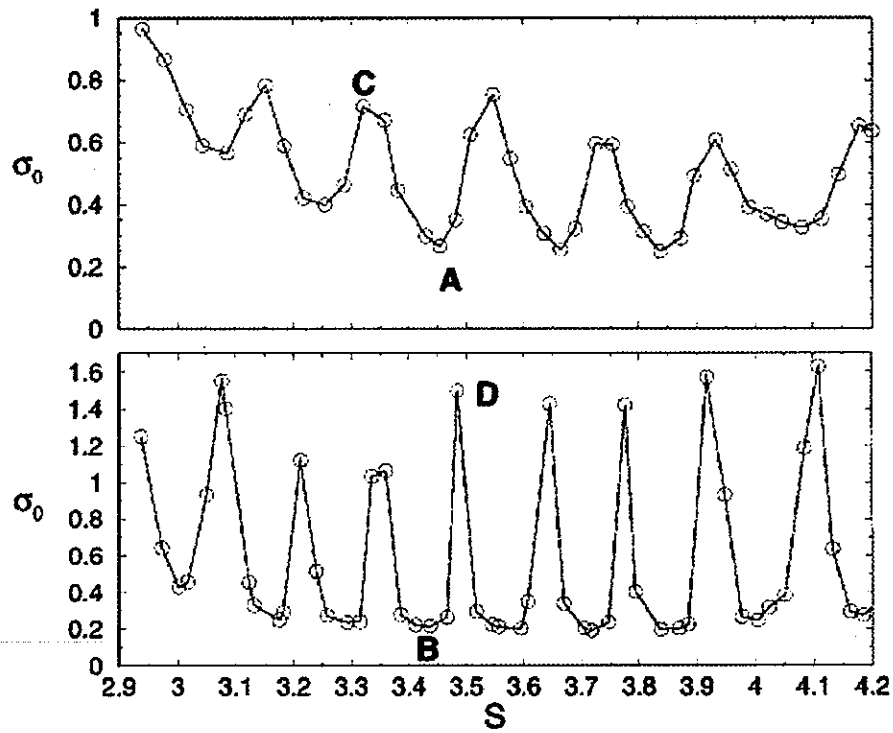

Figure 2.1 Plots of σ_0 vs k_z for growth of 4ML at T = 195K on the $\sqrt{3}\times\sqrt{3}$ phase (top) showing 5-fold oscillations and on the (7×7) phase (bottom) showing 7-fold oscillations. The out-of-phase values of σ_0 for the $\sqrt{3}\times\sqrt{3}$ are smaller than the corresponding values on the (7×7) indicating that larger islands are grown on the $\sqrt{3}\times\sqrt{3}$ phase.

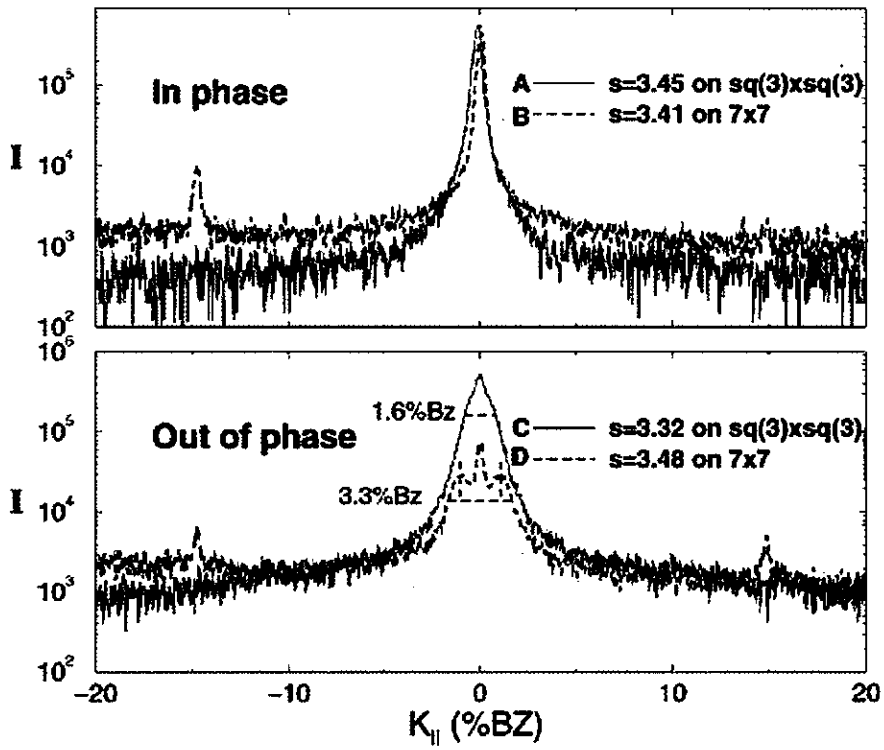

Figure 2.2 Typical profiles for the in-phase (top) and out-of-phase (bottom) for the two interfaces showing sharper profiles (and larger islands) are present on the $\sqrt{3} \times \sqrt{3}$ phase.

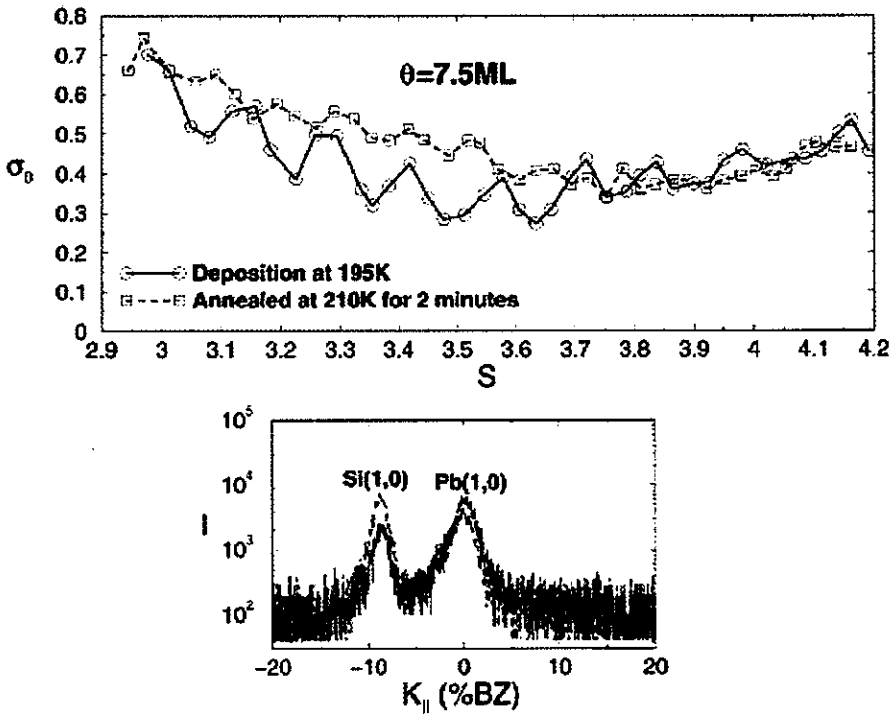

Figure 2.3 For T = 190K and larger Pb deposited amounts on the $\sqrt{3} \times \sqrt{3}$ ($\theta = 7.5$ML) 7-step islands are observed. When the islands are annealed to a higher temperature T = 210K 9-step islands are observed. The transfer of atoms to higher levels can be seen also from the decrease of the Pb(10) spot and the corresponding increase of the Si(10) spot intensity.

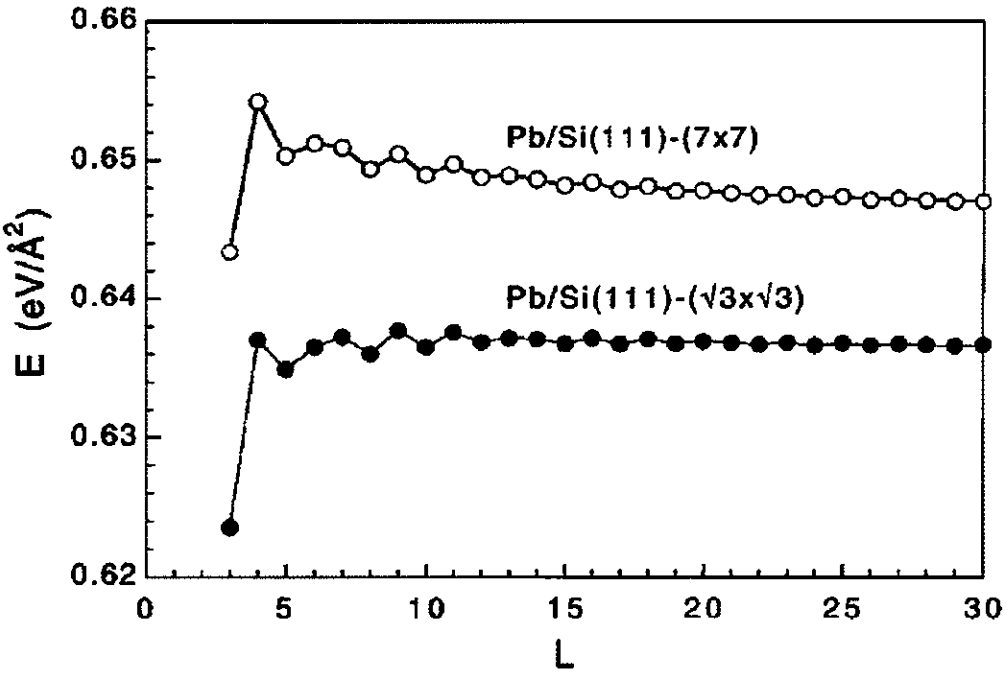

Figure 2.4 Calculated film energy vs film thickness L for the two interfaces showing that the energy curve for the $\sqrt{3} \times \sqrt{3}$ phase lies lower and has a lower minimum at $L = 5$ than the next minimum $L = 8$; for the (7×7) curve the order of the minima is inverted.

CHAPTER 3. Measurement of island density of Pb grown on Si(111)-7×7 with SPA-LEED and tests of the scaling theory of nucleation

Abstract

The number density of 7-step Pb islands grown on Si(111)-7×7 between 185 K and 225 K had been measured with SPA-LEED. Both temperature and deposition rate (0.001 ML/s to 0.01 ML/s) dependence experiments were carried out in attempt to determine the critical cluster size and migration barrier. The rate dependence results show no dependence of saturation island number density on the deposition rate, suggesting a limited applicability of the nucleation theory on this system, therefore a firm conclusion of the critical size cannot be drawn. A theory considering "non-traditional" nucleation behavior has to be developed. However, limited conclusion could still be drawn from the temperature dependence results. For example, our results suggest that the smallest possible stable cluster for Pb/Si(111)-7×7 is a tetramer, i.e., $i \geq 3$. A different STM study showed either $i = 3$ or $i = 4$ based on the shape of the scaling function of island size distribution for different coverage (0.8ML and 1.6ML above wetting layer) deposited at $T = 208$ K, which is consistent with our conclusion.

Introduction

The nucleation theory states that, for *2-D islands* and *complete saturation*, the number density of islands is given by [34]

$$n_x = \eta(\theta, i)\left(\frac{D}{F}\right)^{-\chi}\exp\left(\frac{E_i}{(i+2)kT}\right), \quad \chi = \frac{i}{(i+2)} \tag{3.1}$$

where D denotes the diffusion coefficient, F the deposition rate, i the critical cluster size, E_i its binding energy ($E_1 = 0$), η the dimensionless nucleation density [35]. The critical cluster is the maximum unstable cluster, if one more atom joined in, it would become stable. The critical cluster size i is the number of atoms in the cluster. Therefore, if the critical size $i = 1$ for a specific system, dimers are stable for that system. In the limiting cases, namely $i = 1$ and $i = \infty$, n_x is proportional to $\left(\frac{D}{F}\right)^{-1/3}$ and $\left(\frac{D}{F}\right)^{-1}$, respectively. The diffusion coefficient can be further expressed as $D = \frac{\nu_0}{2d}\exp\left(\frac{-E_m}{kT}\right)$, where ν_0 is the attempt frequency, d the dimensionality of diffusion, and E_m the migration barrier. The binding energy of the critical cluster E_i can be expressed as $E_i = i\overline{E}_i$, where $\overline{E}_i$ is the average binding energy per atom in the critical cluster of size i. Using these expressions of the diffusion coefficient D and the binding energy E_i, the saturation island number density becomes,

$$\begin{aligned} n_x &= \eta(\theta, i)\left(\frac{\nu_0}{4F}\right)^{-\chi}\exp\left(\frac{\chi E_m}{kT}\right)\exp\left(\frac{i\overline{E}_i}{(i+2)kT}\right) \\ &= \eta(\theta, i)\left(\frac{\nu_0}{4F}\right)^{-\chi}\exp\left(\frac{\chi E_m}{kT}\right)\exp\left(\frac{\chi\overline{E}_i}{kT}\right) \end{aligned} \tag{3.2}$$

Taking logarithm on Eq. (3.2) we have

$$\ln(n_x) = \ln\eta - \chi\ln\left(\frac{\nu_0}{4F}\right) + \frac{\chi}{kT}(E_m + \overline{E}_i). \tag{3.3}$$

In Eq. (3.3), the parameters that can be controlled experimentally are the deposition rate F and deposition temperature T. Therefore, one tests the applicability of this theory by fixing one and vary the other. The rate dependence experiments (fixing T)

can be used to determine the critical size through the relation

$$\ln(n_x) = -\chi \ln\left(\frac{\nu_0}{4F}\right) + \text{ const1} = \chi \ln(F) + \text{ const2}, \tag{3.4}$$

while the temperature dependence experiments (fixing F) can give the migration barrier, provided the size and binding energy of the critical size are known, through

$$\ln(n_x) = \frac{\chi}{kT}(E_m + \overline{E}_i) + \text{ const.} \tag{3.5}$$

In rate dependence experiments, one plots $\ln(n_x)$ vs $\ln(F)$, the results should be a straight line with a slope χ. This slope can then determine the critical size. In temperature dependence experiments, one plots $ln(n_x)$ vs $1/T$ and the results are expected to be a straight line with a slope and intersection of

$$s = \frac{\chi}{k}(E_m + \overline{E}_i) \tag{3.6}$$

$$\ln(n_x)|_{1/T=0} = \ln\eta - \chi \ln\left(\frac{\nu_0}{4F}\right). \tag{3.7}$$

One then determines the migration barrier from the slope and the attempt frequency from the intersection. The sum of migration barrier and average binding energy per atom $E_m + \overline{E}_i$ can be extracted from the slope. In most cases, one needs to apply certain model to calculate the binding energy of the critical cluster in order to obtain the migration barrier from Eq. (3.6). However, an upper limit of this barrier for each critical size i can be estimated by

$$E_m \leq \frac{sk}{\chi}. \tag{3.8}$$

Particularly, for the case of $i = 1$, the scaling factor $\chi = 1/3$ and $E_1 = 0$, the migration barrier is given by

$$E_{m,i=1} = 3ks$$

The *attempt frequency* ν_0 can be obtained from the intersection Eq. (3.7), if η is given. The values of η for different coverage and critical size were studied and reported in

Ref [36]. We will use the values of η obtained from Fig. 6(b) and 6(c) therein in the analysis of this work.

In SPA-LEED experiments, one measures K_1 and σ_1, the position and width of the broad component (a shoulder or ring structure) of the (00) spot profile. The average island separation S is then determined via the relation $\frac{K_1}{K_{10}} = \frac{a_0}{S}$ (Eq. 1.13), where $a_0 = 3.84$ Å is the Si(111) lattice constant and $K_{10} = (2\pi/a_0)$. The measured island number density is approximated by $n_m \sim (1/S)^2$. Assuming this is the same as the saturation density, it is then connected to SPA-LEED measurements by

$$n_x \sim \left(\frac{1}{S}\right)^2 = \left(\frac{K_1}{K_{10}}\right)^2 \left(\frac{1}{a_0}\right)^2. \tag{3.9}$$

Experiments

The experiments were performed in an UHV-chamber with a base pressure below 5×10^{-11} torr. Pressure during experiments was kept below 2×10^{-10} torr. Clean Si(111)-7×7 was prepared by flashing the sample to $\sim 1200\,^{\circ}$C for 20 seconds, followed by slowly cooling down to deposition temperatures. When the temperature cooled down to slightly below the deposition temperature, radiation heating was turned on to keep the sample at the desired temperature. A total amount of 4ML of Pb was then deposited onto the surface at a fixed temperature between 185 K and 225 K to make 7-step islands. Deposition rate F was approximately 0.01 ML/s. Although this total coverage is far beyond the saturation regime (0.1ML $< \theta <$ 0.3ML) [34], the surface area that is actually covered by islands is $\sim$ 0.43 ML (1 ML in wetting layer, 3 ML in 7-step islands). In addition, STM study (figure 2(a) in Ref [4]) shows that Pb islands grown by deposition at $T \sim 208$ K has a steady island density between 3 to 5 ML. These two reasons make this system adequate for testing the applicability of nucleation theory in the high coverage limit ($\theta > 0.3$ ML), with the assumption that the measured number density of island is the same as the saturation density for temperatures between 185 K

and 225 K.

Results and discussions

The profiles and g(s) curves

Figure 3.1 shows some (00) spot profiles taken at different temperatures at beam energy $E = 57$eV. This energy fits the out-of-phase condition for both 7-step and single step islands, where the broad component shows itself most significantly, and therefore the best to show any change of it. Position (taken as the local maxima of the broad components) and half width of broad components were obtained by both manual analysis and the fitting program. Manual measurement was done by reading the values out of the graph with a ruler, while fitting program use multiple components: a Gaussian for the central and two Lorentzian-3/2 for the broad. Both show consistent results. Figure 3.1 shows clearly that the positions of the broad components (indicated by the dashed lines) move towards (00) spot, meaning the island separation gets larger, hence island number density decreases, as temperature increases. This is expected since, under the same deposition rate, higher temperature gives higher mobility to atoms and more aggregation to islands. Profiles taken at different energies (figure 3.2) show that the positions of the broad component do not depend on the energy of the electron beam, which is also expected since this position represents the average island separation that should be independent of the incident beam energy. Note that the profiles in figure 3.2 are all multiplied by a constant to their intensities so their shoulders are all at the same level. The central component at different energies has different intensity, which is because of the fact that not all the energies are at the exact out-of-phase conditions. In principle it is also possibly because of the existence of single steps at the sides of islands, but this should have little contribution since it had been pointed out [1] that such islands have steep edges and therefore it is not possible to have many single steps

at their sides. Figure 3.3 shows that K_1 and σ_1 are all larger than the instrument limit in the experiments, which further assures the reliability of their use in determining the average island separation and hence the island number density in this study.

Figure 3.4(a) shows the typical $g(s)$ curves taken at 177 K and 192 K for $\theta \sim 4$ ML, 7-fold oscillation are clearly seen, indicating the surface has mainly 7-step islands. Figure 3.4(b) shows an STM image taken at 190 K for $\theta = 3.5$ ML, mostly 7-step islands with steep edges and flat tops were grown. A $g(s)$ curve reflects the height of islands in atomic steps from the number of oscillations shown within a range of $2\pi/d$ in momentum space, where d is the atomic step height. At temperatures lower than 200 K, all our $g(s)$ curves show a regular 7-fold oscillation, meaning 7-step is the dominant island height. At temperatures greater than 200 K, the $g(s)$ curves are irregular (not shown), indicating coexistence of larger height islands. From our previous studies [4, 1, 37], 2-step islands begin to form on top of 7-step islands at these temperatures, resulting in coexistence of 9-step and 7-step islands. The resultant $g(s)$ curve is therefore a mixture of 7-fold and 9-fold oscillations. Those irregular $g(s)$ curves all show roughly a 7-fold oscillation modulated by a 2-fold oscillation, consistent with the picture of small 2-step islands forming on top of large 7-step islands. In such high temperature cases, the assumption that the measured island number density is the saturation density is still valid because Pb atoms have high mobility and long diffusion length, preventing nucleation in the area between islands and keeping the island number density steady. Although there are small islands nucleated on top of existing ones, it does not affect the separation of the dominant 7-step islands, therefore it does not affect the measured island number density.

Temperature dependence experiments

A plot of $\ln(n_x)$ vs $1000/T$ is shown in figure 3.5. Our data is shown in empty circles while data from Ref [4] is in solid circles. The number density of island, n_x, was calculated using Eq. (3.9). Both data show a very well linear behavior within

the temperature range of the experiments. The sum of migration barrier and average binding energy per atom, $E_m + \overline{E}_i$, determined from the linear fits of the two data sets for critical sizes $1 \leq i \leq 40$, are shown in figure 3.6. Extracted energies from the two curves agree with each other within 5%. If we assume the average binding energy per atom $\overline{E}_i$ varies slowly with critical size i, figure 3.6 should reflect the trend of migration barrier with critical size i. It is seen in figure 3.6 that migration barrier is smaller for larger i, which is reasonable because, under the same deposition rate and temperature, atoms need to diffuse faster to form a bigger stable cluster and then grow islands. The migration barrier limit shown in figure 3.6 ranges from 0.83eV for $i = 1$ down to 0.28eV for $i \geq 40$. In the case of $i = 1$, $\overline{E}_i = 0$, the migration barrier can be determined to be $E_{m,i=1} = 0.83$eV. The attempt frequencies ν_0 determined from the intersections in figure 3.5 with different values of η for $i = 1$ to 40 are shown in figure 3.7. The values of η were obtained from figure 6(b) and 6(c) in Ref[36] (see the caption of figure 3.7 for details). It is seen that the results are insensitive to the value of η for $i \geq 3$. Empty symbols are from our experiments while solid circles from Ref[4]. Figure 3.7 shows that the attempt frequencies determined from our data and that from Ref[4] are essentially of the same order of magnitude for $i \geq 3$. In cases of $i = 1$ and 2, the specific values are around 10^{33} and 10^{21}, respectively. Both are too high to be physical. This suggests that the critical size $i \geq 3$ for this system. A different STM study [5] showed that $i = 3$ by comparing the theoretical scaling function [39, 40, 41, 42] with the shape of the island size distribution for different coverage (0.8ML and 1.6ML above wetting layer) deposited at $T = 208$ K. The theoretical scaling function for the island size distribution $N_s(\theta)$ can be written in the general form [39, 40]

$$N_s(\theta) = \theta S^{-2} f_i(s/S), \tag{3.10}$$

where $S(\theta)$ is the average island size and the scaling function $f_i(s/S)$ depends on the value of critical size i. A plot of the scaling function $f_i(s/S)$ for $i = 1$ to 6, together with

the island size distribution data from Ref[5], are shown in figure 3.8. The experimental data fits the scaling function of either $i = 3$ or $i = 4$. For the case of $i = 3$, as concluded in Ref[5] and pointed out in both figure 3.6 and 3.7, the attempt frequency is in the order of 10^{18} and $E_m + \overline{E}_i$ ~0.43eV. For $i = 4$, however, ν_0 is roughly 10^{16} and $E_m + \overline{E}_i \sim$ 0.41eV. Compared to the typical value of ν_0 for surface diffusion $10^{13\pm2}$, $i = 4$ seems to be more reasonable than $i = 3$.

Determination of attempt frequency

In determining the attempt frequency ν_0, the values of η (the dimensionless nucleation density) in Eq. (3.7) were obtained from Fig. 6(b) and 6(c) of Ref[36]. Apparently we should pick the values of η from Fig. 6(b) of Ref[36], since that is the one for 3-D islands (6(c) is for 2-D islands). However, since the growth of islands is lateral after forming 7-step islands [4, 37], the growth has both two and three dimensional features, we used the values of η from both 2-D and 3-D cases in Ref[36]. It is seen in figure 3.7 that the attempt frequencies are essentially of the same order of magnitude for $i \geq 3$, regardless of the value of η (from 0.08 to 0.4, see figure caption for details). Comparing the estimated diffusion length and the measured island separation, one can test the validity of the attempt frequency. If the diffusion length is much smaller than the island separation, nucleation will occur between existing islands and island number density will increase, which disagrees with our major assumption that the observed island number density is the saturation density. If the diffusion length is comparable to or larger than the island separation, island number density will remain the same and the results will be consistent with that assumption. The diffusion length of a single atom on the surface can be estimated by the relation $l \sim \sqrt{4D/F}$. For the possible candidates, $i = 3$ and $i = 4$, the attempt frequency ν_0 are 5.63×10^{17} and $6.85 \times 10^{15} (\eta = 0.17)$, while the maximum migration barriers are 0.46eV and 0.41eV, respectively (D/F between 10^7 and 10^8). The diffusion lengths calculated for the experimental temperatures (185 K to

Table 3.1 Measured average island size L, average island separation S and, calculated diffusion length l at different temperatures. The diffusion length was calculated for the case of $i = 3(E_m < 0.43\text{eV}$, $\nu_0 = 5.63 \times 10^{17})$. Deposition rate $F = 0.01$ ML/s. Column $n_{x,Ch}$ and L_{Ch} list the island number density and range of island size, respectively, from Ref[4].

T (K)	K_1 (%Bz)	S (Å)	l (Å)	n_x ($10^{10}/cm^2$)	$n_{x,Ch}$ ($10^{10}/cm^2$)	σ_1 (%Bz)	L (Å)	L_{Ch} (Å)
188	1.42	270	21000	13.7	5.0	4.17	140	$170 \sim 300$
192	1.23	310	28000	10.2		3.56	165	
194	1.13	340	32000	8.6		2.99	206	
197	0.78	490	40000	4.1	2.3	2.53	219	$250 \sim 420$
205	0.62	620	67000	3.1	1.2	1.51	431	$330 \sim 540$
220	0.42	915	162000	1.2	0.51	0.55		$840 \sim 970$

225 K), with deposition rate $F = 0.01$ ML/s, range from 2.1×10^4 to 1.6×10^6 Å ($i = 3$) and from 9.4×10^3 to 6.0×10^4 Å ($i = 4$). Compared to the measured island separation (270 to 910 Å) at the same temperatures, these diffusion lengths are 75 to 180 times larger for $i = 3$ and 35 to 65 times for $i = 4$. These obviously long diffusion lengths suggest that the atoms do have enough time to join existing islands before the next atom arrives onto the surface, therefore the number density of island is saturated. If we take into account the average binding energy, the migration barrier will be even lower and the calculated diffusion length will be even longer. It is interesting to note that for $i = 40$, $\nu_0 = 1.14 \times 10^{11}$ and $E_m < 0.29\text{eV}$, the diffusion lengths are from 1800 Å for 188 K to 6400 Å for 225 K, which are not unreasonable and seem to suggest that even $i > 4$ is possible. Table 1 lists the average island separation S, and calculated diffusion length l for $i = 40$ at different temperatures, the island number density n_x obtained from separation S, and average island size L obtained from the width of the shoulder of (00) spot (Eq. (1.15)). The number density and island size from Ref[4] are also listed for comparison. Our island density is larger than theirs by a factor of 2, which could be due to the difference in temperature measurement between our setup and theirs.

Rate dependence experiments

In order to determine the critical size, we performed some rate dependence experiments. The expected result is, according to Eq. (3.4), that a plot of $\ln(n_x)$ vs $\ln(F)$ shall give a straight line with a slope equal to $\chi = \frac{i}{i+2}$, which directly determines the critical size i. The rate dependence experiments were carried out at fixed temperatures of 188 K and 205 K, both showed consistent results. The results of 188 K will be shown here since the shoulder of (00) spot has clear maxima (see figure 3.1). Deposition rate ranges from 0.001 ML/s to 0.01 ML/s (10^{12} to 10^{13} atoms/cm^2 s). In contrast to the expectation of a linear dependence, figure 3.9(a) shows that the saturation island number density is almost independent of the deposition rate. This can also be seen in the raw data (figure 3.9(b)) that the position (maxima) of shoulder (indicated by dashed lines) is roughly constant with deposition rate. This result suggests that the nucleation theory is not applicable in this case and limits the conclusion on the critical size i. A modified theory considering "non-traditional" QSE-based nucleation behavior has to be developed. One possible reason for this limitation of applicability is that the theory assumes atoms stay on surface right after landing on a particular site, while in reality the Pb atoms might bounce off and then back on several times before they finally stay on the surface. After several such bounces the atom can actually stop at a place that is relatively far away from the original landing site. This kind of mobility depends on the kinetic energy of the Pb atoms in the gas phase, but not on the deposition [43]. However, how such "'non-thermal" mobility will affect the island density is still unknown. More studies are needed to understand the effects.

Summary

We had done both temperature and deposition rate dependence experiments on the 7-step islands of Pb/Si(111)-7×7 to test the applicability of nucleation theory. Our rate

dependence results showed no dependence of island density on deposition rate, suggesting that the theory is not applicable in this case. A modified theory needs to be developed to explain the results. The temperature dependence results indicate the smallest possible stable cluster is a tetramer ($i \geq 3$), but do not exclude the possibility of larger sizes. Recent STM study [5] indicated the critical size is either $i = 3$ or $i = 4$, by comparing the theoretical scaling function to the measured island size distribution for different coverage at $T = 208$ K. This result is consistent with our conclusion from temperature dependence experiments that $i \geq 3$. However, the attempt frequencies determined from the same experiments favor $i = 4$. Theoretical calculations on the binding energies of critical clusters are needed to determine the migration barrier.

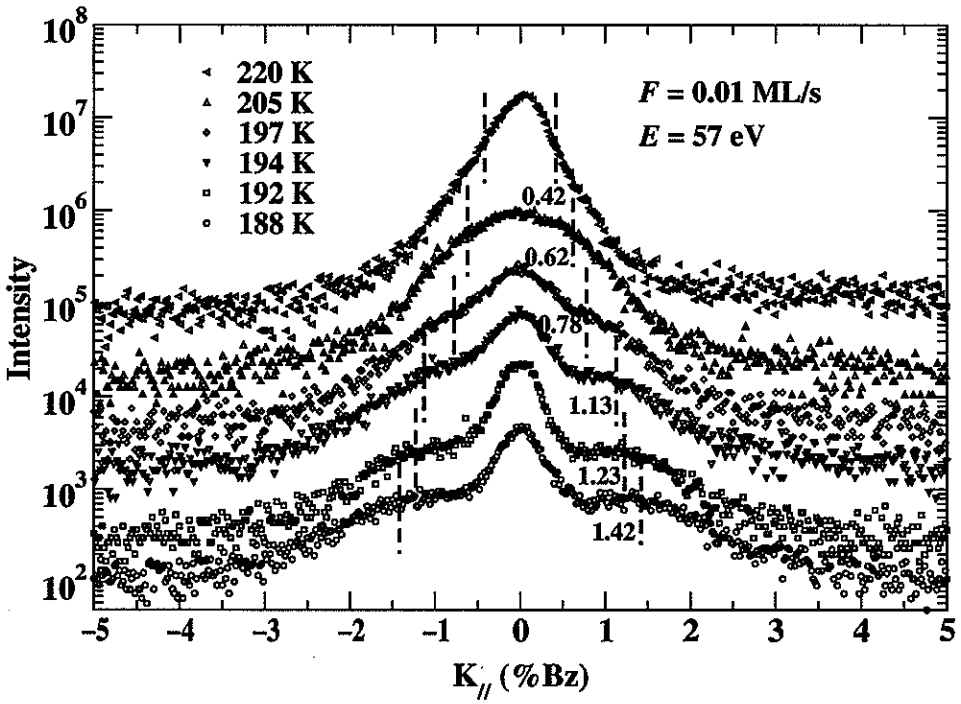

Figure 3.1 Profiles of (00) spot taken at $E = 57$eV (an out-of-phase condition for both 7-step and single step islands) at different temperatures. Total deposition amount is $\theta = 4$ ML, with deposition rate $F \sim 0.01$ ML/s. The shoulders were fitted with two Lorentzian-2/3 functions. Position of shoulders moves towards the center, meaning island separation gets larger, as temperature goes higher. The average island separation changes from 270 Å to 910 Å from 188 K to 220 K.

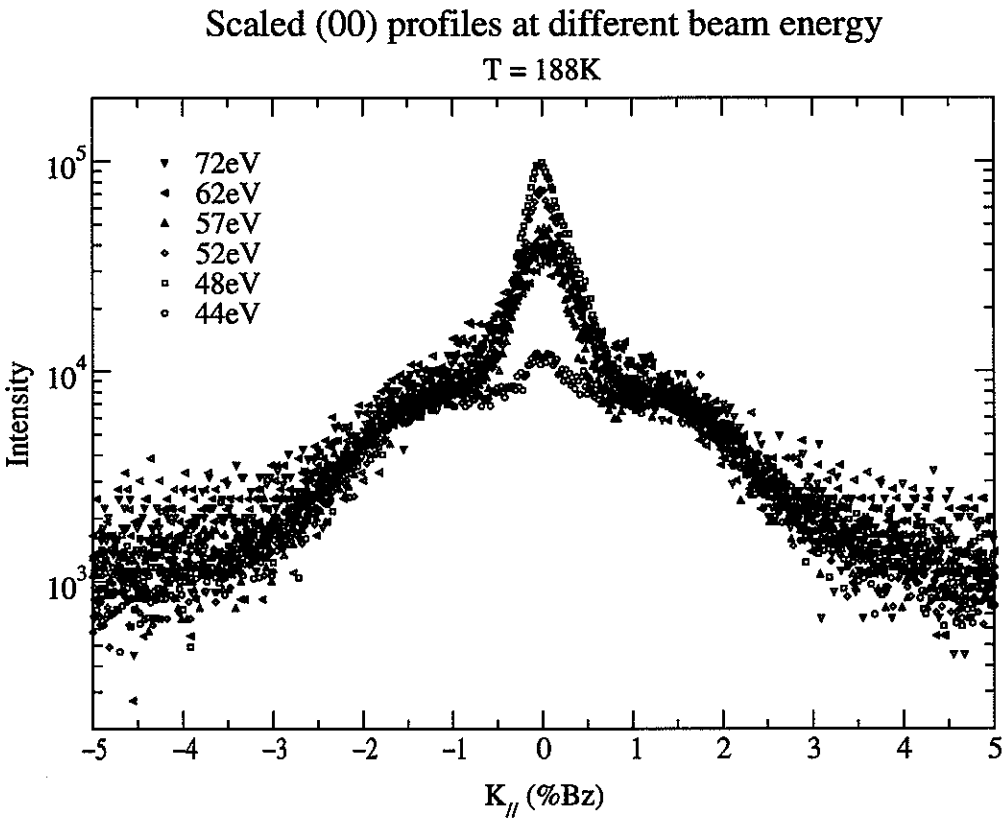

Figure 3.2 Profiles of (00) spot taken after Pb deposited at $T = 188$ K ($\theta = 4.2$ ML) at different out-of-phase energies. All profiles are multiplied by a constant to their intensity so their shoulders are all at the same level. This is to show the fact that the position and shape of the shoulder is independent of the beam energy, so the use of them to determine n_x is reliable, when the temperature is fixed. This is expected because they reflect the average island size and separation, which is not affect by the beam energy. The central component has different intensities at different energies because not all the energies are at the exact out-of-phase conditions for 7-steps.

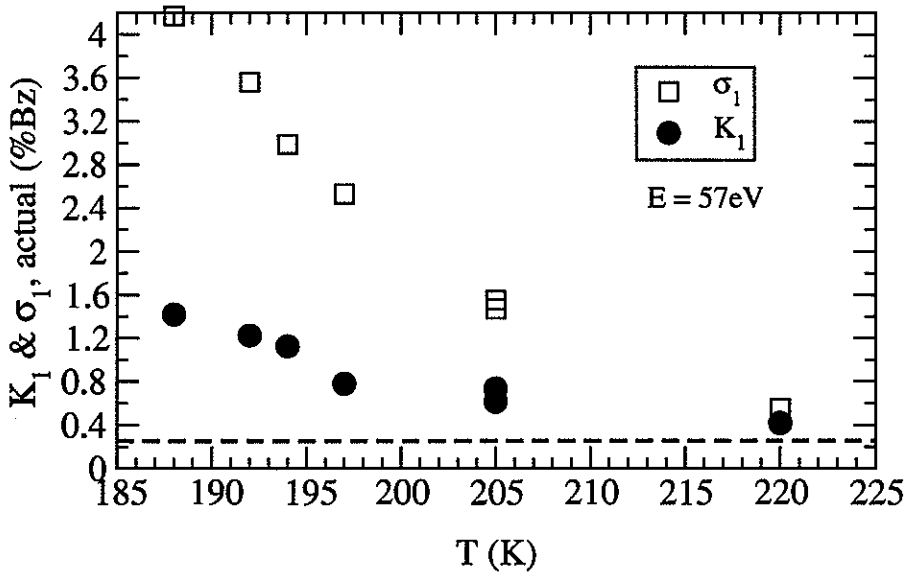

Figure 3.3 Plots of position K_1 (solid symbol) and width σ_1 (empty symbols) of the broad component of (00) spot with temperature. Total coverage is about 4 ML. Incident beam energy $E = 57$eV. Both width and position go down with temperature, meaning both separation and size of islands become larger as temperature goes higher. Note that in the highest temperature case both K_1 and σ_1 approached but are still above the instrument limit (dotted horizontal line), indicating the use of these values is still reliable.

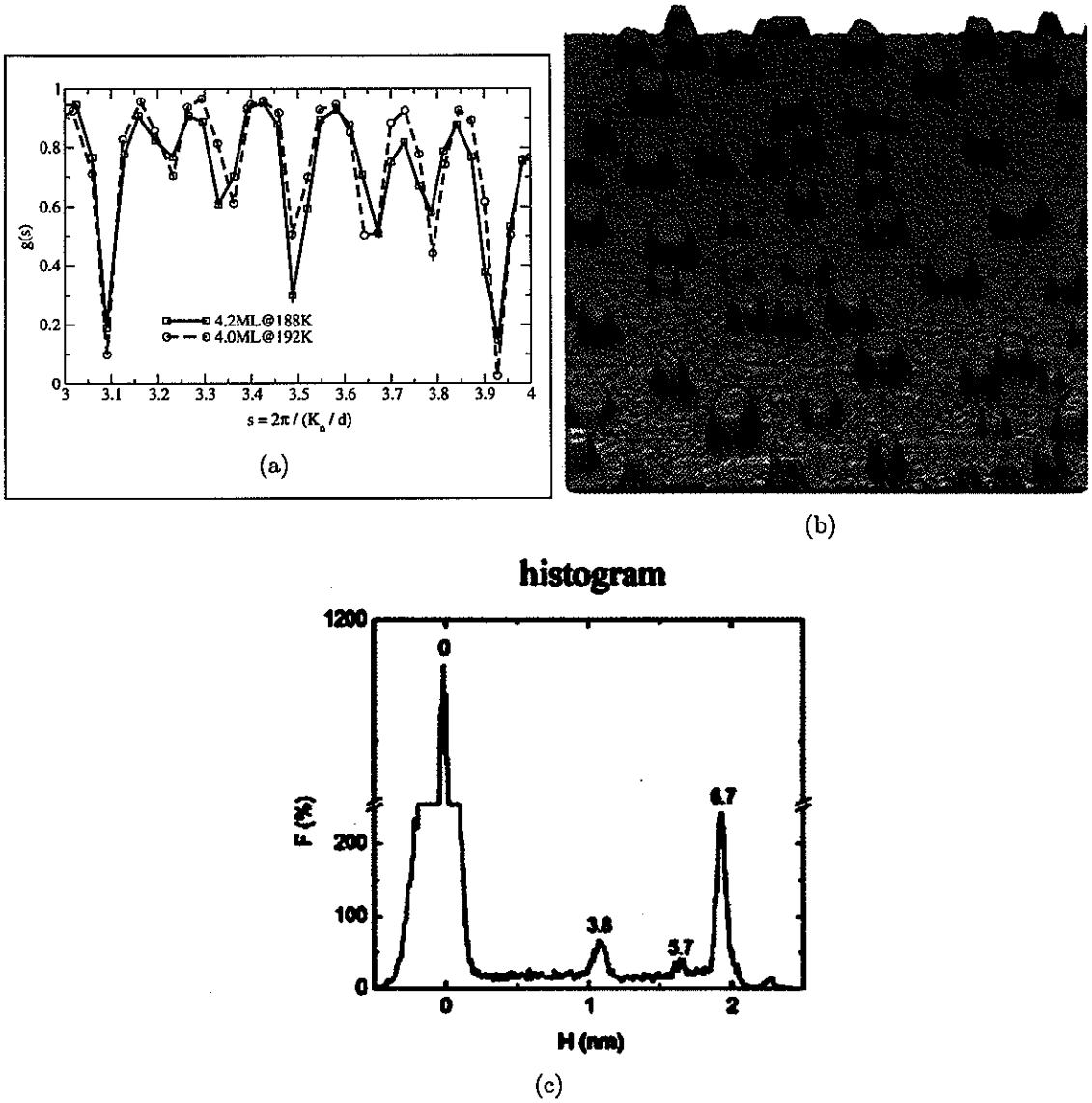

Figure 3.4 (a) Typical $g(s)$ curves taken at 188 K and 192 K for $\theta \sim 4$ML. Both show clearly 7-fold oscillations, meaning that most of the islands have a height of 7 atomic steps. (b) STM image taken at 190 K for $\theta = 3.5$ ML, showing islands with seep edges and flat tops. (c) Histogram of the stm image, showing the island heights are mostly 7-step.

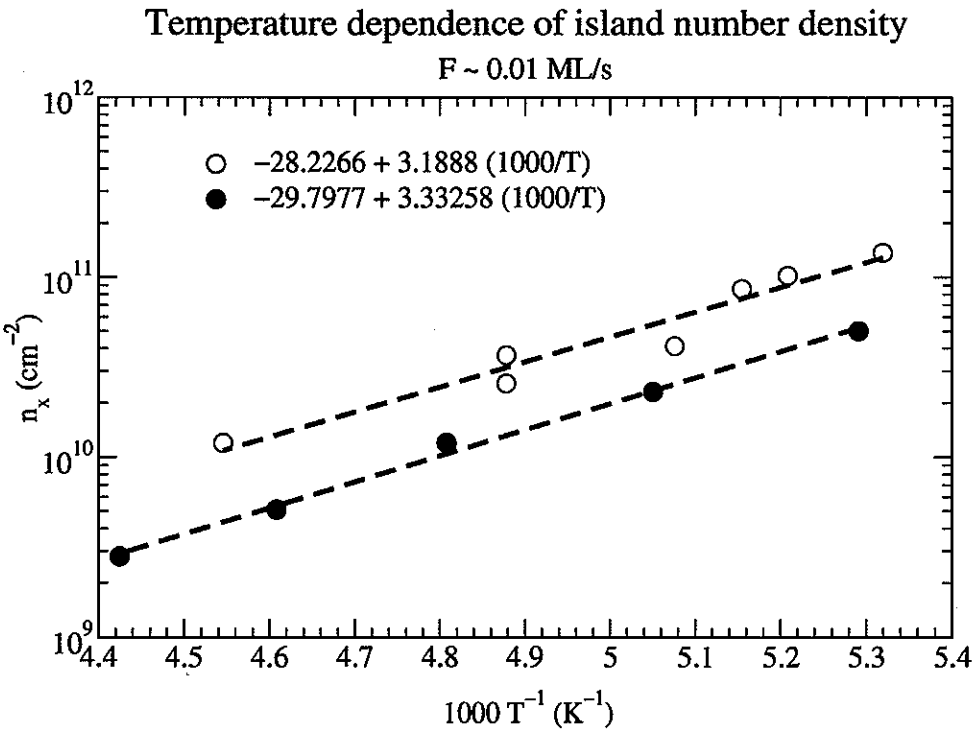

Figure 3.5 Plot of $\ln(n_x)$ vs $1000/T$. Empty circles are our data, solid circles are data from Ref [4]. In our experiments the total coverage was about 4 ML and deposition rate was 0.01 ML/s. In Ref [4] coverage was 3.2 ML and deposition rate 2.7×10^{-3} ML/s (0.16 ML/min). Linear fits are shown as dashed lines. The upper limits of migration barrier derived from the slope of the linear fits are shown in Fig. 3.6. Our data agrees with Chang's within 5%. The difference between the two data sets could be due to the difference in temperature measurements.

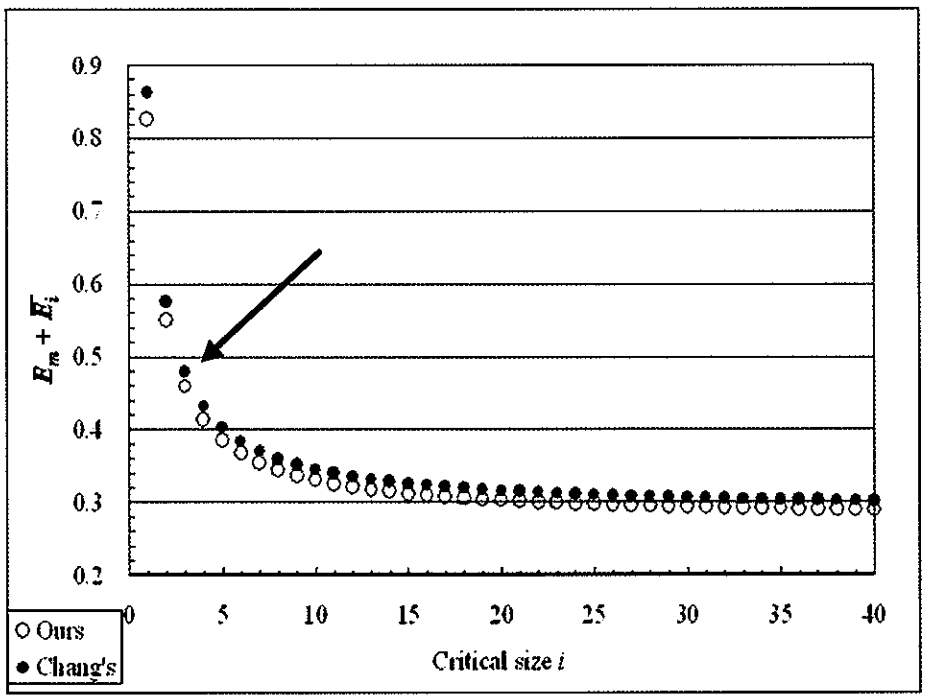

Figure 3.6 Migration barrier E_m plus average binding energy per atom $\overline{E}_i$ for different critical size i, derived from the slope of the linear fit shown in Fig. 3.5. Empty circles are our results while solid circles are from Ref[4]. Both agree with each other within 5%. For the case of $i = 1$, $\overline{E}_i = 0, E_{m,i=1} \sim 0.83$eV. The arrow indicates the result of a recent STM study [5] which concluded that for such a system $i = 3$.

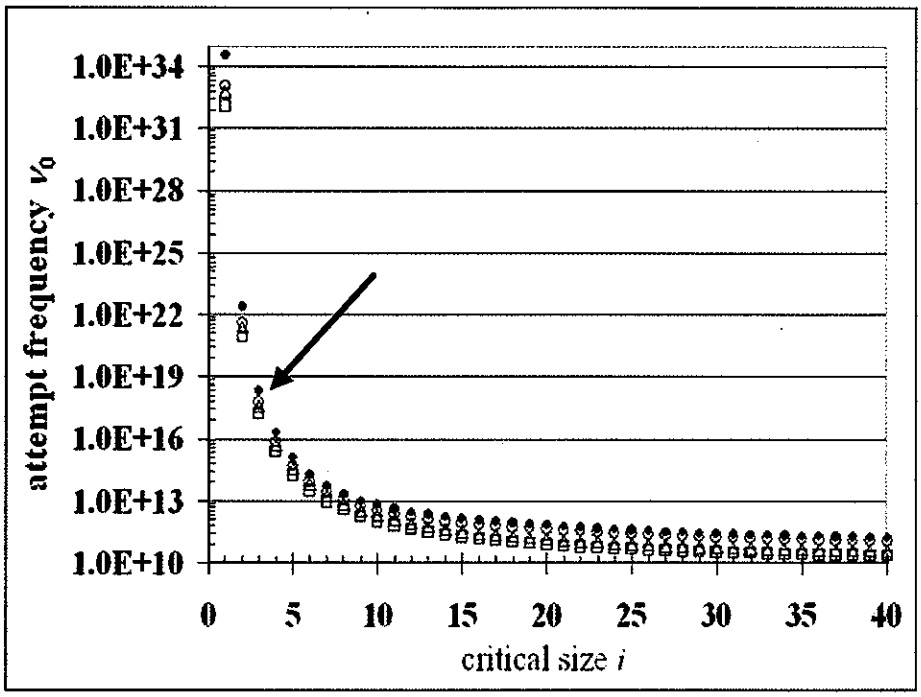

Figure 3.7 Attempt frequency ν_0 determined from the intersection of fig 3.5 with different values of η obtained from figure 6(b) and 6(c) in Ref[36]. Empty symbols are from our experiments while solid symbols from Ref[4]. The attempt frequencies are essentially of the same order of magnitude for $i \geq 3$. Circles were calculated using varying η (0.17 for $i = 1$ to 0.4 for $i = 20$) from 6(c) of Ref[36], which is for 2D islands. Linear interpolation was assumed for the values of critical size that are not given in that figure. For $i > 20$ (the maximum size given in that figure), the same value as $i = 20$ was assumed. Squares and triangles were calculated using fixed values of $\eta = 0.08$ and 0.14, respectively, as given in figure 6(b) of Ref[36] for 3D islands. The attempt frequency ν_0 in this figure is around 10^{33} for $i = 1$ and 10^{21} for $i = 2$, both are too high to be physical. The conclusion of $i = 3$ in Ref[5] is pointed out by an arrow, with an attempt frequency in the order of 10^{18}.

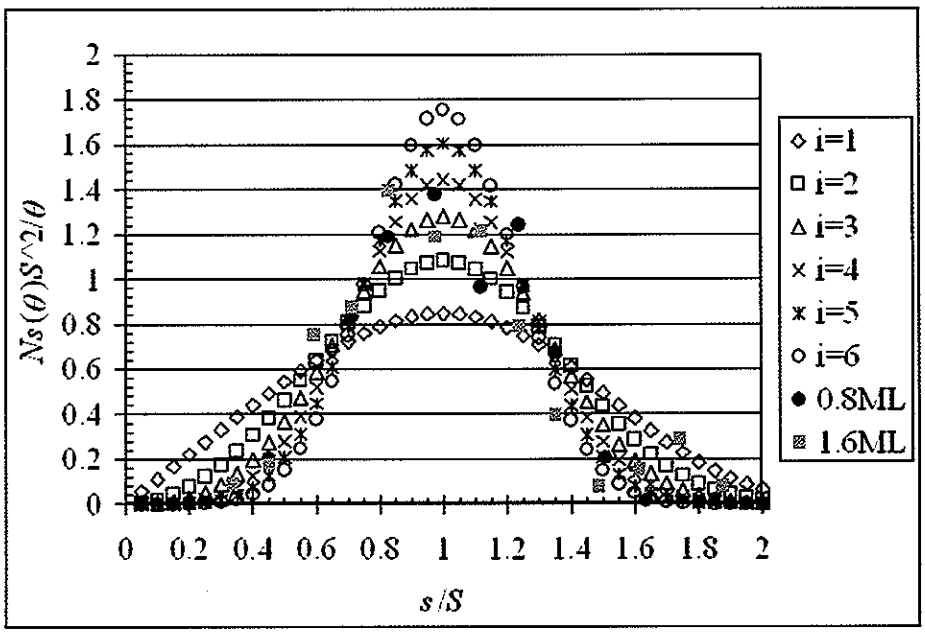

Figure 3.8 Scaling function $N_s(\theta)s^2/\theta$ vs s/S for $i = 1$ to 6. The expression of the function was obtained from Eq. 2(a) and 2(b) of Ref[39]. Island size distribution from Ref[5] for 0.8 ML (solid black circles) and 1.6 ML (solid gray squares) above wetting layer are also shown. This figure shows that the data in Ref[5] fits either $i = 3$ or $i = 4$.

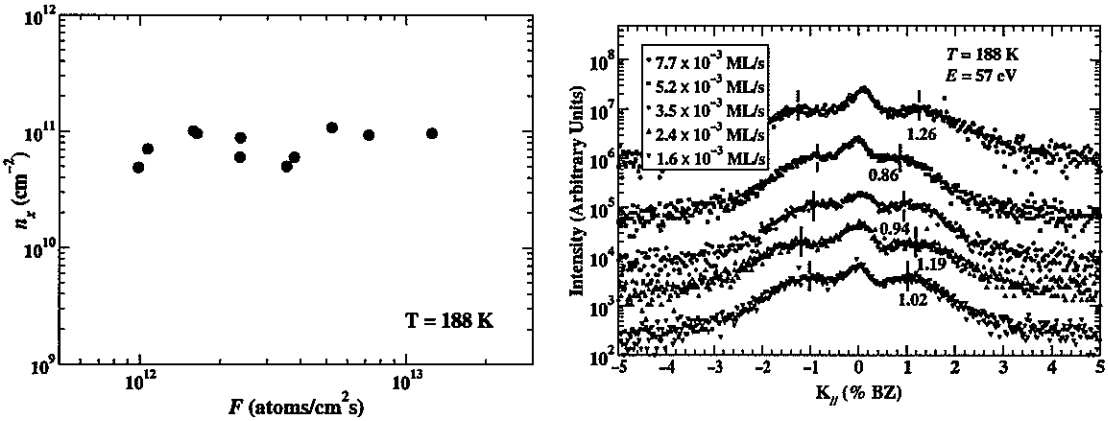

Figure 3.9 Rate dependence experiment of island number density for $\theta =$ 4 ML at $T = 188$ K. The temperature was chosen such that the shoulder of (00) spot has clear maxima (see figure 3.1). The deposition rate ranges from 0.001 ML/s to 0.01 ML/s. (a) Plot of island number density vs deposition rate in (atoms/cm^2 s). The conversion of F is done by 1 ML/s $\sim$ 1 atom/(unit cell area) s $\sim 1/(3.84$ Å$)^2$ s $\sim 6.78 \times 10^{14}$ atoms/cm^2 s. (b) Raw data. In contrast to the linear dependence as expected by Eq. 3.4, (a) shows the saturation island number density is independent of the deposition rate. This can also be seen from the raw data (b) that the position (maxima) of shoulder (indicated by dashed lines) is roughly constant with the deposition rate.

CHAPTER 4. Low temperature formation and change of high symmetry site occupation of the "devil's staircase" phases in Pb/Si(111)

Abstract

It has been a question what phase or phases could be formed on Pb/Si(111) when the coverage is between 6/5 ML and 4/3 ML because 1) more than one phase were reported in publications and 2) there existed inconsistent descriptions about the phases close to 4/3 ML. It was found that actually a novel "devil's staircase" could be formed within this coverage range. Diffraction study on this system had been performed to understand the transitions between those "devil's staircase" phases. It was found that many of such staircase phases could be made by low temperature deposition ($T \sim$ 120K) onto Pb/Si(111)-$\sqrt{7} \times \sqrt{3}$ without thermal annealing, with spatial extent over macroscopic distances ($\sim$0.5 mm). The extraordinary amount of atom rearrangement necessary for these phases to form indicates an unusual degree of self-organization at low temperatures. In order to identify the "devil's staircase" phases from diffraction patterns, kinematic calculations were performed and compared to the experiment. A sudden change in diffraction pattern size and additional spots around (10) spot was observed at $\theta \sim 1.25$ ML, which can be explained by high symmetry site occupation change (some high symmetry atoms changed from H3 to T4).

Linear phases of Pb/Si(111) between 6/5 and 4/3 ML: a novel "devil's staircase"

The discovery

Numerous linear phases of Pb/Si(111) with coverage θ between 6/5 ML and 4/3 ML had been observed with STM [11] by high temperature deposition of Pb onto Pb/Si(111)-$\sqrt{7} \times \sqrt{3}$ phase, or thermal treatment after low temperature deposition onto the same initial surface. These phases were found to consist of two generating phases, the $\sqrt{7} \times \sqrt{3}$ (θ = 6/5 ML) and $\sqrt{3} \times \sqrt{3}$ (θ = 4/3 ML). Theoretical calculations on the θ vs $\Delta\mu$ stability curve of such phases show the feature of a "devil's staircase" (figure 4.1). Mathematically this stability curve is a continuous but non-differentiable function, with infinite number of phases whose coverage is a rational number (see left-top corner of figure 4.1 for example). Some of these phases have significant width $\Delta\mu$ (stable phases) while others not. In experiments those unstable phases will be difficult to observe and one expects to see only the most stable phases as shown in figure 4.1. The "devil's staircase" is one of the outstanding phase diagrams found in theoretical physics which predicts the existence of an infinite number of phases within a narrow coverage range. The infinite phases of the "devil's staircase" and the corresponding hierarchical patterns are built from the combination of two generating phases of coverage's θ_1 and θ_2, according to simple generating rules [44, 45]. Experimentally it has been an outstanding challenge to show a "devil's staircase" since physical phenomena are not expected to be described by non-differentiable functions. To prove the existence of a "devil's staircase", one needs to show 1) there exists a large number of phases within a narrow coverage range; and 2) these phases can be built from two generating phases. The ordered phases of Pb/Si(111) discovered in Ref[11] is an example of "devil's staircase" because 1) twelve stable phases were clearly identified within a narrow coverage range of 0.1 ML (figure 4.2); and 2) all

the observed phases could be built from two generating phases, $\sqrt{7} \times \sqrt{3}$ and $\sqrt{3} \times \sqrt{3}$.

Figure 4.2 shows twelve of those linear phases observed in Ref [11]. In that figure, each bright row is a line of high symmetry Pb atoms. Two close bright rows correspond to a line of $\sqrt{3} \times \sqrt{3}$ phases, while two more distant bright rows are $\sqrt{7} \times \sqrt{3}$ phases. To identify a particular phase from these STM images, one simply counts the number of larger separations (corresponding to $\sqrt{7} \times \sqrt{3}$ unit cells) and the number of smaller separations ($\sqrt{3} \times \sqrt{3}$ unit cells). Take figure 4.2(g) for example, if one counts the number of separations from left to right, every two larger separations are followed by one smaller separation, that is, every two $\sqrt{7} \times \sqrt{3}$ unit cells are followed by one $\sqrt{3} \times \sqrt{3}$ unit cell. It is found that each of these "devil's staircase" phases consists of n $\sqrt{7} \times \sqrt{3}$ and m $\sqrt{3} \times \sqrt{3}$ sub cells in its unit cell and is uniquely labeled as a (n, m) phase. For example, a (2, 1) phase denotes a phase consists of two $\sqrt{7} \times \sqrt{3}$ and one $\sqrt{3} \times \sqrt{3}$ sub cells, which is exactly what figure 4.2(g) shows. Models of (3, 1) and (2, 1) phases and the two generating phases are shown in Figure 4.3. The generating phases are shown on the top, with $\sqrt{7} \times \sqrt{3}$ on the left and $\sqrt{3} \times \sqrt{3}$ on the right. A $\sqrt{7} \times \sqrt{3}$ unit cell has six atoms, five of which are slightly shifted from T1 (off-centered T1) sites (see figure 4.4 for definition of different binding sites) and the high symmetry atom is on H3 site [46]. The $\sqrt{3} \times \sqrt{3}$ unit cell has four atoms, with three on the off-centered T1 sites and one on H3 site [47]. Figure 4.4 shows the Si(111) substrate and the definition of H3, T4 and T1 sites. Figure 4.5 shows the full models of $\sqrt{7} \times \sqrt{3}$ and $\sqrt{3} \times \sqrt{3}$ unit cells, with atom coordinates obtained from x-ray diffraction experiments [46] and first principle calculations [47]. The fact that $\sqrt{7} \times \sqrt{3}$ has more atoms in its unit cell but lower coverage is because its unit cell has a larger size ($\frac{5}{2}a_0 \times \sqrt{3}a_0$ vs $\frac{3}{2}a_0 \times \sqrt{3}a_0$, where $a_0 = 3.84$ Å is the Si(111) lattice constant).

Low temperature formation and macroscopic spatial extent

It was surprising that even more of such phases were observed by merely low temperature deposition ($T \sim 120$ K) [12] without thermal annealing. The starting phase was $\sqrt{7} \times \sqrt{3}$, which was made by depositing ~1.2 ML of Pb on Si(111)-7×7 at low temperature, followed by annealing to 400 K. After the initial phase was made, small amount of Pb ($\Delta\theta \sim 0.006$ ML) was deposited at $T \sim 120$ K in a step-wise manner until the diffraction pattern is close to that of $\sqrt{3} \times \sqrt{3}$ and beyond the resolution of the experimental setup. Figure 4.6 shows the two-dimensional diffraction patterns of all the distinguishable phases in Ref[12]. The diffraction patterns of these phases are essentially an equilateral triangle centered at the commensurate position (1/3, 1/3). The height of the triangle H decreases monotonically with coverage θ. One-dimensional scans along the diagonal of the Brillouin zone (one of the equivalent $[1\bar{1}0]$ directions) corresponding to figure 4.6(e) through (g) (bottom to top) are shown in figure 4.7. These one-dimensional scans show two important results from the low temperature deposition experiments: 1) the majority (nearly 80%) of the surface was covered by only two phases over a macroscopic region (~0.5 mm defined by incident beam size); 2) observable change of phase, indicated by shifts in positions and changes in intensity of spots, happened at $T \sim 120$ K with a coverage difference of only 0.006 ML. These unexpected results indicate that even at low temperature where atoms are not expected to be mobile, a high degree of self-organization is possible in the system of Pb/Si(111).

In order to identify the phases from diffraction pattern, kinematic calculations were performed on simplified model with only high symmetry atoms occupying H3 sites. Figure 4.8 shows the results for the generating phases and the "devil's staircase" phases (7, 1) to (1, 7). The calculations agree with the experiments very well for coverage $\theta \leq$ 1.25 ML. Figure 4.9 shows the comparison for (2, 1) phase, nearly identical patterns are seen. The main difference between the experiment and calculation in figure 4.9 is the

missing corner of the triangle. This missing corner was seen in all equivalent orientations in a larger view in reciprocal space (not shown). It could be due to dynamical effects or the off-centered T1 atoms, which are neglected in the calculations. In one-dimensional scans along $[1\bar{1}0]$, as shown in figure 4.7, phase identification was done by matching the experimental spot positions to the calculations along the same direction of scan. In calculations, the position of any spot of a specific "devil's staircase" phase must be a rational numbers p/q, with p an integer and q the number of total spots determined by the $[1\bar{1}0]$ dimension of the unit cell. In experiments, one tries to match the position of spots to the calculated rational numbers from specific phases. If multiple spots can be indexed by rational numbers with the same denominator, they must be given by the same phase present on the surface. For example, the bottom scan of figure 4.7 has spots at 38.4%Bz (4/18), 57.5%Bz (6/18), and 67.2%Bz (7/18), which are from phase (3, 1), since $5n + 3m = 5 \times 3 + 3 \times 1 = 18$ (Eq. (A.6)); and spots at 26.8%Bz (2/13), 39.8%Bz (3/13), 52.9%Bz (4/13), and 66.4%Bz (5/13), which are from phase (2, 1). Even though some spots are close to each other, such as 66.4%Bz (5/13) and 67.2%Bz (7/18), they can still be identified to be different phases. This is because that if one spot can be indexed by a rational number p_1/q_1, it's distinguishable yet very close neighbors are unlikely to be indexed by another rational number with the same denominator p_2/q_1, unless they happen to be separated by integral multiples of $1/q_1$. If such close neighbors can be identified to be a rational number with a different denominator p_2/q_2, and there exist other spots that can also be indexed by rational numbers with the same denominator q_2, it is very probably that these close neighbors are given by another phase that is also present on the surface.

Change of high symmetry site occupation

Sudden change of diffraction pattern

At coverage $\theta \sim 1.25$ ML, the experiment shows a sudden change in height (half-sized) and orientation (180° rotated) of the triangle (figure 4.6(i) and (j)), and the existence of satellite spots around (10) spot. The calculations with only H3 atoms (H3-H3 occupation) show the triangle simply reduces gradually without changing its orientation and no satellite spots around (10) spot (figure 4.8(g) through (i)). Further calculations including both H3 and T4 atoms (H3-T4 occupation) show that such a mixed occupation of high symmetry atoms can explain these changes in the diffraction pattern. The sudden change of triangle height can be even better seen in one-dimensional scans in figure 4.10: the third scan from bottom, which corresponds to figure 4.6(j), has a much smaller triangle height than the second (figure 4.6(i)). Before and after this sudden change, the evolution of diffraction pattern is always gradual. A plot of the triangle height H vs coverage θ is shown in figure 4.11, a linear relation and a clear break in slope is clearly seen. The linear relationship between H and θ is explained in Appendix A. The break in slope corresponds to the sudden change of triangle height. The minus sign and cross signs are calculations with H3-H3 and H3-T4 occupation, respectively. The solid circles are experimental results. It is seen in the figure that for $\theta < 1.25$ ML, all phases have H3-H3 occupation, while for $\theta > 1.25$ ML they change to H3-T4 occupation. This transition of high symmetry site occupation from H3-H3 to H3-T4 changes the inter-atomic separation in real space, hence introduces new spots and changes the intensity distribution in reciprocal space, and causes the triangle to be half-sized and 180° rotated. Figure 4.12 shows a comparison between the diffraction patterns of H3-H3 occupation and H3-T4 occupation for (1, 3) phase. In modeling the H3-T4 case for calculation, we combined one (1, 3) unit cell on H3 with one cell on T4 sites to form a new unit cell for simplicity. However, the main features observed

in experiments were obtained: 1) the separation between bright spots in H3-T4 case is smaller than that in H3-H3 case; 2) the triangle in H3-T4 case is in opposite orientation as in H3-H3 case; 3) there are satellite spots around (10) in H3-T4 case and not in H3-H3 case.

STM images

Such H3-T4 occupation can also be seen from STM images in real space. Figure 4.13 shows images of the (2, 1) and (1, 3) phases. Each bright row in the figure is a line of high symmetry Pb atoms on either H3 or T4 sites. The red circles correspond to high symmetry Pb atoms occupying H3 sites, while blue circles correspond to atoms on T4 sites. It is seen in the figure that all high symmetry atoms are on H3 sites for the (2, 1) phase, while there are both H3 and T4 atoms for the (1, 3) phase. The parallelograms across dark rows with same color atoms in the figure correspond to the $\sqrt{7} \times \sqrt{3}$ unit cells, which are different from those with atoms of different colors. The top-left of (2, 1) image and center of (1, 3) image show that different cells won't fit into the same atoms, meaning such a change of biding site from H3 to T4 can be observed unambiguously, even though the change only introduces a small shift in real space ($\frac{\sqrt{3}}{6} \times 3.84 = 1.1$ Å in $[11\bar{2}]$). It is interesting to note that such change of binding sites happens only at "$\sqrt{7} \times \sqrt{3}$" cells and not at $\sqrt{3} \times \sqrt{3}$ cells. The smaller parallelograms in the bright rows of the (1, 3) phase image correspond to $\sqrt{3} \times \sqrt{3}$ unit cells, which match all the atoms in the bright rows without having to change the binding sites in adjacent rows.

Satellite spots around (10) spot

The existence of the satellite spots around (10) spot is also a result of the H3-T4 occupation. The satellite spots show up because there is a change in intensity distribution due to a change in $|F(\Delta \boldsymbol{s})|^2$. To understand the reason of such a change, we need to look for the difference in the inter-atomic separation between H3-H3 and H3-

T4 cases, since it is the relative position of atoms that determines the structure factor squared $|F(\Delta \boldsymbol{s})|^2$ (Eq. (1.10)). As shown in figure 4.15, the H3-T4 occupation introduces a separation of $\frac{\sqrt{3}}{6}a_0$ in the $[11\bar{2}]$ direction, in addition to the regular $[11\bar{2}]$ separation $\frac{\sqrt{3}}{2}a_0$ as in the in H3-H3 case. The regular separation $\frac{\sqrt{3}}{2}a_0$ determines fundamental spots (± 10), (± 10), $\cdots$. This additional separation is $\frac{1}{3}\times$ of the regular separation, so it will superimpose a $3\times$ period upon the regular spots. That is, the (± 10) and (± 20) spots shall be different from the regular spots (00) and (± 30). A calculation of diffraction pattern over three Brillouin zones shows that (± 10) and (± 20) spots have satellite spots while (00) and (± 30) do not, exactly the expected $3\times$ period. The satellite spots around (10) spot show up in H3-T4 case because the additional $\frac{\sqrt{3}}{6}a_0$ separation gives a phase shift to the (10) spot and lowers its intensity in the structure factor part $|F(\Delta \boldsymbol{s})|^2$, which should be a local maximum in a H3-H3 case. To conserve the total intensity (since the total number of scattering atoms is not changed by the high symmetry site occupation change), the structure factor squared $|F(\Delta \boldsymbol{s})|^2$ has to be broadened and hence open up a wider range around the (10) spot. If the minimal separation of spots of a particular phase is within this view of the $|F(\Delta \boldsymbol{s})|^2$, some weak spots will show up around, those are the satellite spots we see around (10) spot. The position of the spots measured from (10) spot should be the delta function separation of the particular phase. Figure 4.14 shows that for $\theta > 1.25$ ML these spots are indeed at their expected positions. This evidence supports the idea that these satellite spots come from H3-T4 occupation even though experimentally we cannot make observations beyond the first Brillouin zone to observe the superimposed $3\times$ period. We also had seen such satellite spots when the main phase on the surface was slightly below 1.25 ML, and their positions seem to stay constant ($\sim$9.4%Bz) until $\theta > 1.25$ ML. The constant position suggests that those spots come from the same phase. However, the reason why they show up at $\theta < 1.25ML$ is unclear. Further calculations on modified models are needed to understand this effect.

Summary

In summary we have discovered the existence of a "devil's staircase" on Pb/Si(111). Many of those phases could be prepared by low temperature deposition without thermal annealing, with spatial extent over nearly 0.5 mm, indicating a high degree of self-organization at low temperatures is possible for Pb/Si(111). High resolution LEED studies on the transitions with temperature between those staircase phases were performed and will be given elsewhere [50]. Kinematic calculations were done on simplified models with only high symmetry atoms on H3 sites to identify the phases in reciprocal space. Unambiguous phase identification was achieved by matching the position of all the spots from experiments with that from calculations in one-dimensional scans along $[1\bar{1}0]$. A sudden change in the size and orientation of diffraction pattern and the existence of satellite spots around (10) spots, which can be explained by high symmetry site occupation change from H3-H3 to H3-T4, was observed and discussed. The changes in diffraction pattern due to H3-T4 occupation are attributed to an additional inter-atomic separation introduced by the H3 and T4 atoms across a "$\sqrt{7} \times \sqrt{3}$" cell.

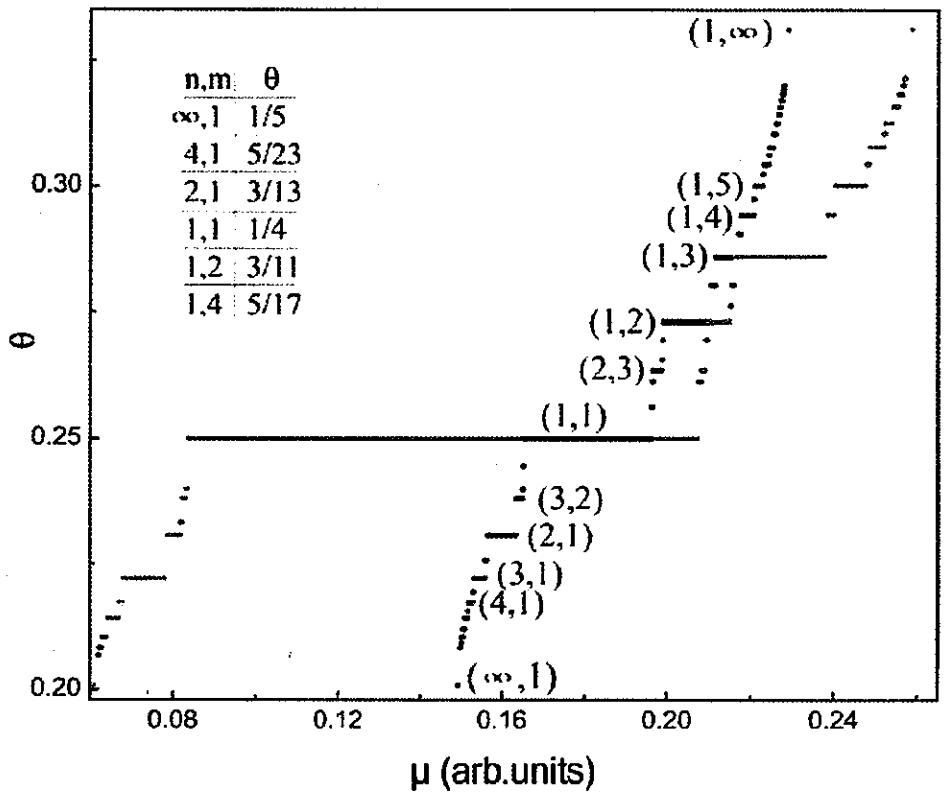

Figure 4.1 Stability curve (black) of a novel "devil's staircase" discovered on the system of Pb/Si(111) between coverage 6/5 ML and 4/3 ML. The generating phases are $\sqrt{7} \times \sqrt{3}$ ($\theta = 6/5$ ML) and $\sqrt{3} \times \sqrt{3}$ ($\theta = 4/3$ ML). These two generating phases have their $[1\bar{1}0]$ dimensions differ by two lattice constants $a_0/2$, while for a normal staircase they differ by one. The stability curve (red) of a normal staircase is also given for comparison. The novel staircase is much steeper. Mathematically this is a continuous function, with infinite number of phases whose coverage is a rational number (see left-top corner of figure for example). Some phases have significant width $\Delta\mu$ (stable) while others not. In experiments one expects to see only the most stable phases as shown in this figure.

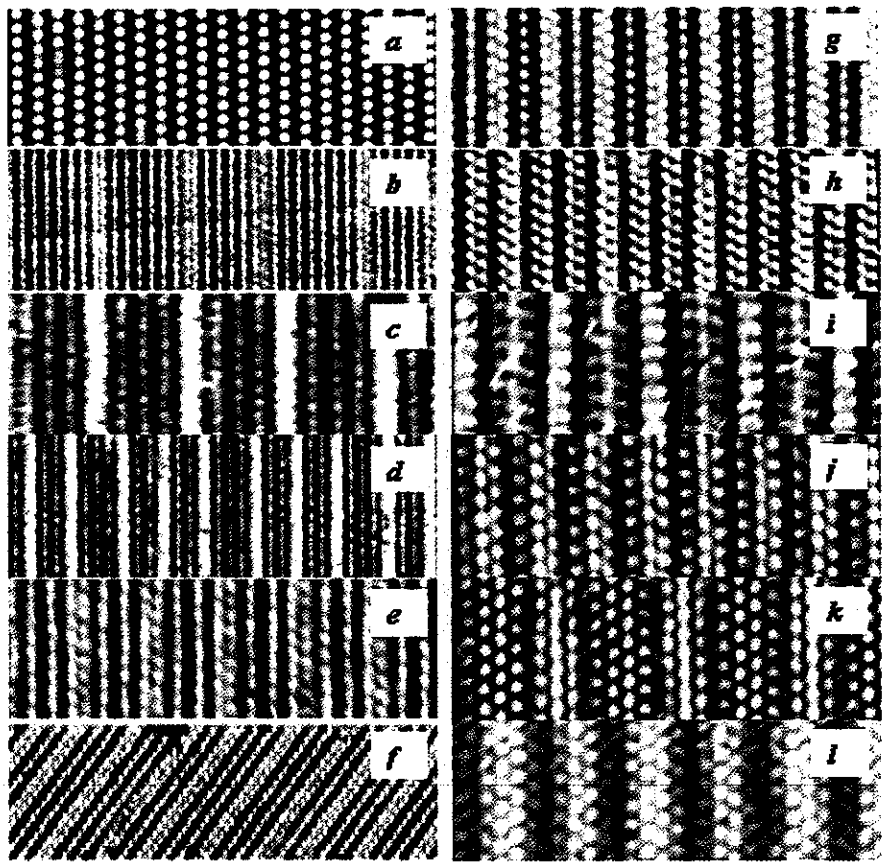

Figure 4.2 STM images (tunneling voltage 1.5V) showing small patches of linear phases observed for Pb/Si(111) with coverage between 6/5 ML and 4/3 ML. The dark columns are $\sqrt{7}\times\sqrt{3}$while the bright columns are $\sqrt{3}\times\sqrt{3}$ sub cells. (a) Initial phase $\sqrt{7}\times\sqrt{3}$, θ = 6/5 = 1.2 ML; (b) (7, 1) and (5, 1), θ = 1.21 ML; (c) (4, 1), θ = 1.217 ML; (d) (4, 1) and (3, 1), θ = 1.220 ML; (e) (3, 1), θ = 1.222 ML; (f) (3, 1) and (2, 1), θ = 1.223 ML; (g) (2, 1), θ = 1.231 ML; (h) (1, 1), θ = 1.25 ML; (i) (1, 1) and (1, 2), θ = 1.263 ML; (j) (1, 2), θ = 1.27 ML; (k) (1, 2) and (1, 3), θ = 1.28 ML; and (k) (1, 3), θ = 1.285 ML.

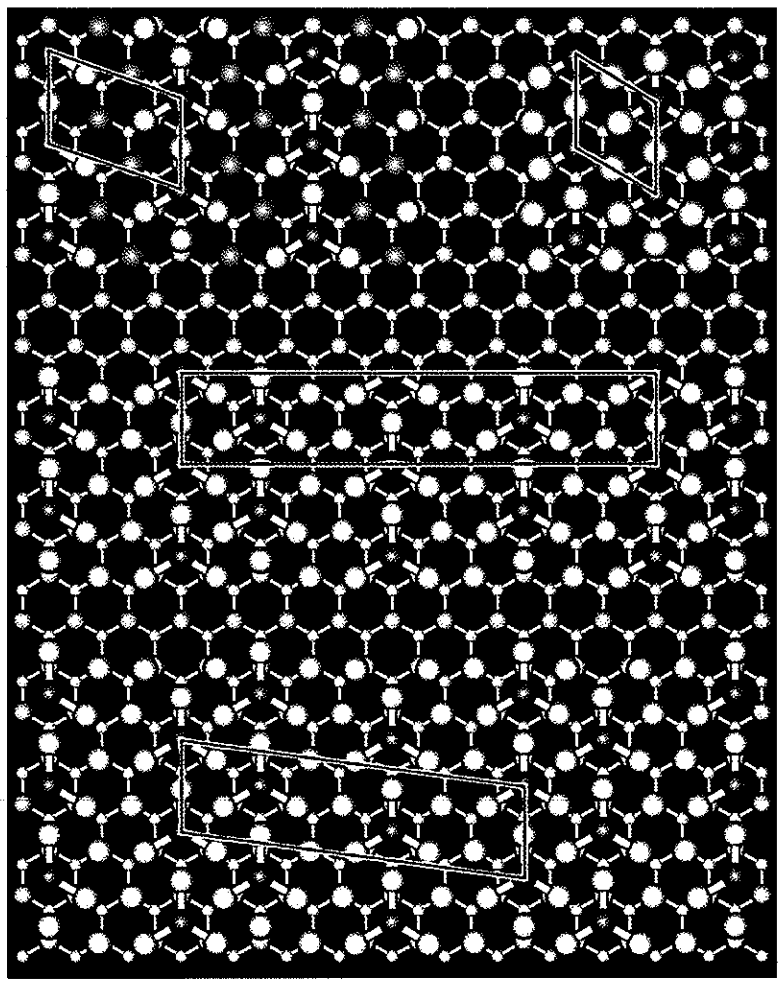

Figure 4.3 Model of tow of the "devil's staircase" phases of Pb/Si(111) and the generating phases, with high symmetry atoms (red) occupying H3 sites. Silicon atoms are in yellow color, while green and gray atoms are off-centered T1 Pb atoms. The top left is a $\sqrt{7} \times \sqrt{3}$ unit cell, while the top right is $\sqrt{3} \times \sqrt{3}$. The middle is the unit cell of (3, 1) phase, i.e., there are three $\sqrt{7} \times \sqrt{3}$ and one $\sqrt{3} \times \sqrt{3}$ sub cells in the unit cell. The bottom is a (2, 1) unit cell.

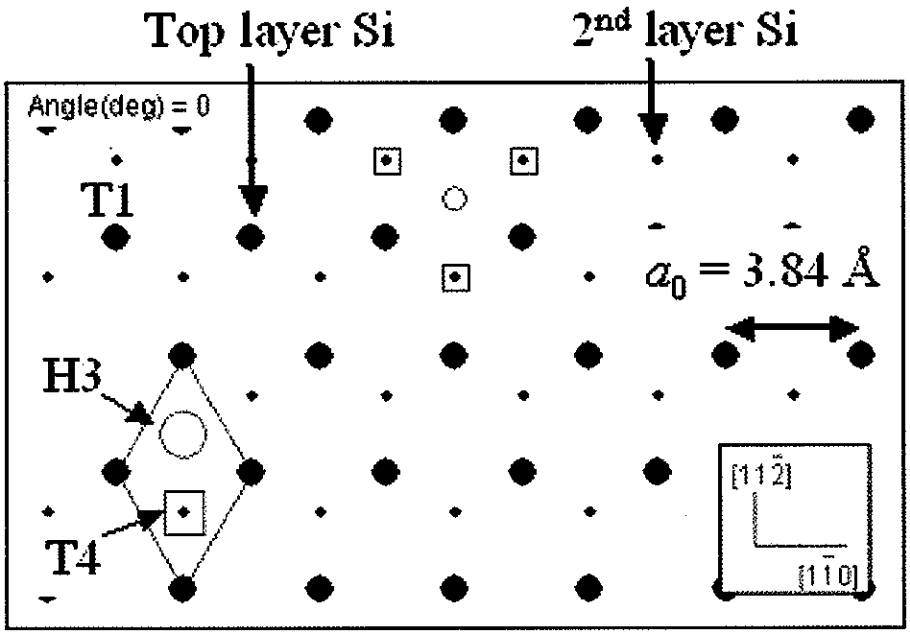

Figure 4.4 Si(111) surface with a rhombic unit cell. The lattice constant is $a_0 = 3.84$ Å. Large filled circles are top layer Si atoms, while small dots are second layer Si atoms. The high symmetry sites H3 and T4 are drawn in empty circles and empty squares, respectively. H3 site is a "hole" with three nearest neighbors. T4 sites are on top of a second layer atom with four nearest neighbors. Each H3 (T4) site is surrounded by three T4 (H3) sites, as shown in the top center of the figure. The binding energy of a H3 is slightly lower (4 meV/atom [48]) than that of a T4 site. A T1 site is on top of a top-layer Si atom that has only one nearest neighbor, as indicated in the figure.

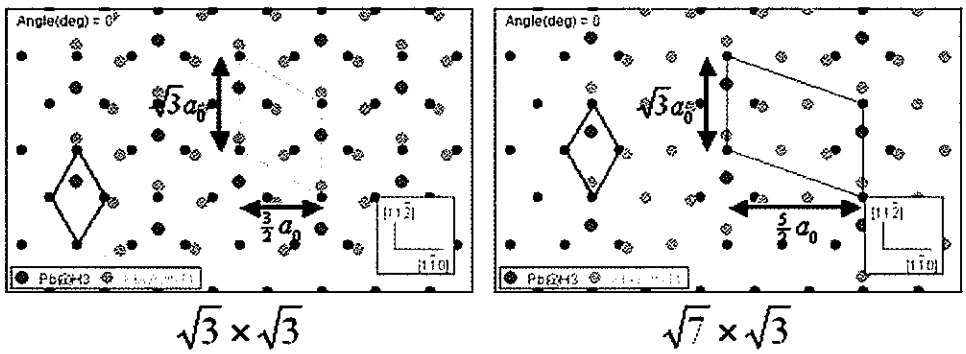

Figure 4.5 Full model of $\sqrt{3} \times \sqrt{3}$ ($\theta = 4/3$ ML, dimensions $\frac{3}{2}a_0 \times \sqrt{3}a_0$) and $\sqrt{7} \times \sqrt{3}$ ($\theta = 6/5$ ML, dimensions $\frac{5}{2}a_0 \times \sqrt{3}a_0$) phases. Black circles are top layer Si atoms, red and gray circles are Pb atoms. The $\sqrt{3} \times \sqrt{3}$ phase has four Pb atoms in its unit cell, three of them (gray) are slightly shifted from the center of T1 (off-centered T1) sites and the high symmetry atom (red) is on H3 site. The $\sqrt{7} \times \sqrt{3}$ phase has six atoms in its unit cell, five of them (gray) are on off-centered T1 sites and the high symmetry atom (red) on H3 site. The coordinates of atoms are obtained from x-ray diffraction experiments [46] and first principle calculations [47]. In this work only high symmetry atoms were used in the calculations to reduce the complexity.

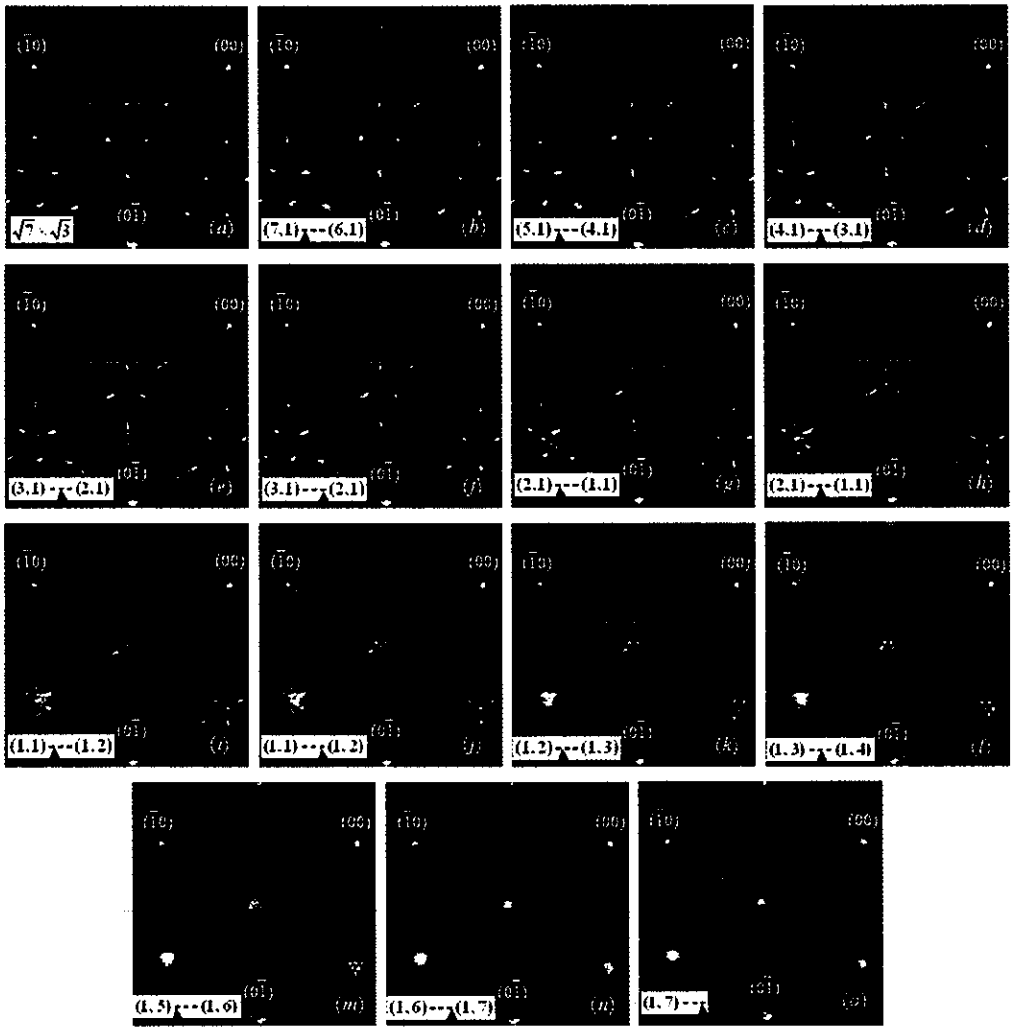

Figure 4.6 Two-dimensional diffraction patterns (1.2Bz×1.2Bz, centered at $(\overline{1}/3, \overline{1}/3)$ position) of some of the "devil's staircase" phases of Pb/Si(111), obtained after step-wise low temperature deposition ($T_{dep} \sim 120$ K, $\Delta\theta \sim 0.006$ ML). Coverage is lowest for (a) and highest for (o). The dashed triangles correspond to the pattern of $\sqrt{7} \times \sqrt{3}$. The main phases identified are listed at the lower left corner in each sub figure. The corresponding coverage's on the surface are indicated by a small black triangle. The patterns are essentially an equilateral triangle centered at the $(\overline{1}/3, \overline{1}/3)$ position, with the height decreases monotonically with coverage from $\frac{\sqrt{3}}{5}$ Bz in (a) to almost 0 in (o). The sudden change in height and orientation of triangle from (i) to (j) corresponds to a change in high symmetry site occupation.

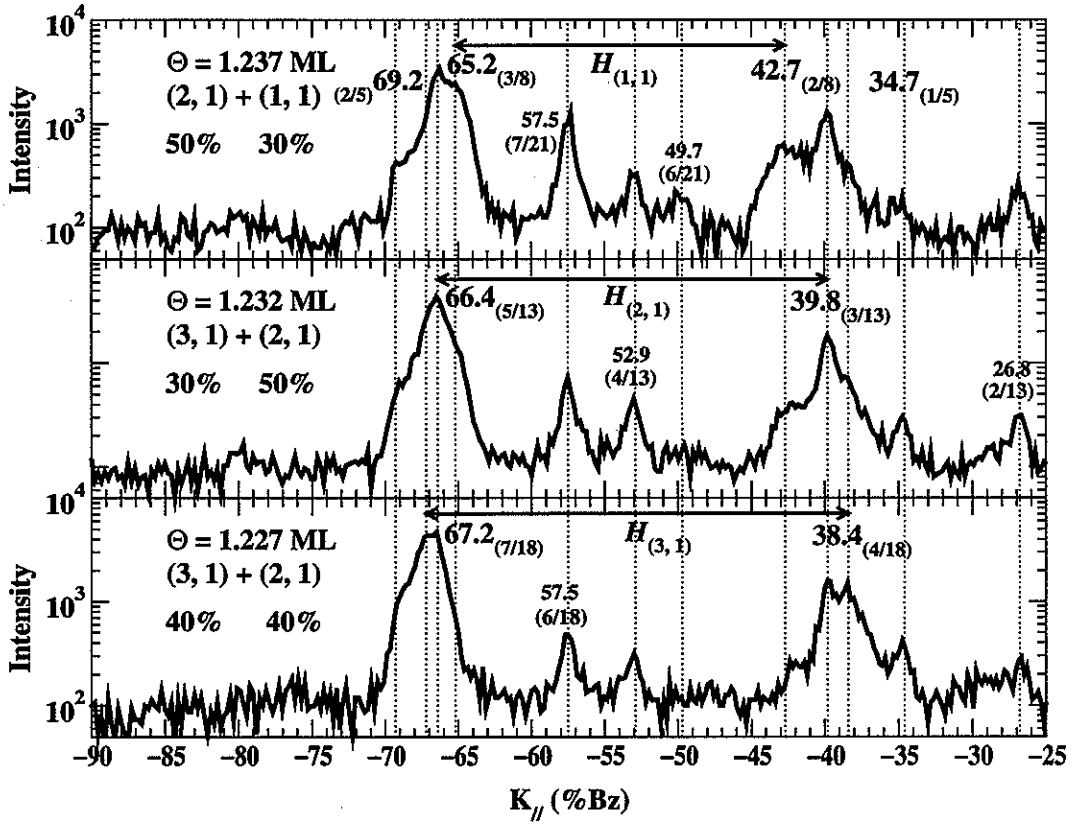

Figure 4.7 One-dimensional diffraction patterns that correspond to figure 4.6(e) through (g) (bottom to top). These scans show the followings: 1) the majority (nearly 80%) of the surface was covered by only two phases; 2) observable change of phase, indicated by shifts in positions and changes in intensity of spots, happened at $T \sim 120$ K with a coverage difference of only 0.006ML. Positions of spots and their corresponding fractional indices are listed. Spots from the same phase shall have the same denominator in their indices. For example, the bottom scan has spots at 38.4%Bz (4/18), 57.5%Bz (6/18), and 67.2%Bz (7/18), which are from phase (3, 1); and spots at 26.8%Bz (2/13), 39.8%Bz (3/13), 52.9%Bz (4/13), and 66.4%Bz (5/13), which are from phase (2, 1). The triangle height H of one of the main phases are indicated by arrows.

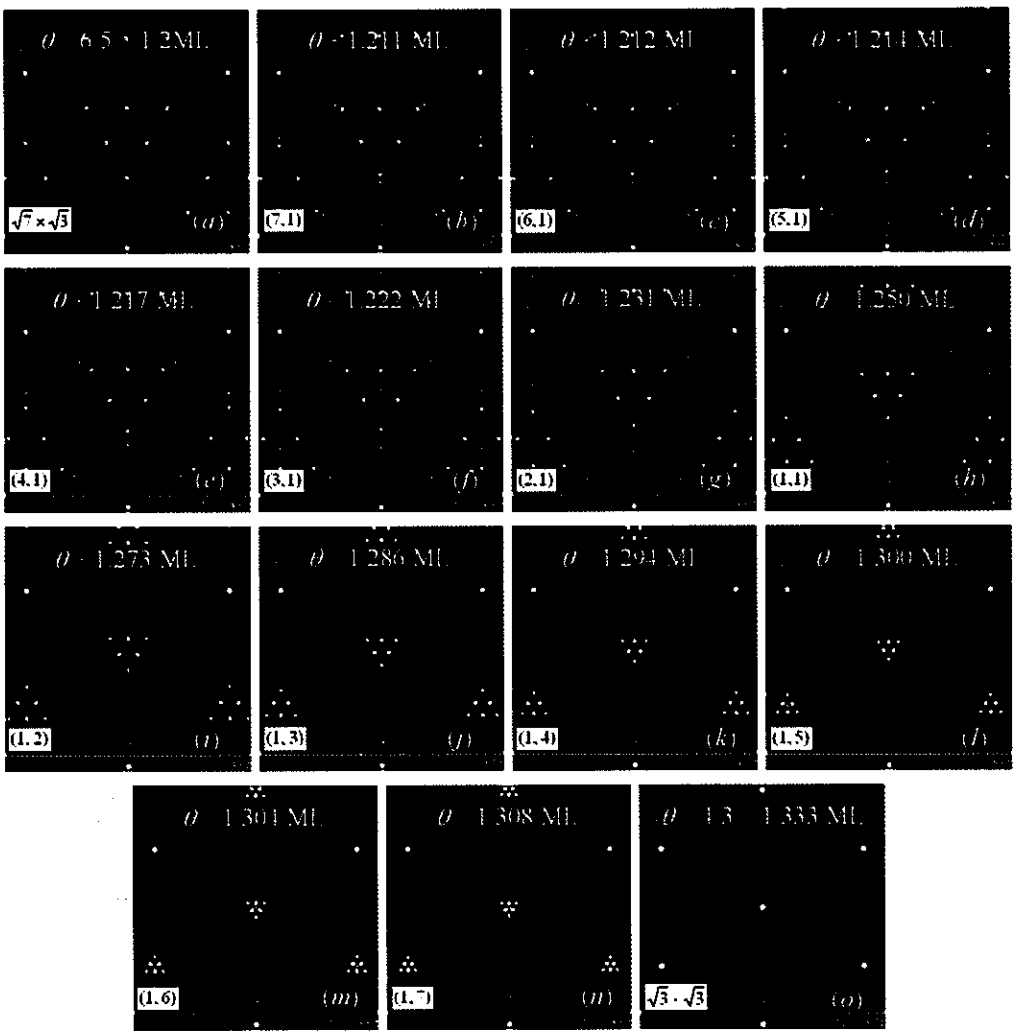

Figure 4.8 Kinematic calculations, including only high symmetry atoms on H3 sites, of diffraction pattern of some of the "devil's staircase" phases (1.2Bz × 1.2Bz, centered at (1/3, 1/3)). Triangles in dashed lines correspond to the $\sqrt{7} \times \sqrt{3}$ pattern. The patterns are essentially equilateral triangles centered at (1/3, 1/3) and (2/3, 2/3) spots. Starting from the lowest coverage 6/5 ML up to the highest 4/3 ML, the pattern evolves from a triangle with a height of $\frac{\sqrt{3}}{5}$ Bz down to a single spot at its center. The sudden change of height and orientation of triangle in figure 4.6 from (i) to (j) is not seen here. Further calculations show that this sudden change corresponds to a change in high symmetry site occupation.

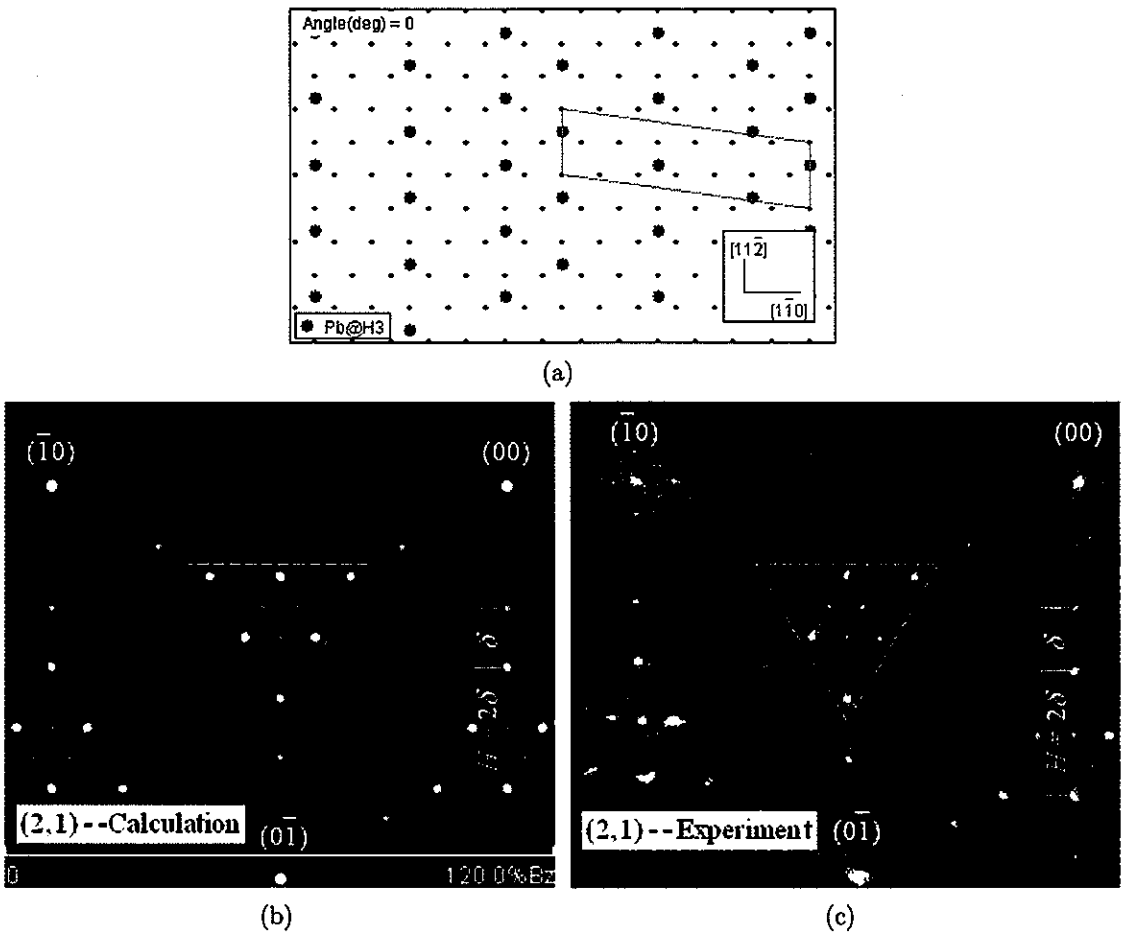

Figure 4.9 Comparison between experimental results and kinematic calculation of the diffraction pattern of (2, 1) phase ($\theta = 1.231$ ML). (a) Model of (2, 1) phase including only high symmetry atoms on H3 sites. (b) Kinematic calculation. (c) Experimental results made by depositing 0.3 ML of Pb on $\sqrt{7} \times \sqrt{3}$ phase at 120 K, followed by annealing to 400 K. The extra Pb atoms could have possibly formed small islands at step edges [49]. The dashed triangles correspond to the diffraction pattern of $\sqrt{7} \times \sqrt{3}$ phase. The calculation (b) shows six bright spots forming a triangle, three weaker spot outside, and three even weaker ones inside. The experiment shows exactly the same pattern, except that one corner of the triangle is missing. This missing corner was seen in all equivalent orientations in a larger view. Such a result could be due to dynamical effects or the off-centered T1 atoms, which are neglected in the calculations. Note that the relation $H = n\delta$ (Appendix A) is seen from both calculation and experiment.

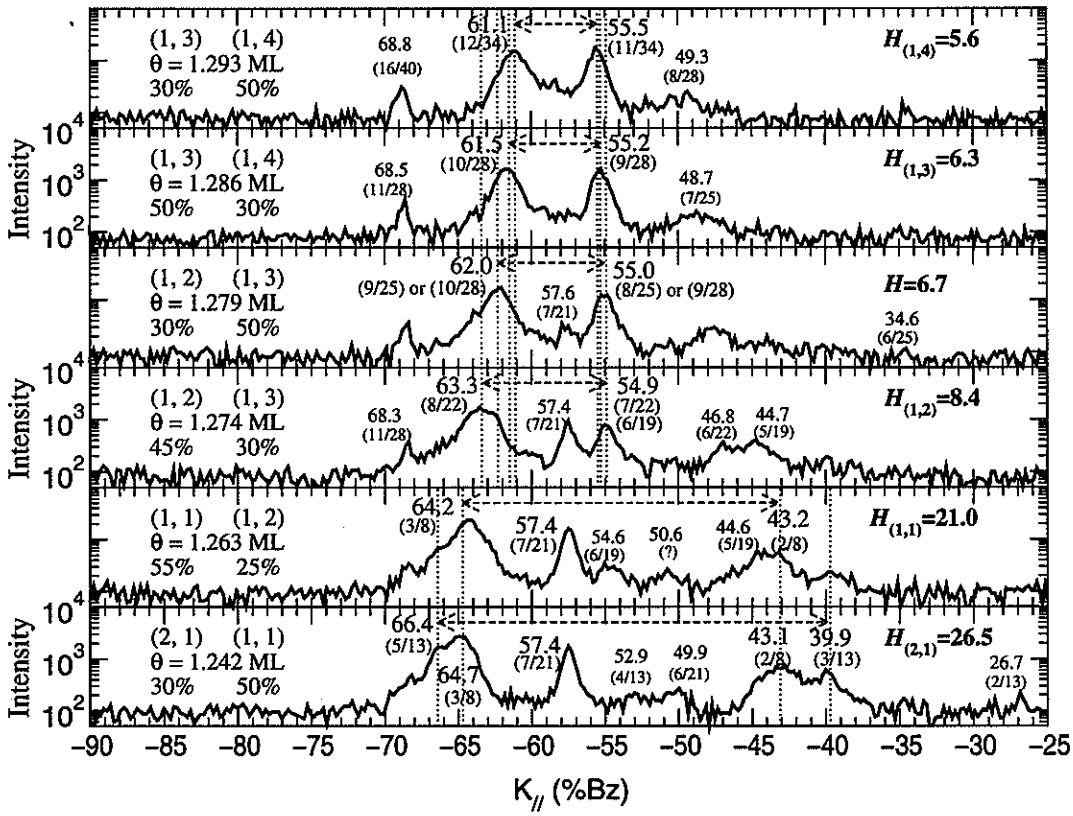

Figure 4.10 One-dimensional scans along the diagonal of the Brillouin zone, taken after successive steps of deposition ($\Delta\theta \sim 0.006$ ML). Observable changes are seen after each step. Coverage is lowest at the bottom and highest at the top. The triangle height has a sudden change between the second and third scans, corresponding to the "break" at $\theta \sim 1.25$ ML in figure 4.11. The H3-T4 occupation change can explain such a change.

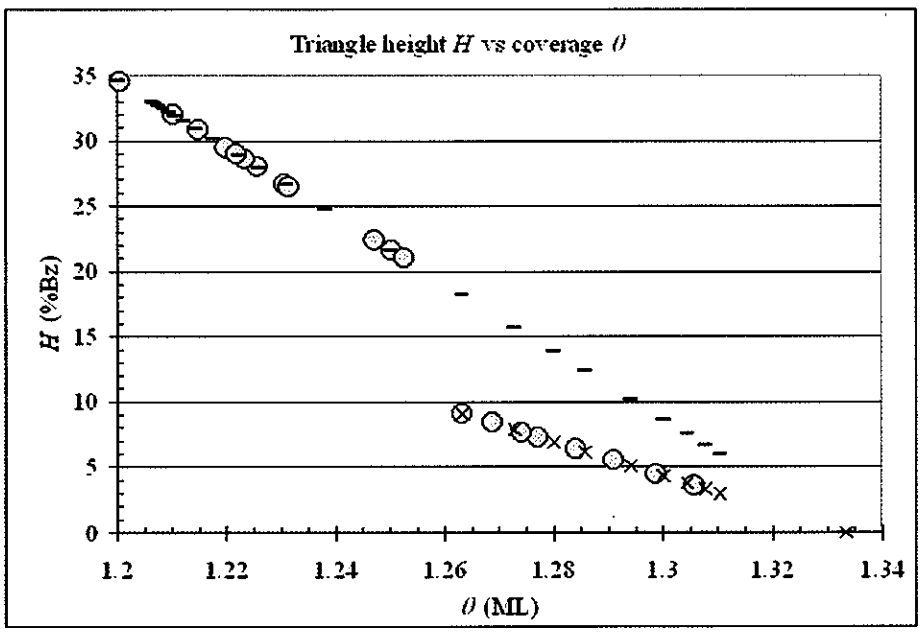

Figure 4.11 Triangle height H vs coverage θ from both experiments and calculations, a linearly decreasing relation is clear seen. Experimentally phases were identified by matching spots in 1D scans along $[1\bar{1}0]$, then coverage calculated by Eq. (A.5). Minus (H3-H3) and cross sings (H3-T4) are from kinematic calculations of the $(n, 1)$ and $(1, m)$ phases. Solid circles are experimentally measured. For $\theta < 1.25$ ML, all phases have high symmetry atoms on H3 sites only. At $\theta > 1.25$ ML, experimental data coincide with H3-T4 line instead of the H3-H3 line. The break at $\theta \sim 1.25$ ML, corresponding to the sudden change in triangle height in figure 4.6(j).

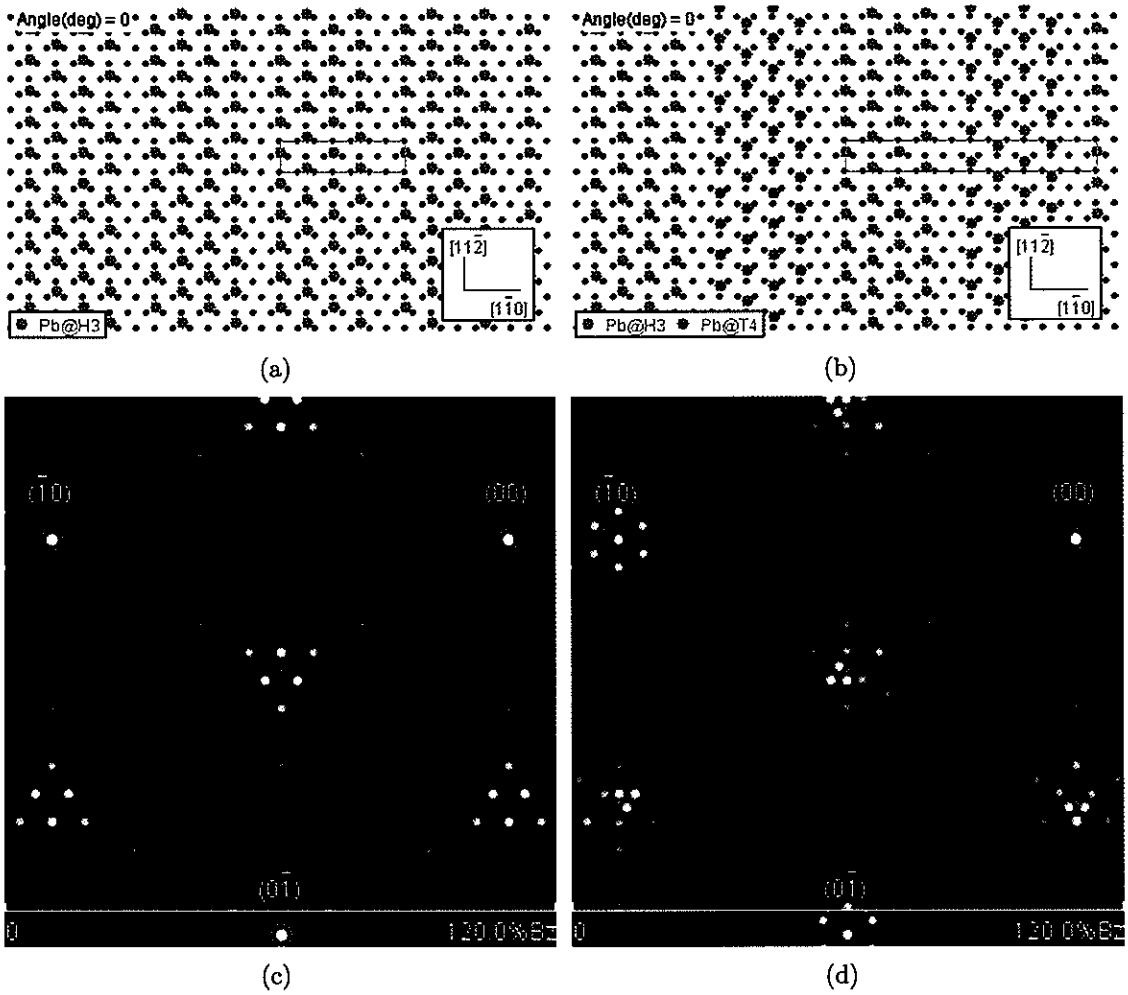

Figure 4.12 Comparison between the diffraction patterns of H3-H3 occupation and H3-T4 occupation for (1, 3) phase. The left column shows the H3-H3 case, while the right column shows the H3-T4 case. The main differences between them are: 1) the separation between bright spots in H3-T4 case is smaller than that in H3-H3 case; 2) the triangle in H3-T4 case is in opposite orientation as in H3-H3 case; 3) there are satellite spots around (10) in H3-T4 case and not in H3-H3 case. For simplicity in modeling the H3-T4 case for calculation, we combined one (1, 3) unit cell on H3 with one cell on T4 sites to form a new unit cell, the three main features observed in experiments were obtained.

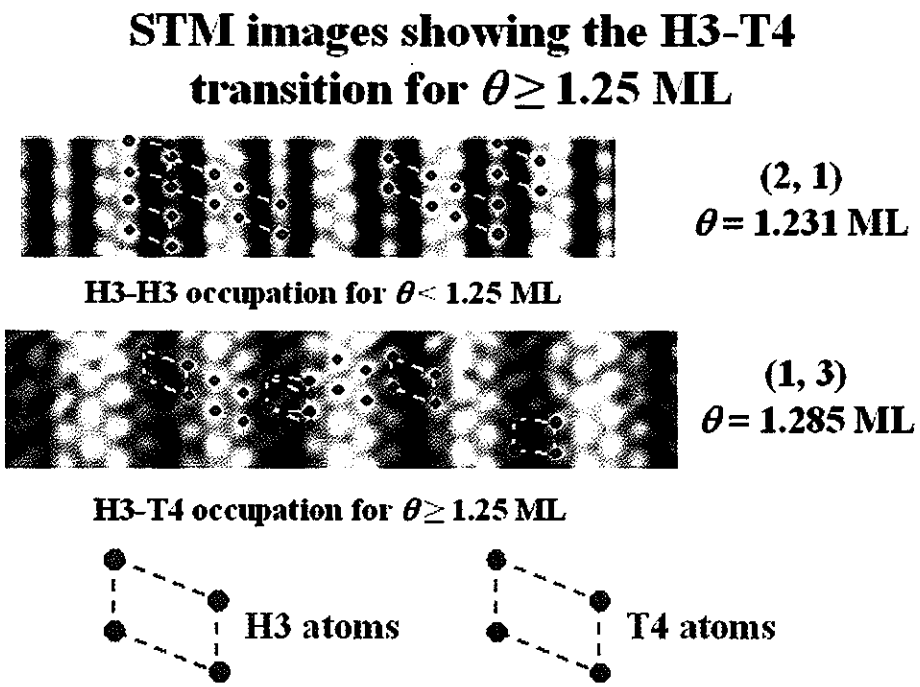

Figure 4.13 STM images (tunneling voltage 1.5V) of the (2, 1), and (1, 3) phases, showing H3-H3 occupation for $\theta < 1.25$ ML (the (2, 1) phase) and H3-T4 occupation for $\theta \geq 1.25$ ML (the (1, 3) phase). The red circles correspond to Pb atoms occupying H3 sites, while blue circles correspond to atoms on T4 sites. All high symmetry atoms are on H3 sites for the (2, 1) phase, while there are both H3 and T4 atoms for the (1, 3) phase. The parallelograms across dark rows with same color atoms correspond to the $\sqrt{7} \times \sqrt{3}$ unit cells, which are different from those with atoms of different colors. The top-left of (2, 1) image and center of (1, 3) image show that atoms fit into one cell won't fit into the other. It is interesting to note that such change of binding sites happens only at "$\sqrt{7} \times \sqrt{3}$" cells and not at $\sqrt{3} \times \sqrt{3}$ cells. The smaller parallelograms in the bright rows of the (1, 3) phase image correspond to $\sqrt{3} \times \sqrt{3}$ unit cells, which match all the atoms in the bright rows without having to change the binding sites in adjacent rows.

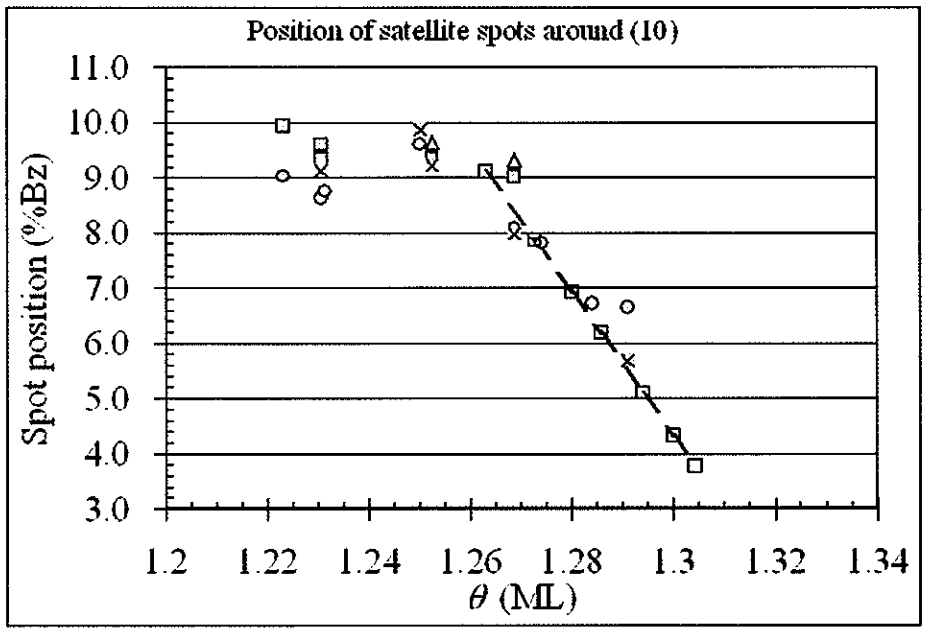

Figure 4.14 Position of satellite spots around (10) spot, measured from (10) spot, with coverage. The coverage is not the total coverage of the surface, but rather of the main phases present on the surface. The positions are roughly constant when $\theta < 1.25$ ML, and starts to move towards (10) spot at $\theta \sim 1.25$ ML, where the sudden change of triangle height happens. The empty squares on the dashed line are the expected spot position for $(1, m)$ phases with H3-T4 occupation. Experimental results (solid symbols) agree with this line very well for $\theta > 1.25$ ML.

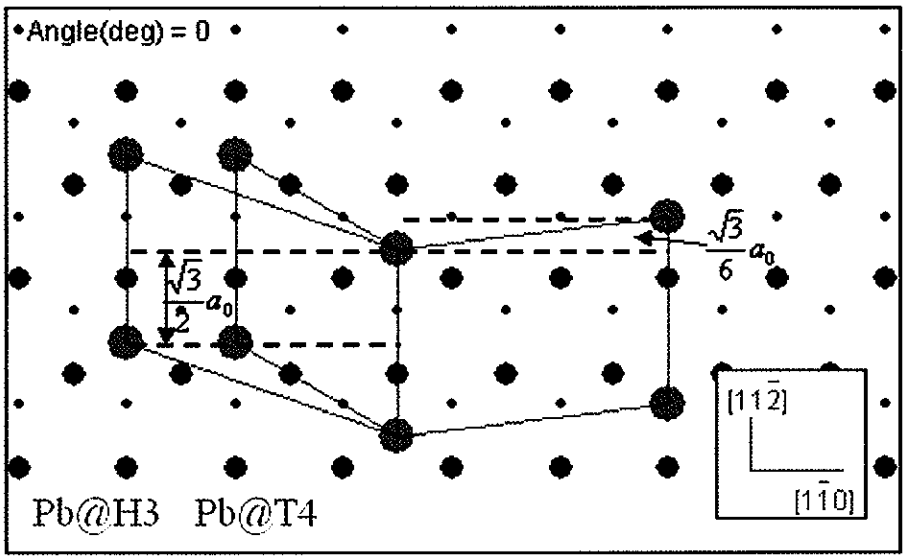

Figure 4.15 Schematic of inter-atomic separation between H3 sites and T4 sites across a $\sqrt{3} \times \sqrt{3}$ and $\sqrt{7} \times \sqrt{3}$ unit cell. The $[11\bar{2}]$ separation between two such H3 sites is $\frac{\sqrt{3}}{2}a_0$, while that between a H3 and a T4 site is $\frac{\sqrt{3}}{6}a_0$. The $\frac{\sqrt{3}}{2}a_0$ between H3 sites determines the fundamental diffraction spots (± 10), (± 10), $\cdots$ in $[11\bar{2}]$. When a unit cell of a certain phase has both kinds of high symmetry atoms, the additional $\frac{\sqrt{3}}{6}a_0$ separation, which is $\frac{1}{3} \times \frac{\sqrt{3}}{2}a_0$, will superimpose a $3\times$ period onto the regular spots in $[11\bar{2}]$. That is, the (± 10) and (± 20) spots will be different from the regular spots (00) and (± 30).

CHAPTER 5. General conclusions

This thesis was developed to address the following questions for the Pb/Si(111) system:

1. Is it possible to control the nano-structure growth by changing the initial substrate?
2. Is the nucleation theory applicable to the case of the 7-step growth mode?
3. What phase or phases could be formed between coverage 6/5 ML and 4/3 ML?

The first question was answered in chapter 2, different growth results were observed for different initial substrate, suggesting the possibility of controlling nano-structure growth by selecting the initial substrate. The applicability of nucleation theory was determined to be unclear in chapter 3, from the results that the saturation island density does not depend on deposition rate, in contrary to the prediction of nucleation theory. Chapter 4 revealed a novel "devil's staircase" in Pb/Si(111) within the coverage range 6/5 ML and 4/3 ML. Low temperature deposition experiments showed high order of self-organization in such a system. Theoretical studies are needed to understand such a low temperature behavior.

In general, this thesis provides possibilities of controlling nano-structure growth, which can be possibly an indication for future application. It also raises interesting questions in fundamental researches: a modified theory of nucleation is needed, and a detailed study of low temperature behavior is required. Details of the conclusions in each of the chapters are collected in the following sections.

Control of nano-structure growth

Self-organized islands of uniform heights can form at low temperatures on metal/semiconductor systems as a result of quantum size effects (QSE), i.e., the occupation of discrete electron energy levels in the film. We have examined the role of the metal/semiconductor interfaces by comparing the growth mode on two different substrates (Si(111)-(7×7) vs Si(111)-Pb($\sqrt{3} \times \sqrt{3}$)) measured with Spot Profile Analysis (SPA-LEED). For the same growth conditions (of coverage and temperature) 7-step islands are the most stable islands on the (7×7) phase while 5-step (but larger islands) are the most stable islands on the ($\sqrt{3} \times \sqrt{3}$). A theoretical calculation, based on the difference in the Fermi levels across the interface, suggests that the height selection on the two interfaces can be attributed to differences in their electronic structure and the amount of charge transfer at the interface. The practical significance of these experiments is that they demonstrate that it is possible to select in another way ,(i.e. by varying the starting phase of the substrate), the preferred island height and to control the type of nano-structures formed in epitaxy.

Applicability of nucleation theory

In the nucleation study, both temperature and deposition rate dependence experiments were carried out to determine the applicability of the theory. The rate dependence results show no dependence of saturation island number density on the deposition rate, in contrary to the expectation, suggesting a limited applicability of the nucleation theory on this system. A different theory considering "non-traditional" QSE-based nucleation behavior has to be developed. The temperature dependence results indicate that most likely the smallest possible stable cluster is a tetramer. Recent STM study [5] indicated the critical size is either $i = 3$ or $i = 4$, by comparing the theoretical scaling function to the measured island size distribution for different coverage at $T = 208$ K. This result

is consistent with our conclusion. However, the attempt frequencies determined from the same experiments favor $i = 4$. Theoretical calculations on the binding energies of critical clusters are needed to determine the migration barrier.

A novel "devil's staircase"

The discovery of a "devil's staircase" in Pb/Si(111) between 6/5 ML and 4/3 ML answered the question in the literature about the correct phase or phases formed during this coverage range. Step-wise deposition experiments showed different "devil's staircase" phases can be observed after only a change of $\Delta\theta \sim 0.006$ ML, at low temperatures ($T \sim 120$K) where atoms are not expected to be mobile. The extraordinary amount of atom rearrangement necessary for these phases to form indicates an unusual degree of self-organization at low temperatures is possible. Further theoretical studies are needed to understand such an unexpected low temperature behavior.

APPENDIX A. Diffraction pattern of the "devil's staircase" phases of Pb/Si(111)

Coverage of a (n, m) phase

In real space, these phases have high symmetry Pb atoms, occupying H3 sites, lined up and separated by $\sqrt{3}a_0$ in $[11\bar{2}]$, and have different repeated structure for different phases in $[1\bar{1}0]$, that is, their unit cell dimensions vary only in $[1\bar{1}0]$ and therefore their diffraction patterns vary only in the diagonal of Brillouin zone. As shown in figure 4.5 the unit cell dimensions of $\sqrt{7} \times \sqrt{3}$ and $\sqrt{3} \times \sqrt{3}$ phases are,

$$\begin{aligned} 5/2a_0 \times \sqrt{3}a_0 \qquad & \text{for } \sqrt{7} \times \sqrt{3} \\ 3/2a_0 \times \sqrt{3}a_0 \qquad & \text{for } \sqrt{3} \times \sqrt{3}. \end{aligned} \tag{A.1}$$

Therefore, for any of the (n, m) phases, the unit cell dimensions are given by

$$(\frac{5}{2}n + \frac{3}{2}m)a_0 \times \sqrt{3}a_0. \tag{A.2}$$

The fractions of the surface area covered by each of the two generating phases are then given by, respectively,

$$\begin{aligned} x_3 &= \frac{\frac{3}{2}ma_0 \times \sqrt{3}a_0}{\frac{5n+3m}{2}a_0 \times \sqrt{3}a_0} = \frac{3m}{5n+3m}, \\ x_5 &= \frac{\frac{5}{2}na_0 \times \sqrt{3}a_0}{\frac{5n+3m}{2}a_0 \times \sqrt{3}a_0} = \frac{5n}{5n+3m}. \end{aligned} \tag{A.3}$$

The quantity x_3 means the fraction of the surface area covered by $\sqrt{3} \times \sqrt{3}$, while x_5 means that by $\sqrt{7} \times \sqrt{3}$. The reason for using 3 and 5 as subscripts is because the

dimensions of the two phases in $[1\bar{1}0]$ are $\frac{3}{2}a_0$ and $\frac{5}{2}a_0$. Obviously the two quantities must satisfy the relation

$$x_3 + x_5 = 1 \tag{A.4}$$

The fraction x_3 goes up from 0 to 1, while x_5 goes down from 1 to 0, as the phase changes from $\sqrt{7} \times \sqrt{3}$ to $\sqrt{3} \times \sqrt{3}$. The coverage of such a phase is given by,

$$\theta = \frac{6}{5}x_5 + \frac{4}{3}x_3 = \frac{6n+4m}{5n+3m}, \tag{A.5}$$

which lies between 6/5 ML and 4/3 ML.

The diffraction pattern

As mentioned earlier, a (n, m) phase consists of n $\sqrt{7} \times \sqrt{3}$ and m $\sqrt{3} \times \sqrt{3}$ sub cells in its unit cell. Therefore, the higher the value of n is, the more $\sqrt{7} \times \sqrt{3}$ sub cells there are in the unit cell, and hence the lower coverage the phase is. On the other hand, the higher the value of m is, the more $\sqrt{3} \times \sqrt{3}$ sub cells are present, and the higher coverage of the phase. The diffraction patterns of the two generating phases are well known. The $\sqrt{3} \times \sqrt{3}$ phase has two spots in addition to the fundamental spots, located at (1/3, 1/3) and (2/3, 2/3) positions (figure A.1(a)). The $\sqrt{7} \times \sqrt{3}$ phase has two equilateral triangles with triangle height equals $\frac{\sqrt{3}}{5}$ Bz, centered at (1/3, 1/3) and (2/3, 2/3), respectively. Each of the two triangles consists of six spots, three at corners and three at the center of sides (A.1(b)). These patterns can be understood by comparing their atomic separations within the unit cell with that of the substrate. Take $\sqrt{7} \times \sqrt{3}$ for example, it is seen in figure 4.4 that the $\sqrt{7} \times \sqrt{3}$ has the same atomic separation $\frac{\sqrt{3}}{2}a_0$ in $[11\bar{2}]$ as the substrate Si(111). This means in reciprocal space there should be no difference between them in $[11\bar{2}]$. However, in $[1\bar{1}0]$, the substrate has atomic separation $\frac{1}{2}a_0$, while $\sqrt{7} \times \sqrt{3}$ phase has $\frac{5}{2}a_0 = 5 \times \frac{1}{2}a_0$. This indicates that in reciprocal space in $[1\bar{1}0]$, which is along the diagonal of the Si(111) Brillouin zone,

the $\sqrt{7} \times \sqrt{3}$ will have five spots. Since for Si(111) the diagonal of Brillouin zone has a length of $\sqrt{3}$ Bz (Bz $= |a_0^*|$, see Eq. (1.7)), the $\sqrt{7} \times \sqrt{3}$ spots are separated by $\frac{\sqrt{3}}{5}$ Bz in $[1\bar{1}0]$. The triangular shape formed by the six spots in $\sqrt{7} \times \sqrt{3}$ pattern is due to the 3-fold rotational symmetry of the substrate. Those six spots are the (1/5, 1/5) and (2/5, 2/5) spots in the three equivalent $[1\bar{1}0]$ orientations. Figure A.2 illustrates such a construction and the resultant triangle height. The center of the triangle is right at (1/3, 1/3) because the center of an equilateral triangle is 2/3 H away from its top vortex, which is the (1/5, 1/5) spot in this case, hence its distance from (00) spot in $[1\bar{1}0]$ is $\frac{\sqrt{3}}{5} \times (1+2/3) = \frac{\sqrt{3}}{5} \times 5/3 = \frac{\sqrt{3}}{3}$ Bz, exactly the position of the commensurate spot (1/3, 1/3). The pattern of $\sqrt{3} \times \sqrt{3}$ phase can be understood in the same way. The reason why it doesn't form a triangle is because the (1/3, 1/3) position is the intersection of the three equivalent $[1\bar{1}0]$ directions.

For a (n, m) phase such that $n \gg m$, the unit cell has much more $\sqrt{7} \times \sqrt{3}$ than $\sqrt{3} \times \sqrt{3}$ sub cells, the structure factor squared $|F(\Delta \boldsymbol{s})|^2$ is simply a broadened $\sqrt{7} \times \sqrt{3}$ pattern. While in the other limit, it is a broadened $\sqrt{3} \times \sqrt{3}$ pattern. The left column of figure A.3 shows the expected behavior of $|F(\Delta \boldsymbol{s})|^2$ for (7, 1) phase (bottom, $\theta =$ 1.211 ML) and (1, 7) phase (top, $\theta = 1.308$ ML): (7, 1) has a $\sqrt{7} \times \sqrt{3}$ like pattern while (1, 7) has $\sqrt{3} \times \sqrt{3}$ like pattern. After multiplying the long range cell factor $|G(\Delta \boldsymbol{s})|^2$, one expects that only the delta functions that are close to the local maxima of the structure factor can have significant intensity and others not. The center column of figure A.3 shows the $|G(\Delta \boldsymbol{s})|^2$ of the two phases, large number of spots are expected by this factor due to the large $[1\bar{1}0]$ dimension of their unit cells ($\frac{5}{2} \times 7 + \frac{3}{2} \times 1 = 19a_0$ for (7, 1) and $\frac{5}{2} \times 1 + \frac{3}{2} \times 7 = 13a_0$ for (1, 7)). The right column shows the product of $|F(\Delta \boldsymbol{s})|^2 |G(\Delta \boldsymbol{s})|^2$, many of the spots that are far away from the maxima of $|F(\Delta \boldsymbol{s})|^2$ do not survive. Because of these effects, if we start from the $\sqrt{7} \times \sqrt{3}$ phase and increase the coverage, the diffraction pattern of the "devil's staircase" phases should evolve from a $\sqrt{7} \times \sqrt{3}$ like pattern to a $\sqrt{3} \times \sqrt{3}$ like. A simple relation $H = n\delta$ between the

triangle height H and the minimum spot separation of the phase δ, was obtained from calculation. Figure 4.9 shows this relation $H = n\delta$ is easily verified both in calculation and experiment. A plot of the triangle height of $(n, 1)$ and $(1, m)$ phases vs their coverage (figure 4.11) shows that the triangle height decreases not only monotonically, but also linearly with coverage. This linear relationship can be shown to be a consequence of the simple relation $H = n\delta$.

Triangle height and the delta function separation — $H = n\delta$

As stated in Chapter 1, the spot positions are determined by the delta function part $|G(\Delta \boldsymbol{s})|^2$, therefore the height of the triangle must be an integral multiple of the delta function separation for that particular phase. The delta function separation for any of the "devil's staircase" phases (n, m) is given by

$$\delta = \frac{\sqrt{3}}{5n + 3m}. \tag{A.6}$$

It is so because the $[1\bar{1}0]$ spacing of its unit cell is $(5n + 3m)$ times that of the substrate (Eq. (A.2)). Hence such a phase shall have $5n + 3m$ spots along the diagonal of the Brillouin zone. The triangle height of this (n, m) phase is therefore

$$H = q\delta = \frac{q\sqrt{3}}{5n + 3m}, \tag{A.7}$$

where q is an integer. It was observed both in calculations and experiments that the value of q is exactly n, the number of $\sqrt{7} \times \sqrt{3}$ cells in the unit cell of the (n, m) phase. This relation can be understood for the $(n, 1)$ and $(1, m)$ phases as follows. For a $(n, 1)$ phase, the triangle height $H = q\delta$ is less than that of $\sqrt{7} \times \sqrt{3}$ phase, which is $\frac{\sqrt{3}}{5}$ Bz, that is,

$$\frac{q\sqrt{3}}{5n + 3m} < \frac{\sqrt{3}}{5} \rightarrow \frac{q}{5n + 3} < \frac{1}{5} \rightarrow q < n + \frac{3}{5}. \tag{A.8}$$

In earlier discussions we mentioned that only the delta functions that are closest to the maxima of structure factor can have significant intensity. In the case of a $(n, 1)$ phase,

the maxima of structure factor are close to the $\sqrt{7} \times \sqrt{3}$ pattern (see bottom-left of figure A.3). For the strongest spots to get as close to these maxima as possible, the separation $q\delta$ between them has to be as close to $\frac{\sqrt{3}}{5}$ Bz as possible. In other words, the number q has to take its maximum possible value, which is n by Eq. (A.8).

For the $(1, m)$ phases, the maxima of structure factor are close to $\sqrt{3} \times \sqrt{3}$ pattern (see top-left of figure A.3). The strongest spots are simply in the vicinity of (1/3, 1/3) spot. Since the unit cell length in $[1\bar{1}0]$ of a $(1, m)$ phase is always greater than that of the $\sqrt{3} \times \sqrt{3}$ phase, its delta-function separation is always smaller than $\frac{\sqrt{3}}{3}$ Bz. Therefore, the triangle height of a $(1, m)$ phase is simply equal to delta-function separation, or, $q = n = 1$.

For the experimentally observed $(n, 2)$ and $(2, m)$ phases, such a relation can also be obtained by assuming that monotonic decreasing relation is still true for these phase. See appendix B for details.

Triangle height H and coverage θ — linear, monotonically decreasing relation

We have argued that for the experimentally observed "devil's staircase" phases of Pb/Si(111), the triangle height is given by $H = n\delta$, where n is the number of $\sqrt{7} \times \sqrt{3}$ cells in their unit cells. We will show now that the triangle height H actually has a linear dependence on the coverage for the phases that satisfy the relation $H = n\delta$. Using the variables x_3 and x_5 defined by Eq. (A.3), and the relation Eq. (A.4), we can rewrite the triangle height and the coverage as

$$\theta = \frac{6}{5}x_5 + \frac{4}{3}(1 - x_5) = \frac{4}{3} - \frac{2}{15}x_5. \tag{A.9}$$

$$H = n\delta = \frac{\sqrt{3}}{5}x_5. \tag{A.10}$$

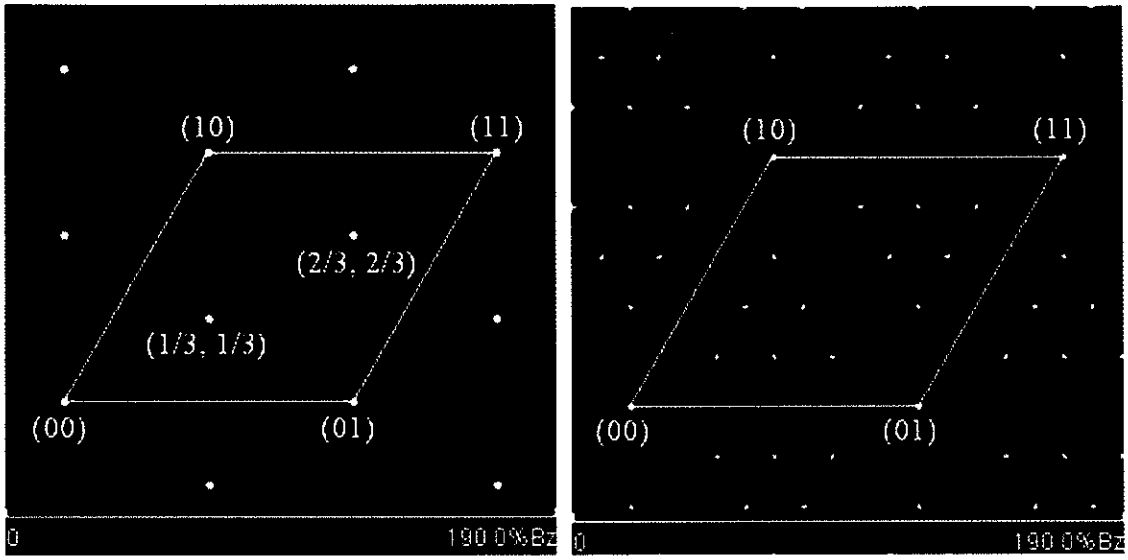

Figure A.1 Diffraction pattern of (a) ideal $\sqrt{3} \times \sqrt{3}$ and (b) ideal $\sqrt{7} \times \sqrt{3}$. The $\sqrt{3} \times \sqrt{3}$ phase has two spots in addition to the fundamental spots, located at (1/3, 1/3) and (2/3, 2/3) positions. The $\sqrt{7} \times \sqrt{3}$ phase has two equilateral triangles centered at the (1/3, 1/3) and (2/3, 2/3) positions. Each of the triangles consists of six spots, three at the corners, and three at the center of sides.

Eq. (A.9) and (A.10) state that both coverage and triangle height are linear in x_5, so they must be linearly dependent on each other. Combining the two we will get the explicit form

$$H = \frac{3\sqrt{3}}{2}(\frac{4}{3} - \theta). \tag{A.11}$$

Eq. (A.11) says that the triangle height is actually proportional to the coverage difference between the $\sqrt{3} \times \sqrt{3}$ and the (n, m) phase.

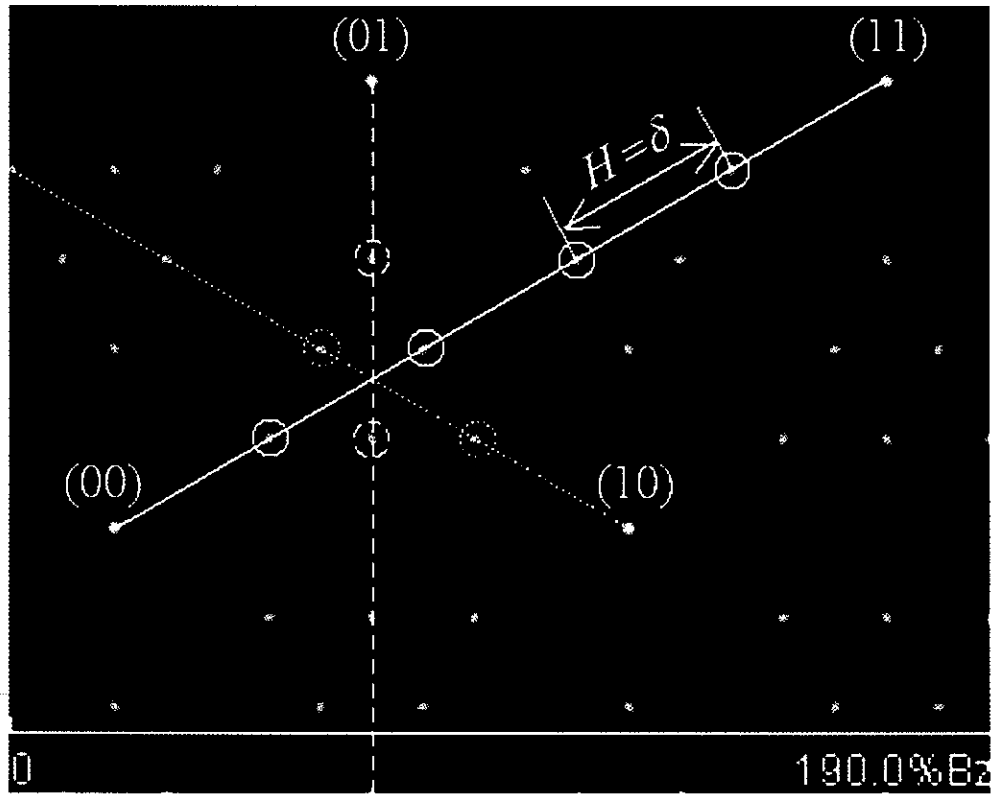

Figure A.2 Diffraction pattern of $\sqrt{7} \times \sqrt{3}$ phase: a triangle made of six spots (three at corners, three at the center of sides). The six spots are the (1/5, 1/5) and (2/5, 2/5) in all three equivalent $[1\bar{1}0]$ directions. The height of the triangle H is the separation between that two spots. The center of the triangle is the intersection of the three equivalent $[1\bar{1}0]$ lines, which is the commensurate (1/3, 1/3) position.

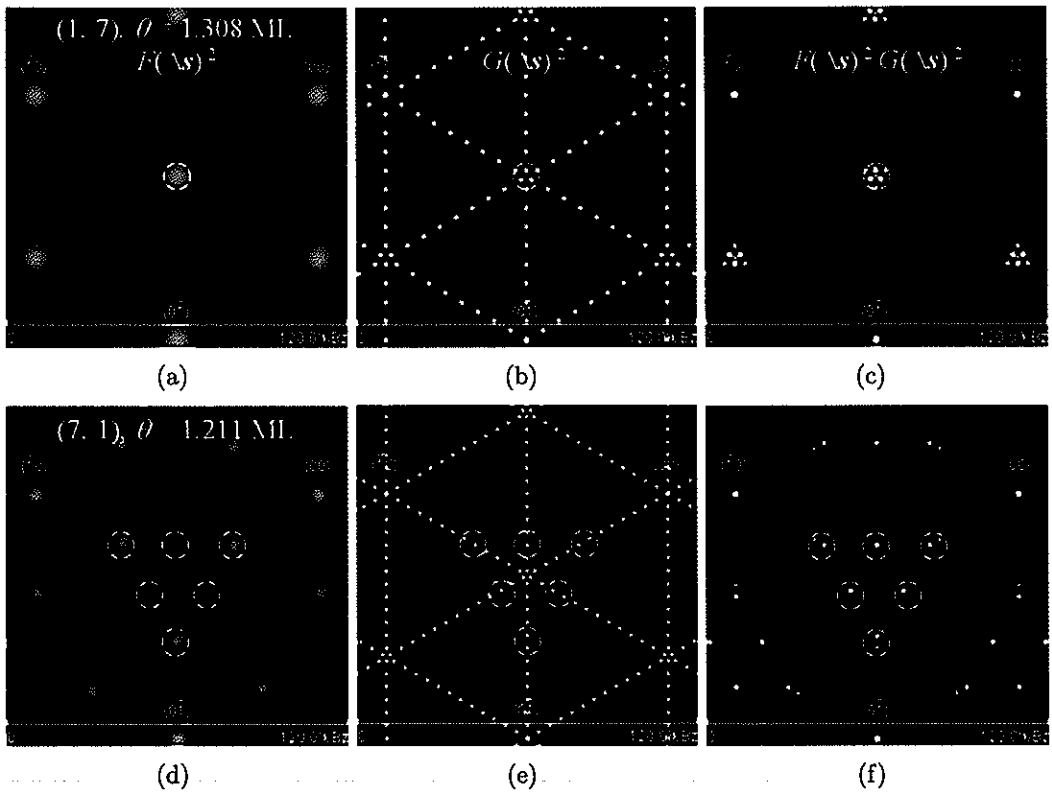

Figure A.3 Calculated structure factor squared $|F(\Delta \boldsymbol{s})|^2$ (left column), long range cell contribution $|G(\Delta \boldsymbol{s})|^2$ (center column), and diffraction pattern $|F(\Delta \boldsymbol{s})|^2 |G(\Delta \boldsymbol{s})|^2$ (right column) of (1, 7) phase (top, $\theta = 1.308$ ML) and (7, 1) phase (bottom, $\theta = 1.211$ ML). All calculations are centered at ($\overline{1}/3$, $\overline{1}/3$) commensurate position. This figure shows the followings: 1) for a $(n \gg 1, 1)$ phase its structure factor squared $|F(\Delta \boldsymbol{s})|^2$ is like a $\sqrt{7} \times \sqrt{3}$ pattern (equilateral triangle centered at (1/3, 1/3)), while that of a $(1, m \gg 1)$ phase is like a $\sqrt{3} \times \sqrt{3}$ (a single spot at (1/3, 1/3)). 2) Not all of the spots given by $|G(\Delta \boldsymbol{s})|^2$ will show up in the diffraction pattern, only the spots close to the local maxima (dashed circles) of $|F(\Delta \boldsymbol{s})|^2$ can survive.

APPENDIX B. $H = n\delta$ for the experimentally observed $(n, 2)$ and $(2, m)$ phases

We have argued that $H = n\delta$ holds for all of the $(n, 1)$ and $(1, m)$ phases in Appendix A, now we want to show that it is also true for the experimentally observed $(n, 2)$ and $(2, m)$ phases. Those phases include (5, 2), (3, 2), (2, 3) and (2, 5). All of them are constructed by two neighboring $(n, 1)$ or $(1, m)$ phases. For example, (5, 2) is constructed by combining (3, 1) and (2, 1) in its unit cell, while (2, 5) is by (1, 2) and (1, 3). Obviously, to better reflect their structures, (5, 2) phases should be labeled as [(3, 1), (2, 1)], and (2, 5) phases as [(1, 2), (1, 3)]. However, we will still keep the notation (5, 2) and (2, 5) because of 1) that they reflect the total number of generating phases in their unit cells and 2) that they give the same relation between triangle height and delta-function separation, $H = n\delta$ (to be shown below), as their parent phases. Actually, for any $(n, 2)$ or $(2, m)$ phase that can be constructed in the same way, we can show that the relation $H = n\delta$ will hold, assuming that monotonic decreasing relation is still true for these phase. Consider a $(n, 2)$ phase of such kind, it is constructed by two neighboring phases $(n1, 1)$ and $(n1 + 1, 1)$, with the requirement that the following relation be satisfied,

$$n = 2n_1 + 1. \tag{B.1}$$

In addition, we note that the triangle size of a $(n, 2)$ phase has to be between that of its two parent phases. This is understood by considering the fact that the coverage of a child generation phase is between that of its two parents, and the observation that the

triangle height decreases monotonically with coverage. These will lead to

$$
\begin{aligned}
& H_{(n_1,1)} < H_{(n,2)} < H_{(n_1+1,1)} \\
\rightarrow \quad & n_1\delta_{(n_1,1)} < q\delta_{(n,2)} < (n_1+1)\delta_{((n_1+1),1)} \\
\rightarrow \quad & \tfrac{n_1}{5n_1+3} < \tfrac{q}{5n+3(2)} < \tfrac{n_1+1}{5(n_1+1)+3} \\
\rightarrow \quad & \tfrac{n_1}{5n_1+3} < \tfrac{q}{5(2n_1+1)+3(2)} < \tfrac{n_1+1}{5(n_1+1)+3} \\
\rightarrow \quad & \tfrac{n_1[5(2n_1+1)+3(2)]}{5n_1+3} < q < \tfrac{(n_1+1)[5(2n_1+1)+3(2)]}{5(n_1+1)+3} \\
\rightarrow \quad & (2n_1+1) - \tfrac{3}{5n_1+3} < q < (2n_1+1) + \tfrac{3}{5(n_1+1)+3} \\
\rightarrow \quad & n-1 < q < n+1 \rightarrow q = n. \qquad \text{(B.2)}
\end{aligned}
$$

In the last step of Eq. (B.2) we have made use of Eq. (B.1) and the fact that $\frac{3}{5(n_1+1)+3} < \frac{3}{5n_1+3} < 1$.

For the $(2, m)$ phases, we follow the same procedure,

$$
\begin{aligned}
& \delta_{(1,(m_1+1))} < q\delta_{(2,m)} < \delta_{(1,m_1)} \\
\rightarrow \quad & \tfrac{1}{5+3(m_1+1)} < \tfrac{q}{5(2)+3(2m_1+1)} < \tfrac{1}{5+3m_1} \\
\rightarrow \quad & \tfrac{[5(2)+3(2m_1+1)]}{5+3(m_1+1)} < q < \tfrac{[5(2)+3(2m_1+1)]}{5+3m_1} \\
\rightarrow \quad & 2 - \tfrac{3}{5+3(m_1+1)} < q < 2 + \tfrac{3}{5+3m_1} \\
\rightarrow \quad & 2-1 < q < 2+1 \rightarrow q = n = 2. \qquad \text{(B.3)}
\end{aligned}
$$

Again we have used the fact that $\frac{3}{5+3(m_1+1)} < \frac{3}{5+3m_1} < 1$. Eq. (B.2) and (B.3) show that the relation $H = n\delta$ is true for all the $(n, 2)$ or $(2, m)$ phases that are constructed by two neighboring $(n, 1)$ or $(1, m)$ phases.

Bibliography

[1] K. Budde, E. Abram, V. Yeh, and M.C. Tringides, Phys. Rev. B 61, 10602 (2000).

[2] M. Hupalo, S. Kremmer, V. Yeh, L. Berbil-Bautista, E. Abram, M.C. Tringides, Surf. Sci. 493, 526-538 (2001).

[3] S. Stepanovskyy, V. Yeh, M. Hupalo, M.C. Tringides, Surf. Sci. 515, 187-198 (2002).

[4] S.H. Chang, W.B. Su, W.B. Jian, C.S. Chang, L.J. Chen, and Tien T. Tsong, Phys. Rev. B 65, 245401 (2002).

[5] W.B. Su, S.H. Chang, H.Y. Lin, Y.P. Chiu, T.Y. Fu, C.S. Chang, and Tien T. Tsong, Phys. Rev. B 68, 033405 (2003).

[6] L. Seehofer, G. Falkenberg, D. Daboul, and R.L. Johnson, Phys. Rev. B 51, 13503 (1995).

[7] K. Horikoshi and X. Tong, T. Nagao and S. Hasegawa, Phys. Rev. B 60, 13287 (1999).

[8] A. Petkova, J. Wollschlager, H.-L. Gunter, M. Henzler, Surf. Sci. 471, 11 (2001).

[9] H.H. Weitering, D.R. Heslinga, T. Hibma, Phys. Rev. B 45, 5991 (1992).

[10] F. Grey, R. Feidenhans'l, M. Nielsen, and R.L. Johnson, J. Phys. (Paris) 50, 7181 (1989).

[11] M. Hupalo, J. Schmalian, and M.C. Tringides, Phys. Rev. Lett. 90, 216106 (2003).

[12] M.K.Yakes, V. Yeh, M. Hupalo, and M.C. Tringides (submitted).

[13] C.S. Lent, and P.I. Cohen, Surf. Sci. 193, 121 (1984).

[14] P.R. Pukite, C.S. Lent, and P.I. Cohen, Surf. Sci. 161, 39 (1985).

[15] L. H. Zhao, E.Z. Luo, and M. Henzler, Appl. Phys. A 50, 595 (1990).

[16] M. Henzler, Appl. Phys. A 34 (1984) 205.

[17] Gavioli, K. R. Kimberlin, M. C. Tringides J. F. Wendelken, and Z. Zhang, Phys. Rev. Letts. 82, 129 (1999).

[18] J. Braun, J. P. Toennies, and Ch. Woll, Phys. Rev. B60, 11707, (1999)

[19] A. R. Smith, K. J. Chao, Q. Niu, C. K. Shih, Science 273, 226 (1996).

[20] L. Huang, S. Jay Chey, J. H. Weaver, Surf. Sci. 416 L1101 (1998).

[21] F. K. Schulte, Surf. Sci. 55, 427 (1976).

[22] P. J. Feibelman, Phys. Rev. B 27, 1991 (1983).

[23] P. J. Feibelman and D. R. Hamann, Phys. Rev. 29, 6463 (1984).

[24] I. P. Batra et. Al. Phys. Rev. B 34, 8246 (1986).

[25] N. Trivedi and N. Aschroft, Phys. Rev. B 38, 12298 (1988).

[26] B. J. Hinch, C. Koziol, J. P. Toennies, G. Zhang, Europh. Letts. 10(4), 341 (1989).

[27] M. Jalochowski, M. Hoffmann, and E. Bauer, Phys. Rev. B 51, 7231 (1995).

[28] A. Grottini, D. Cvetko, L. Floreano, R. Gotter, A. Morgante, and F. Tommasini, Phys. Rev. Letts. 79, 1527 (1997).

[29] I. B. Altefeder, D. M. Chen, and K. A. Matveev Phys. Rev. Lett. 78, 2815 (1997);Phys. Rev. Letts. 80, 4895 (1998).

[30] Z. Y. Zhang, Q. Niu, and C. K. Shih, Phys. Rev. Letts. 80, 5381 (1998).

[31] X. Tong, K. Horikosshi, S. Hasegawa Phys. Rev. B 60, 5653 (1999).

[32] D. R. Heslinga, H. H. Weitering, D. P. van der Werf, T. M. Klapwijk, and T. Hibma Phys. Rev. Lett. 64, 1589 (1990); H. H. Weitering, A. R. H. F. Ettema, T. Hibma, Phys. Rev. B 45, 9126 (1992).

[33] W. B. Su, S. H. Chang, W. B. Jian, C. S. Chang, L. J. Chen, and Tien T. Tsong, Phys. Rev. Lett. 86, 5116 (2001).

[34] H. Brune, Surf. Sci. Rep. 31, 121 (1998) and the references therein.

[35] J.A. Venables, Phys. Rev. B 36, 4153 (1987).

[36] J.A. Venables, G D T Spiller and M Hanbucken, Rep. Prog. Phys. 47, 399 (1984).

[37] V. Yeh, L. Berbil-Bautista, C.Z. Wang, K.M. Ho, and M.C. Tringides, Phys. Rev. Lett. 85, 5158 (2000).

[38] A. Menzel, M. Kammler, E.H. Conrad, V. Yeh, M. Hupalo, and M.C. Tringides, Phys. Rev. B 67, 165314 (2003).

[39] Jacques G. Amar and Fereydoon Family, Phys. Rev. Lett. 74, 2066 (1995).

[40] M. C. Bartelt, J. W. Evans, Phys. Rev. B 46, 12675 (1992).

[41] M. C. Bartelt, M. C. Tringides, J. W. Evans, Phys. Rev. B 47, 13891 (1993).

[42] J. W. Evans, M. C. Bartelt, Phys. Rev. B 66, 235410 (2002).

[43] R. Biswas, K. Roos, M.C. Tringides, Phys. Rev. B 50, 10932 (1994) and the references therein.

[44] M.E. Fisher and W. Selke Phys. Rev. Lett. 44 1502 (1980).

[45] P.Bak and R. Bruinsma Phys. Rev. Lett. 49 249 (1982).

[46] C. Kumpf, O. Bunk, J.H. Zeysing, M.M. Nielsen, M. Nielsen, R.L. Johnson, R. Feidenhans'l, Surf. Sci. 448, L213 (2000).

[47] T.L. Chan, C.Z. Wang, M. Hupalo, M.C. Tringides, Z.Y. Lu, and K.M. Ho, Phys. Rev. B 68, 045410 (2003).

[48] M. Hupalo, T.L. Chan, C.Z. Wang, K.M. Ho, and M.C. Tringides, Phys. Rev. B 66, 161410 (2002).

[49] M.F. Reedijk, J. Arsic, D. Kaminski, P. Poodt, J.W. M van Kessel, W.J. Szweryn, H. Knops, and E. Vlieg, Phys. Rev. Lett. 90, 056104-1 (2003)

[50] M.K. Yakes, *et al*, to be published.

ACKNOWLEDGMENT

All the work in this thesis was done in a collaborating manner. A good part of the experiments and analysis were performed by the following people: Myron Hupalo, Knut Budde, Michael Yakes. Some part was done by Eric Abram, Sascha Kremmer, and Louis Berbil-Bautista. Special thanks to Myron Hupalo and Michael Yakes for fruitful discussions and tremendous amount of help, to Knut Budde for the training I received from him. Visiting scientis, Stepan Stepanovskyy and Martin Kammler, and a visiting student, Andreas Menzel, all had their contributions through collaboration in other projects. My major professor and I worked together closely on all the projects. We had frequent discussions from which I received many comments and suggestions.

This work was performed at Ames Laboratory under Contract No. W-7405-Eng-82 with the U.S. Department of Energy. The United States government has assigned the DOE Report number IS-T 1995 to this thesis.